Convection and diffusion in a micro flow injection system

Eelco van Akker

Van Akker, Eelco

Convection and diffusion in a micro flow injection system
Thesis, University of Twente, Enschede

ISBN 90-3651339-1

CONVECTION AND DIFFUSION IN A MICRO FLOW INJECTION SYSTEM

PROEFSCHRIFT

ter verkrijging van
de graad van doctor aan de Universiteit Twente,
op gezag van de rector magnificus,
prof. dr. F.A. van Vught,
volgens besluit van het College voor Promoties
in het openbaar te verdedigen
op vrijdag 1 oktober 1999 te 15.00 uur.

door

Eelke Bauke van Akker

geboren op 16 januari 1968

te Nijmegen

Dit proefschrift is goedgekeurd door de promotor
prof. dr. W.E. van der linden
en de assistant-promotor
dr. ir. M. Bos

IK WIL HIER
BEST WAT LEREN

MAAR IK BEN GEEN
DOM SPONSJE

Loesje

Summary

Much has been written about the theoretical background of Flow Injection Analysis (FIA) systems. Until now the prediction of the dispersion in a FIA system was restricted to the use of simple formulae or two-dimensional numerical models. Through recent developments in computer hardware and, at the same time, the development of efficient computational fluid dynamics software it is possible, with the use of a three dimensional model (based on the Navier-Stokes equations), to make a 1 to 1 translation between experimental systems and systems based on numerical calculations. A 1 to 1 translation means that only (fundamental) parameters are necessary in the numerical description without the need for fit or match factors. All the known phenomena, such as convection and diffusion, are incorporated in this description. The fundamental parameters in this thesis are: the concentrations, the diffusion coefficients, the geometry, the flow rates and in case of a reaction, the reaction constant, the reaction equation and reaction order.
Next to these macro FIA systems the micro FIA systems are emerging. These systems have many advantages compared to the traditional macro systems. Two examples are: a considerable reduction in analyte consumption and the development of portable systems. One disadvantage of the current microsystems, is the expensive development. It would be very helpful, money wise, if numerical calculations could be used for the development of an optimal microsystem. In this thesis the results of a three dimensional numerical model, based on the Navier-Stokes equations, are compared with experimental results. This has been done for channels of different geometries, different flow rates and a simple reaction.

Chapter 1 contains a general introduction into the area of FIA systems (macro and micro). This chapter describes the advantages and disadvantages of the two systems and problems that can be expected to occur with microsystems.
In chapter 2 a general explanation of convection and diffusion and the partial differential equations (Navier-Stokes) these two phenomena are based on, is given.
In chapter 3 an introduction to computational fluid dynamics is given. Different topics are being treated in this chapter. It boils down to solving the partial differential equations (in adapted form) mentioned in chapter two. From this chapter, it is clear that the numerical problems with convection can best be solved with the use of the “QUICK” or “CCCT” scheme. The maximum element length is 15 μm, in the areas with a steep variation of the dependent variable. The use of a non-uniform grid is advised and validated. The calculation of the flow profile is done separately from the convection-diffusion calculation to reduce the calculation time. It is demonstrated that this separation is allowed.
In chapter 4 the effect of a rectangular or smooth bend on the dispersion of a sample injected into a carrier stream is investigated. These investigations are conducted experimentally and numerically. It appears that the difference between a rectangular or smooth bend, with regard to the dispersion of a

sample is minimal. This conclusion is supported by the experimental as well as the numerical results.
In chapter 5 the effect of different flow rates, stopped and pulse flow on the dispersion of a sample injected into a carrier stream is investigated.
It can be concluded that convection still plays a very important role in the dispersion process. This is in contrast to the general opinion that the diffusion mechanism would overrule the convection mechanism. The influence of stopped flow on the dispersion of the sample is comparable with the effects seen in macro FIA systems. Furthermore this chapter shows that the flow doesn’t have to be pulse-free. Under certain restrictions, there is not much difference between a pulsed and pulse-free carrier stream.
In chapter 6 a simple reaction is investigated. The reaction is investigated at different flow rates and with the stopped flow principle. This investigation is performed experimentally and numerically. This chapter shows that it is possible to predict the dispersion of a sample in a carrier stream with a reaction present

Samenvatting

Over de theoretische achtergrond van Flow Injection Analyse (FIA) systemen is veel geschreven. Tot nu toe beperkte zich dit echter tot simpele formules of twee-dimensionale numerieke modellen om de dispersie in een FIA systeem te voorspellen. Door de recente ontwikkeling in computer hardware en de ontwikkeling van efficiënte “computational fluid dynamics” software is het nu mogelijk om met behulp van een drie dimensionaal model (op basis van de Navier-Stokes vergelijkingen) een 1 op 1 vertaling te maken tussen experimentele systemen en systemen op basis van numerieke berekeningen. Een 1 op 1 vertaling betekent dat er alleen (fundamentele) parameters nodig zijn voor de numerieke beschrijving en geen fit of “match” factoren. In deze numerieke beschrijving worden alle bekende verschijnselen, zoals convectie en diffusie, meegenomen. De fundamentele parameters in dit proefschrift zijn: de concentraties, de diffusie coëfficiënten, de geometrie, de stroomsnelheden en, in geval van een reactie, de reactiesnelheidsconstante en de reactievergelijking en orde.
Naast de bestaande macro-FIA systemen zijn micro-FIA systemen in opkomst. Deze systemen bieden vele voordelen ten opzichte van de bestaande macro-systemen. Te denken valt daarbij aan een aanzienlijke reductie in gebruikte chemicaliën en bijvoorbeeld de ontwikkeling van draagbare systemen. Een nadeel van de huidige micro-systemen is dat de ontwikkeling op dit moment erg kostbaar is. De hoge kosten van zo’n micro-system zijn toe te schrijven aan het feit dat dit gebied zich nog in een ontwikkelingsfase bevindt. Het zou, vanwege de kosten, zeer voordelig zijn als men aan de hand van numerieke berekeningen zou kunnen aangeven hoe een optimaal micro-system er uit zou moeten zien. In dit proefschrift worden de resultaten van een drie-dimensionaal numeriek model op basis van de Navier-Stokes vergeleken met experimentele resultaten. Dit gebeurt voor verschillende geometrieën, verschillende stroomsnelheden en een eenvoudige reactie.

Het eerste hoofdstuk is een algemene inleiding op het gebied van FIA-systemen (macro en micro). Dit hoofdstuk behandelt de voor - en nadelen van de twee systemen en problemen die kunnen optreden bij micro-systemen.
In hoofdstuk 2 wordt een algemene beschouwing gegeven van convectie en diffusie en de partiële differentiaalvergelijken (Navier-Stokes) die hier aan ten grondslag liggen.
In hoofdstuk 3 volgt een inleiding in het domein van de “computational fluid dynamics”. Verschillende onderwerpen worden hier behandeld. Het komt er op neer dat de in hoofdstuk twee afgeleide vergelijkingen (in gewijzigde vorm) numeriek worden opgelost. In dit hoofdstuk blijkt dat de numerieke problemen met convectie het best kunnen worden voorkomen met behulp van het “QUICK” of “CCCT” schema. De maximale elementlengte is 15 μm, in de buurt van gebieden met een grote variatie van de afhankelijke grootheid. De maximale tijdstap voor het probleem in dit hoofstuk is 0.01 seconden. Verder

wordt het gebruik van een “non-uniform” grid aangeraden en dit wordt onderbouwd. Om de rekentijd te verkorten wordt de berekening van het stromingsprofiel losgekoppeld van de convectie-diffusie berekening. Er wordt aangetoond dat deze ontkoppeling toelaatbaar is.
In hoofdstuk 4 wordt het effect van haakse of geleidelijke bochten op de dispersie van een in een dragerstroom geïnjecteerd monster volume bekeken. Dit gebeurt zowel experimenteel als numeriek. Het blijkt dat er weinig effect te zien is van de keuze voor één van de beide type bochten op de dispersie van het monster. Deze conclusie wordt ondersteund door zowel de experimentele als de numerieke resultaten.
In hoofdstuk 5 wordt het effect van verschillende stroomsnelheden, “stopped flow” en “pulsed flow” op de dispersie van een in een dragerstroom geïnjecteerd monster bekeken. Het blijkt dat convectie en diffusie beiden nog een grote rol spelen, in tegenstelling tot de algemene veronderstelling dat diffusie overheersend zou moeten zijn. De effecten van “stopped flow” op de dispersie van het monster is te vergelijken met een macro FIA-systeem. Verder laat dit hoofdstuk zien dat de dragerstroom niet volledig “pulse” vrij hoeft te zijn. Onder bepaalde randvoorwaarden is er weinig verschil tussen een puls-vrije of gepulseerde dragerstroom.
In hoofdstuk 6 komt een eenvoudige reactie aanbod. De reactie wordt met verschillende stroomsnelheden en het “stopped flow” principe bekeken en vergeleken met een numeriek model. Dit hoofdstuk laat zien dat het mogelijk is numeriek een voorspelling te doen over de dispersie van een monster in een dragerstroom in samenhang met een reactie.

Contents

Chapter 1

Introduction

1.1 Flow injection analysis

Flow injection analysis (FIA) was introduced in the mid seventies [1]. There is some debate about the first FIA system but the term FIA was introduced in 1975 by Růžička, and Hansen [2]. In the last two and a half decades, this technique has gained a prominent place in today's analytical chemistry. There are several reasons for the success of FIA. Some of these reasons are its simplicity, versatility, low cost and reproducibility. These reasons are closely linked to the elements that are used in building a FIA system.

The basic principle of FIA can be explained with Figure (1.1).

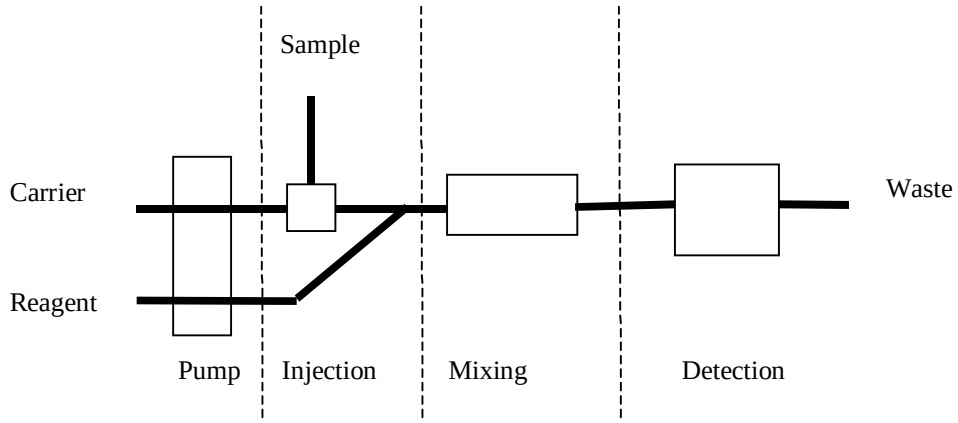

Figure (1.1) A simple flow injection system

The carrier transports the injected sample to the mixing section, where it is mixed with the reagent. The sample reacts with the reagent to a (reaction) product that can be detected in the last section. In Figure (1.1) the process of taking a sample, bringing it to the laboratory, adding a reagent, mixing and recording a detector read-out is replaced with one FIA system. The simple system depicted shows the essential modules of a FIA system: the pump, the injection device, the transport (mixing) and the detection module. The mixing

device is sometimes omitted if only the transport functions are important, such as in FI-AAS. The possibilities for the different modules are countless, but in practice a few configurations predominate.

- The pump module usually is build based on a peristaltic pump. Some other options are pressure based pumps and syringe pumps. The flow has to be reproducible, pulse-free, constant and regular.
- The injection module has to introduce accurately, reproducibly a sample into the carrier stream. Different options are the use of a rotary valve, hydrodynamic injection and time-based injection.
- The transport module can be roughly subdivided into several smaller modules: tubing, connectors, reactors and mixing devices.
- The detection module in a FIA system depends on the product that has to be detected. Usually a photometric absorption detector is used, but electrochemical detectors or mass detectors are also being used.

There are of course different flow systems possible. One of these is a segmented flow system. Air bubbles are used to create segments of fluid with air in between. One segment now can be transported through the system like a mini reactor. The air bubbles have to be removed, just before the detector.

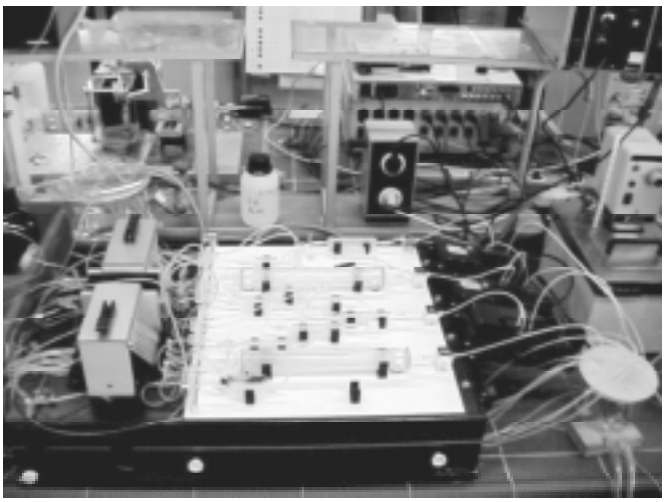

Figure (1.2) A continuous flow air-segmented analyzer from Skalar

The different categories of FIA-systems and their working areas are dealt with in [1] and [3]. One thing that needs special mentioning is the ability of a FIA system to have a high sample throughput. This can be up to 300 samples/hr. Closely linked to the sample throughput is the phenomenon called dispersion. The sample (introduced in Figure (1.1)) undergoes dispersion when it is transported through the flow system. The dispersion is defined as the dilution of a sample volume injected into a flowing stream. The phenomena causing this dilution will be explained in depth in Chapter 2. It is clear that a high dilution

(large dispersion) reduces the sample throughput. The characterization of systems as shown in Figure (1.1) is mostly experimental.

1.2 Micro flow injection systems

A FIA system lends itself for miniaturization. With miniaturization some disadvantages of a FIA system can be overcome while keeping the advantages. A μFIA (micro Flow Injection Analysis) system reduces the amount of reagents used, speeds up the sample processing and makes the system portable. Figure (1.3) shows the μ-device, with 5 channels, used throughout this thesis.

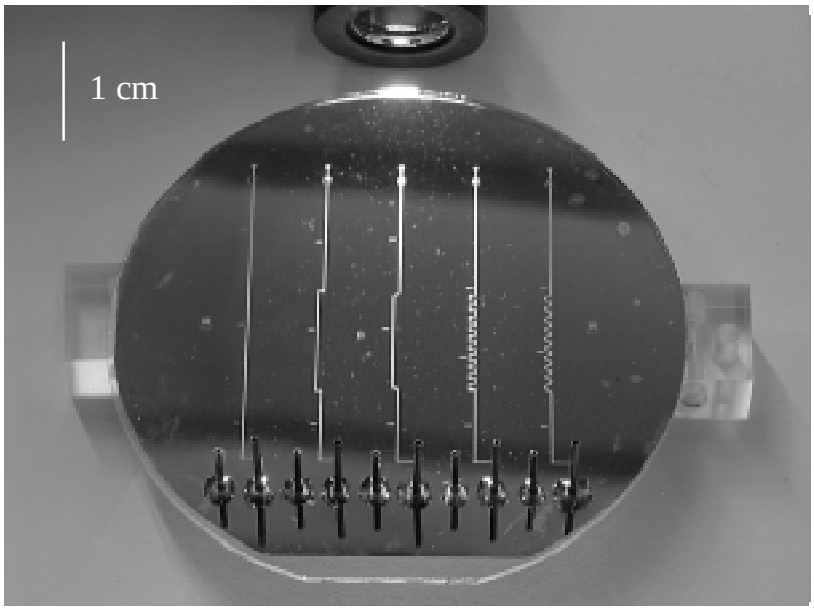

Figure (1.3) A simple μflow injection system

The channel width is about 200 μm. In Chapter 5, for example, the left channel is used to study different flow conditions. In this case the channel volume was 1 μl, the injection volume was 0.067 μl and the detection volume was about 0.047 μl. A simple flow injection system for the determination of chloride [1] has the following dimensions : injection volume 30 μl, detection volume 10 μl and system volume of 196 μl. The decrease in volume of the reagents used is obvious.
To further illustrate the difference Figure (1.3)could be compared to Figure (1.2). Although the μ-FIA system (Figure (1.3)) is not that versatile as the Skalar analyzer (Figure (1.2)), the difference in portability is clearly visible.

There are of course also disadvantages.

- The injection volume decreases. The demands of a ‘macro’ FIA system on the injection apply also to a μ-FIA system. The injection volume, in the μ-flow system, should be decreased with a factor of about 450 with relatively the same accuracy and reproducibility. This means that the hardware, used for the injection, also has to be miniaturized. Since miniature pumps and valves are not (at this moment) off the shelves products this causes a problem.
- The detection volume has to be decreased as well in order to maintain the same spatial resolution. This fact causes an even greater problem than the injection. The detector has to be adjusted or the ‘macro’ equivalent must be used with special adaptation or concessions have to be accepted.
- The pump module should be miniaturized too. There is fortunately the possibility to work with very accurate syringe pumps. These pumps can generate the flow that is needed for a micro system (μl/min range).
- The transport module (and all the other modules) are easily clogged, because of the small diameters. Particularly with the use of real (non-laboratory) samples this poses a big problem. Special measures have to be taken, for example filtering.

At present the availability of micro valves and micro pumps is still a problem. The total integrated solution (with micro pumps, micro valves and micro detection) is referred to as the ‘Micro Total Analysis System’ (μ-TAS). The first workshop on this subject was held in 1994 [4]. Although much progress has been made, it is still a problem to get all the items (valves, pumps and detector) integrated into the micro system. For a detailed review of the different mechanical pumps, we refer to [5].

Another way to propel the solution is to make use of electroosmotic flow (EOF). EOF is used in macro FIA system for it’s separation ability and has gained in popularity in the micro community.
The generation of an EOF to pump reagents and samples through a μ-FIA system is, however, subject to certain physico-chemical limitations [6]. The previous literature reference [6] also presents a review of micro flow injection systems. Although the author focuses on EOF-systems, he also discusses the fabrication process of a micro flow system (in silicon).

In this thesis concessions were done to be able to work with a micro flow system. The integration of pumps and valves into the system shown in Figure (1.3) was not feasible. This problem was solved with a time-based injection and the flow was established with accurate syringe pumps. The problems with a detector were solved on one hand by using a higher concentration of sample and on the other hand by using a very sensitive measuring setup.

1.3 Numerical simulation

While μ-devices are still in the research phase the manufacturing of a device is expensive. The advantage of a numerical pre-analysis is clear. Although the basic equations for describing the flow and sample transport through a flow injection system are known for a long time, the recent increase in computer power makes it possible too calculate the three dimensional fluid dynamics of such a system.
In Chapter 2 the Navier-Stokes [7] equations that describe the fluid dynamics will be explained. Numerical simulation makes it possible to see the effect of different geometries, injection, detection volumes without the costly manufacturing of the devices. Before numerical simulation can be used, we have to make sure that the results obtained in this manner correspond to experimental results. In Chapter 3 a basic introduction to computational fluid dynamics will be given. In this thesis the different basic building blocks of an μ-FIA system will be investigated numerically and experimentally. It shows some promising results. In Chapter 4 the effect of straight and smooth bends are investigated. In Chapter 5 the use of different flow conditions (normal, pulse and stopped flow) are investigated and in Chapter 6 attention is focussed on reactions.
An overview of the literature and the different models used to predict dispersion phenomena in flow injection can be found in a thesis by Hull [8]. This reflects the situation until 1993 and of course for macro flow systems. Hull discussed different models. The “tanks-in-series” model, the axially-dispersed plug flow model and the convection-diffusion model. All these models are simplified representations of the reality. The convection-diffusion model, based on the Navier-Stokes equations also used in this thesis, as used by Hull is only two dimensional with a fixed (analytical) velocity profile. The axially-dispersed plug flow model ignores the radial diffusion and the tanks-in-series model describes the dispersion with the use of a number of ideal stirred tanks placed in series. In this thesis a three-dimensional model is used and the flow profile is also calculated. There are several advantages when comparing the model used in this thesis to the models used by Hull. For example, an arbitrary manifold can be used, the flow profile is available, the pressure distribution is available and the concentration distribution of the sample throughout the channel is available (all three-dimensional and, if necessary, time-dependent).
In principle the numerical simulations should hold for micro systems as well. The problem is that the numerical simulations, used in this thesis, are based on the Navier-Stokes equations. As long as the Navier-Stokes equations hold, the numerical simulations should give good results. There is literature that indicates that unusual behavior may occur with regard to heat and flow in micro channels [9]. That article, however, concentrates on the transition from laminar to turbulent. The flow conditions used in this paper are well within the laminar regime, even according to the definitions in this article.

Besides this thesis, other studies also indicate that numerical simulation based on the Navier-Stokes equations could be used to model accurately the fluid dynamics within complex microstructures. Harper [10] models mass flow of the carrier in different channel geometries and concludes that Computational fluid dynamics is a valid technique to model accurately the fluid dynamics down to a scale of 25 µm. Earlier work from Zemel et. al. [11,12,13] mentioned by Harper, shows that, using particular organic liquids, the Navier-Stokes equations can predict flows down to a scale of 0.1 µm. Although computational fluid dynamics is used extensively, three-dimensional (one on one) numerical investigations concerning flow injection systems (macro and micro) is minimal.
In this thesis convection and diffusion of a sample injected into a micro flow system is modeled.

1.4 References

[1] M. Valcárcel and M.D. Luque de Castro, Flow-Injection Analysis; principles and applications, Ellis Horwood Limited, English Edition, Chichester, 1987
[2] J. Růžička, and E.H. Hansen, Anal. Chim. Acta, 78(1975)145
[3] J. Růžička, and E.H. Hansen,Flow Injection Analysis, second edition, John Wiley & Sons, New York, 1988
[4] A. van den Berg,and P Bergveld, Micro Total Analysis Systems (Proceedings of the µTAS '94 Workshop, Kluwer Academic Publishers, Dordrecht,1994
[5] J. van Kuijk, Numerical Modelling of Flows in Micro mechanical Devices, PhD. Thesis university of Twente, 1997
[6] S.J. Haswell, Analyst, 122(1997)1R.
[7] R.B. Bird, W.E. Stewart, E.N. Lightfoot, 'Transport phenomena', John Wiley & Sons Inc, New York, 1963
[8] R.D. Hull, Flow injection dispersion phenomena : simulation and evaluation of theoretical models, UMI Dissertation Services, 1993
[9] C.P. Tso, S.P. Mahulikar, International Journal of Heat and Mass Transfer, 42(1999)1813
[10] M.J. Harper C.M. Turner and J.E.A. Shaw, Proceedings of the 1st International Conference on Simulation and Design of Microsystems and Microstructures MicroSIM95, editors: R.A. Adey, A. Lahrmann, and C. Lessmolman, Comp. Mech. Publications, UK 1995, p. 155-163
[11] J. Pfahler, J. Harley, H. Bau and J. Zemel, Sensors and Actuators, A21-A23(1990)431
[12] H. Bau, J. Harley, S. Hava, J. Pfahler, A. Toroa, P. Wiilding, W. Urbanek, T.K. Wang, A. Weisberg and J. Zemel;, "Energy and Mass Transport in Mesoscale Structures", Proceedings of the 8th Symp. On Energy Engineering Sciences: Micro / Macro Studies of multiphase Media, (1991)71
[13] W. Urbanic, J.N. Zemel, H.H. Bau, J. Micromech. Microeng. 3(1993)399

Chapter 2

Convection and diffusion

Dispersion (or mixing) of a sample in a flow injection system is caused by two phenomena: convection and diffusion. Both these phenomena can be explained by a simple example. If you put an aqueous drop of dye in a glass of water it takes some time before the dye spreads out. After a certain time the dye drop is gone and you are left with a uniform dye solution. This process is called diffusion. Diffusion equalizes concentration differences. The use of stirring speeds up the equalization. A little stick could be used for stirring and (in this case) speeds up the mixing of the dye. An external imposed flow profile influences the mixing.

2.1 Introduction

In a basic flow injection system several aspects concerning the dispersion of the sample have to be considered. In order to accomplish a high throughput of samples, the mixing (or dispersion) should be limited. However in a ‘small’ part of a flow system mixing is a desirable property (even mandatory). For example: if we want two substances to react, they have to be in contact. A higher contact ratio results in a higher yield of product and more product results (among other things) in a lower detection limit. So dispersion in a flow system isn’t as simple as the “drop of dye” example at the beginning of this chapter. It pays off to know exactly what is going on.
In this chapter an explanation of convection and diffusion will be given and it will be shown that in fact the effects of convection and diffusion (regarding the dispersion of a sample in a flow system) do not necessarily reinforce each other.
The last part of this chapter tries to give the reader some insight into convection and diffusion behavior of a sample in a (micro) flow system.

2.2 The theory behind convection and diffusion

The basic phenomena of convection and diffusion have been explained previously. Before any explanation of these processes can be given with regard to the flow injection system, a more general view about transport processes should be presented [1,2,3,4].

There are three laws that describe the transport in general. The laws of mass (Lavoisier), momentum (Newton) and energy (Joule) conservation. There are two ways of looking at the conservation laws, a macroscopic view and a microscopic view. In each case a balance of the desired quantity is made over a control volume. In case we are interested in, for example, an average value of a quantity in a control volume a macroscopic balance is made. If we are interested in the distribution of this quantity in a control volume a microscopic balance is made.

The following quantities are of interest to us (φ_v represent the volume flowrate (m^3/s)):

- a mass transfer $\varphi_v \rho$ (kg/s) where ρ is the density of the fluid (kg/m^3)
- a molar transfer $\varphi_v c_i$ (kmol/s) where c_i is the concentration ($kmol/m^3$) of material I
- an energy transfer $\varphi_v \rho u$ (J/s) where u is the thermal energy per mass unity (J/kg)
- a momentum transfer $\varphi_v \rho \bar{v}$ (N) where $\bar{v}$ is the fluid velocity (m/s)

A general balance for the quantities is shown in Figure (2.1) and Equation (2.1).

$$\frac{d}{dt}(XV) = \varphi_{v,in} X_{in} - \varphi_{v,out} X_{out} + rV \qquad \text{Equation (2.1)}$$

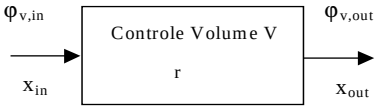

Figure (2.1) General balance

Where:

$\varphi_{v,in}$ and $\varphi_{v,out}$ are the volume flows in and out of the control volume (m^3/s).
V is the control volume (m^3).
r is the production of the quantity X per volume-unit and per time-unit.
x_{in} and x_{out} are what goes in and out of the quantity per volume-unit.

The Navier Stokes equations give us the distribution of this quantity in a control volume. Since we are interested in deriving the Navier Stokes equations and the theoretical background for that purpose, only microscopic balances will be part of this thesis. A division can be made between molecular transport and convective transport of a quantity. In case of molecular transport the

transported quantity is only “passed along” (this happens even when the fluid is not in motion), for example the diffusion case in the pre introduction section. In case of convective transport the transported quantity is carried along with the fluid, for example the convective case in the pre introduction section.

2.2.1 Molecular transport

The Brownian motion of the molecules is mainly responsible for the molecular transport of a quantity. Molecular transport can be separated into three different items. The quantity that is transported could be momentum (internal friction), heat (conduction) and mass (diffusion). These three quantities are described by three different equations (the rate equations). These equations are, however, very similar and follow a general form. Before these three equations are mentioned a few definitions have to be introduced.

2.2.1.1 The steady state molecular transport equations

Flux density.

Flux F is the transfer rate of some quantity. When expressed per unit surface area S (the surface is perpendicular to the direction of the transport), it is flux density Φ

$$\Phi \equiv \lim_{\Delta S \to 0} \frac{\Delta F}{\Delta S} n \qquad \text{Equation (2.2)}$$

where n is a unit vector.

Field intensity

Field intensity ∇ P refers to the strength of a field. It is expressed in terms of position. A high field intensity gives rise to a high flux density, and vice versa. The flux density and field intensity are proportional to each other. Expressing the field intensity as the change of a property P with respect to coordinate dimensions results in the general molecular transport equation,

$$d \cong \nabla P$$

or

$$d = -C \nabla P \qquad \text{Equation (2.3)}$$

where ∇P is the gradient of property P, the operator ∇ being defined by

$$\nabla \equiv i\frac{\partial}{\partial x} + j\frac{\partial}{\partial y} + k\frac{\partial}{\partial z}$$ Equation (2.4)

in the rectangular coordinate system and C is a constant of proportionality; i, j and k are unit vectors in the orthogonal directions. The gradient of P is sometimes referred to as the potential gradient and represents a driving force.

Fick's diffusion equation.

Fick's first law governs the steady state molecular mass transport (diffusion). For a species i and in 1 dimension with constant density of the medium:

$$\Phi''_{mol,i} = -D_i \frac{dc_i}{dx}$$ Equation (2.5)

where $\Phi''_{mol,i}$ is the mass flux of molecular species i (kg/m^{2}s), D_i is the diffusion coefficient (m^2/s) and $\frac{dc_i}{dx}$ is the concentration gradient.
The mass flux of molecular species i is proportional to the concentration gradient of species i. This concentration gradient is the driving force for the molecular mass transport. The molecular mass transport will stop if the concentration of species i is the same along the x-axis.

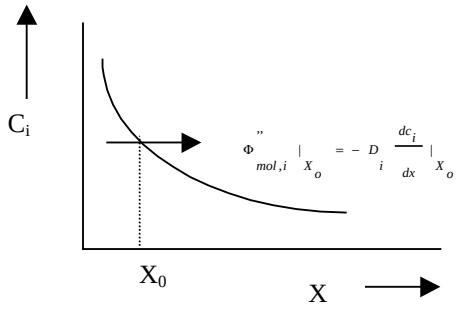

Figure (2.2) Illustration of Fick's law

Fourier's heat-conduction equation

Fourier's first law of heat conduction governs the molecular heat transport (conduction).

$$\Phi''_h = -\lambda \frac{dT}{dx}$$ Equation (2.6)

Where T is the temperature (K), λ is the thermal conductivity (W/(m*K)) and Φ''_h is the heat flux (J/(m^2*s)).

If we include a thermal diffusivity α (m^2/s), defined as

$$\alpha \equiv \frac{\lambda}{\rho C_p} \qquad \text{Equation (2.7)}$$

where ρ is the mass density (kg/m^3) of the material and C_p (J/(kgK)) is its specific heat capicity(at constant pressure) we get the following result

$$\Phi_h'' = -\alpha \frac{d(\rho C_p T)}{dx} \qquad \text{Equation (2.8)}$$

Equation (2.8) agrees with the general form of Equation (2.3).

Newton's viscosity equation.

Newton's law of viscosity governs the molecular momentum transport (internal friction).
For a steady state one-dimensional flow this will be:

$$\Phi_{i,yx}'' = -\eta \frac{dv_x}{dy} \qquad \text{Equation (2.9)}$$

Where η is the dynamic viscosity ($Ns/(m^2)$), v_x is the velocity component in the x-direction and $\Phi_{i,yx}''$ is the momentum flux (N/m^2) in the y-direction.

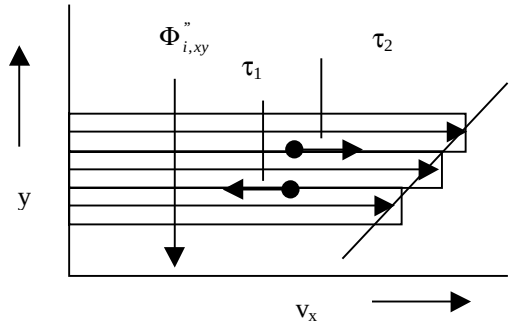

Figure (2.3) Illustration of momentum transport

Imagine two parallel plates at a distance Y. When the highest plate (regarding to y) is set in motion (with a certain velocity) after some time a velocity profile is established. Figure (2.3) visualizes this flow profile. In this figure we have a positive velocity profile in the x-direction and a velocity gradient in the y-direction. The situation in Figure (2.3) means that we have convective momentum transport in the x-direction but there is no x dependency.
In the very neighbourhood of the moving surface at Y the fluid acquires a certain amount of x-momentum. This fluid, in turn, transfers some of its momentum to the adjacent "layer" of liquid causing it to remain in motion in the

x-direction. Hence x-momentum is transferred through the fluid in the y-direction. The $\tau_{1 \text{ and }} \tau_2$ are the forces working on such a fluid layer. Of course, in reality the layers are infinitely small. This is shown in Figure (2.3).
It may be seen from Equation (2.9) that the viscous momentum flux is in the direction of the negative velocity gradient; that is the momentum tends to go in the direction of decreasing velocity. A velocity gradient can thus be thought of as a "driving force" for momentum transport. If Equation (2.9) is rewritten, the general form of Equation (2.3) is eminent.

$$\Phi''_{i,yx} = -\nu \frac{d(\rho v_x)}{dy} \qquad \text{Equation (2.10)}$$

Where ν has now the same unit as the diffusion coefficient (m^2/s) and is defined as η / ρ.

2.2.1.2 The transient molecular transport equations

The previous section was about steady state molecular transport. For the transient behavior of molecular transport we have to look at the conservation laws. The principle of conservation holds for heat, mass and momentum, individually or coupled. Neglecting the internal generation of the different quantities this can be expressed in transfer rates:

$$\text{Rate at which quantity enters} = \text{rate at which quantity leaves} + \text{rate of quantity accumulation} \qquad \text{Equation (2.11)}$$

This equation, sometimes referred to as the equation of change, applies to any transfer process. To develop the analogy, consider a region of unit depth bounded by planes at y and y + Δy (and x and x + Δx). Letting F be the flux density and P the quantity per unit volume which changes with time, Equation (2.11) becomes

$$\Delta x \, F\big|_y = \Delta x \, F\big|_{y+\Delta y} + \frac{\partial P}{\partial t} \Delta x \Delta y \qquad \text{Equation (2.12)}$$

Dividing by $\Delta x \Delta y$ and taking the limit as Δy approaches zero, i.e., description of the condition at point y, we get

$$\lim_{\Delta y \to 0} \frac{F\big|_y - F\big|_{y+\Delta y}}{\Delta y} = \frac{\partial P}{\partial t} \qquad \text{Equation (2.13)}$$

The left side of the previous equation is the negative form of the definition of the derivative.

Hence

$$-\frac{\partial F}{\partial y}=\frac{\partial P}{\partial t} \qquad \text{Equation (2.14)}$$

Equation (2.14) is the equation of change which is valid for one-dimensional transfer processes. Replacing the flux density and the property which changes with time by their equivalents for the fields under consideration [refering to Equation (2.5), Equation (2.8) and Equation (2.10)] we get the conservation equations :

Momentum :

$$\frac{\partial}{\partial y}\left(\eta\frac{\partial v}{\partial y}\right)=\rho\frac{\partial v}{\partial t} \qquad \text{Equation (2.15)}$$

Heat :

$$\frac{\partial}{\partial y}\left(\lambda\frac{\partial T}{\partial y}\right)=\rho C_p\frac{\partial T}{\partial t} \qquad \text{Equation (2.16)}$$

Mass (of species) :

$$\frac{\partial}{\partial y}\left(\rho D_{ij}\frac{\partial c_i}{\partial y}\right)=\rho\frac{\partial c_i}{\partial t} \qquad \text{Equation (2.17)}$$

Equation (2.17) is also known as Fick’s second law.
If for example the viscosity is constant, Equation (2.15) would turn into

Momentum :

$$\eta\frac{\partial^2 v}{\partial y^2}=\rho\frac{\partial v}{\partial t} \qquad \text{Equation (2.18)}$$

2.2.2 Convective transport

As stated earlier convective transport carries the quantity along with the fluid. This type of transport will be included in the next section where the Navier Stokes equations are being treated.

2.2.3 The Navier Stokes equations

The governing equations of flow, heat and mass transfer are called the Navier Stokes equations. It should be emphasized that the equations are valid for laminar and turbulent flows. Turbulent flows are just very complex unsteady laminar flows.

2.2.3.1 The transport equations.

The continuity equation

The first of the transport equations is the continuity equation. This equation will be derived here to give the reader some insight in what is required for such a process. Subsequently the equations will be given with an explanation but without derivation. The equation can be developed by writing a mass balance over a stationary volume element $\Delta x \Delta y \Delta z$ through which fluid is flowing (see Figure (2.4)). In this figure u_x represent the velocity in the x-direction and U the total velocity vector ($U=(u_x,u_y,u_z)$).

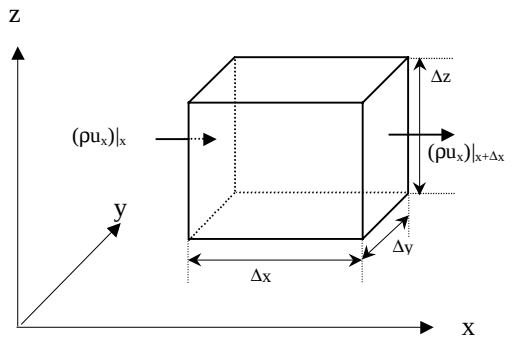

Figure (2.4) Region of volume fixed in space through which a fluid is flowing

A mass balance could be:

$$\begin{Bmatrix} rate\ of \\ mass \\ accumulation \end{Bmatrix} = \begin{Bmatrix} rate\ of \\ mass \\ in \end{Bmatrix} - \begin{Bmatrix} rate\ of \\ mass \\ out \end{Bmatrix} \qquad \text{Equation (2.19)}$$

We begin by considering the pair of faces perpendicular to the x-axis. The rate of mass entering through the face at x is $(\rho u_x)|_x \Delta y \Delta z$ and the rate of mass leaving through the face at $x+\Delta x$ is $(\rho u_x)|_{x+\Delta x} \Delta y \Delta z$. Similar expressions may be written for the other two pair of faces. The rate of mass accumulation within the volume element is $(\Delta x \Delta y \Delta z)$ $(\delta\rho/\delta t)$. The mass balance then becomes

$$\Delta x\Delta y\Delta z \frac{\delta\rho}{\delta t} = \Delta y\Delta z\left[(\rho u_x)|_x - (\rho u_x)|_{x+\Delta x}\right] + \Delta x\Delta z\left[(\rho u_y)|_y - (\rho u_y)|_{y+\Delta y}\right] + \Delta x\Delta y\left[(\rho u_z)|_z - (\rho u_z)|_{z+\Delta z}\right] \qquad \text{Equation (2.20)}$$

By dividing this entire equation by $(\Delta x \Delta y \Delta z)$ and taking the limit as these dimensions approach zero, we get

$$\frac{\delta\rho}{\delta t} + \left(\frac{\delta}{\delta x}\rho u_x + \frac{\delta}{\delta y}\rho u_y + \frac{\delta}{\delta z}\rho u_z\right) = 0 \qquad \text{Equation (2.21)}$$

This is the equation of continuity, which describes the rate of change of density at a fixed point resulting from the mass velocity vector (ρu).
We may write Equation (2.21) in a more conveniently vector notation:

$$\frac{\delta\rho}{\delta t} + (\nabla \cdot \rho U) = 0 \qquad \text{Equation (2.22)}$$

Here $(\nabla \cdot \rho U)$ is called the "divergence" of ρU. Note that the vector ρU is the mass flux and its divergence has a simple significance: it is the net rate of mass efflux per unit volume. So Equation (2.22) states that the rate of increase of the density within a small volume element fixed in space is equal to the net rate of mass influx to the element divided by its volume.
For an incompressible fluid this becomes

$$(\nabla \cdot U) = 0 \qquad \text{Equation (2.23)}$$

There are different ways of writing and developing this equation but this should give the reader enough information to understand the remaining equations in this chapter.

The momentum equation

In the previous section we saw the development of the continuity equation. The development of the momentum equations is done similarly, although a bit harder to do because of more components that have to be taken care of in the momentum balance.

$$\frac{\partial \rho U}{\partial t} = -[\nabla \cdot \rho UU] - \nabla p - [\nabla \cdot \tau] + \rho g \qquad \text{Equation (2.24)}$$

$\frac{\partial \rho U}{\partial t}$	rate of increase of momentum per unit volume
$\nabla \cdot \rho UU$	rate of momentum gain by convection per unit volume
∇p	pressure force on element per unit volume
$\nabla \cdot \tau$	rate of momentum gain by viscosity transfer per unit volume
ρg	gravitational force on element per unit volume
τ	stress vector (N/m^2)

The $[\nabla \cdot \rho UU]$ and $[\nabla \cdot \tau]$ are not simple divergences (used in Equation (2.22)) because of the tensorial nature of $\nabla \cdot \rho UU$ and τ. The physical interpretation is, however, analogous to that of $\nabla \cdot \rho U$ in the previous section, whereas $(\nabla \cdot \rho U)$ represents the rate of loss of mass (a scalar) per unit volume by fluid flow, the quantity $[\nabla \cdot \rho UU]$ represent the rate of loss of momentum (a vector) per unit volume by fluid flow. The τ term should be replaced with an expression before

a velocity distribution can be determined. This is, however, not necessary for this discussion.
For constant ρ and constant ν the previous equation can be simplied to

$$\frac{\partial U}{\partial t} = -(U \cdot \nabla) U - \frac{1}{\rho} \nabla p + \nu \nabla^2 U \qquad \text{Equation (2.25)}$$

The operator $\nabla^2 = \frac{\partial^2}{\partial x^2} + \frac{\partial^2}{\partial y^2} + \frac{\partial^2}{\partial z^2}$ is called the Laplacian operator.

The energy equation

The equation will not be explained nor used in this thesis.

$$\frac{\partial \rho H}{\partial t} + \nabla \cdot (\rho U H) - \nabla \cdot (\lambda \nabla T) = \frac{\partial p}{\partial t} \qquad \text{Equation (2.26)}$$

where H is the total enthalpy (J/kg) and λ is the thermal conductivity W/((m*K)).

Now we have the three basic equations: the continuity equation, the momentum equation and the energy equation. Normally one needs a few extra equations (equation of state, equation of viscosity, constitutive equation) to assess all the variables in these equations.
To describe an isothermal flow problem with constant density and constant viscosity only the continuity equation and the momentum equation are needed.

The binary diffusion equation

One more equation is necessary to describe the distribution of a species in the flow system:

$$\frac{\partial \rho Y_A}{\partial t} + \nabla \cdot (\rho U Y_A) - \nabla \cdot (\rho D_{AB} \nabla Y_A) = r_A \qquad \text{Equation (2.27)}$$

D_{AB} is the binary diffusivity of A in B (m^2/s). The symbol r_A represents the production (or consumption) of species A ($kg_A/(m^3.s)$ The concentration, C_A of species A is the mass per unit volume of species A (kg_A/m^3). The mass fraction, Y_A of A at a point is the ratio of mass of A to the total mass of the mixture, in a small control volume, around the point.

$$Y_A = \frac{C_A}{\rho}$$ Equation (2.28)

2.3 Implications for a flow injection system

In the previous section many equations have been introduced. These equations describe the flow profile and the transport of a species A in a flow system.
The remainder of this chapter shows the effect of convection and diffusion in a flow system. The effect they have in a flow injection system can best be explained with an example. For this purpose a micro flow system is used. A basic flow system consists of a channel with two inlets and 1 outlet. Through one inlet the carrier (the transport medium) is driven with an external pressure. The sample is injected through the other inlet. At the end of the channel a detection cell is placed. Just after the injection of the sample Figure (2.5) shows the situation. In this figure I represents the injection point and D the detection point.

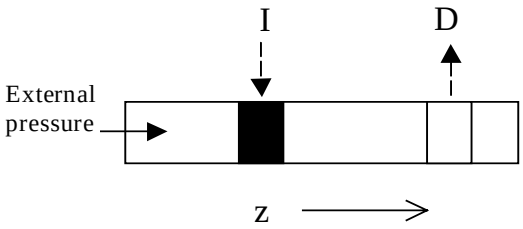

Figure (2.5) Basic flow injection system

After the injection the carrier stream transports the injection plug to the detection cell. During this transport dispersion occurs. Like in the pre-introduction section convection and diffusion take place simultaneously. There are three situations that we can look at. The first one is when there is no convection but only diffusion. The second one when there is only convection and no diffusion. The third case is where both convection and diffusion occur. The situation where there is only diffusion is rather simple. The distribution of the sample is described by a three dimensional version of Equation (2.5). There is no external pressure, so the convection is absent and the sample is only transported by diffusion. In Figure (2.6) the concentration along the z-axis for different times is shown. This figure shows that initially the injected block is a square (t_0). After some time the species A diffuses along the z-axis ($t_0<t_1<t_2$). Species A leaves the system through the inlet and outlet (behind the inlet and outlet an imaginary infinite reservoir of carrier solution is assumed) resulting in a zero concentration curve (t_∞) throughout the system after a very long time.

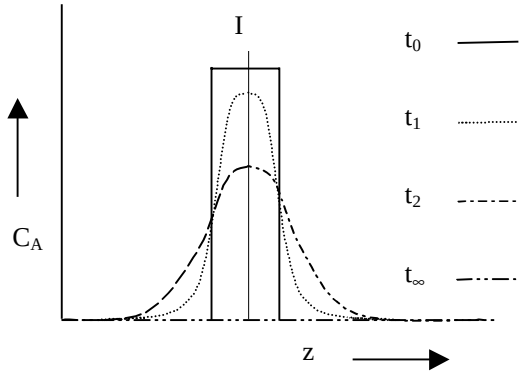

Figure (2.6) Illustration of diffusion (without convection)

To explore the other two situations we use a system as shown in Figure (2.7).

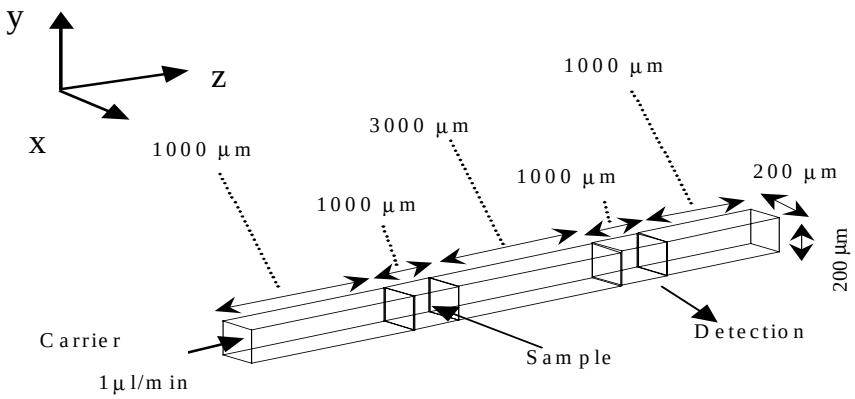

Figure (2.7) Test micro flow system

For these two situations we use numerical solutions to the Navier Stokes equations. This numerical work will be explained in the next chapter but for this moment it is assumed to be correct without further discussion. This allows us to investigate the different options and show some pictures of the actual dispersion. A standard way of looking at the dispersion, in a flow injection system, is plotting the response of the detector against time and inspecting the resulting curve. This curve is called the response curve.

The response curves for the example with diffusion and convection are shown in Figure (2.8). The effect of different diffusion coefficients is clearly visible. Assuming that there is no material consumption or production the following rule applies: a peak height is a measure for dispersion. A greater peak height means less dispersion. The peak width is of course a better measure for the dispersion but for this section the peak height is enough indication.

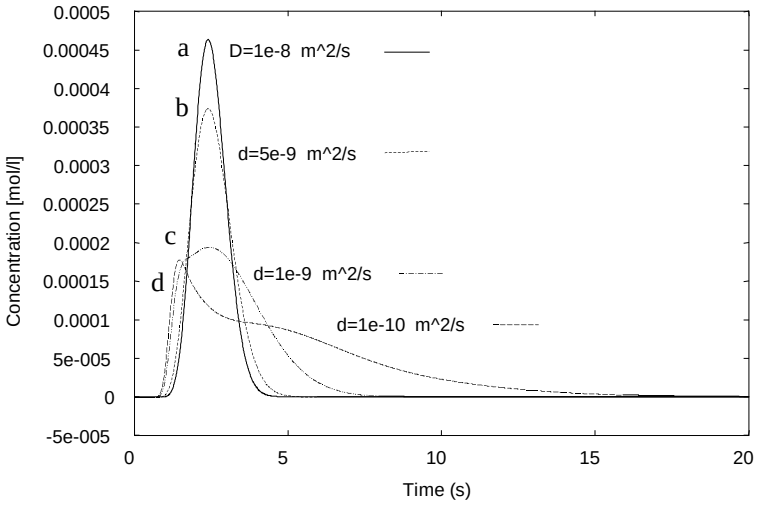

Figure (2.8) Response curve for different diffusion coefficients

From Figure (2.8) we can see four curves, with four different diffusion coefficients. Curve a represents the situation where the diffusion is the dominant mechanism. The sample is transported like a broadening band through the flow system. This becomes manifest as a gaussian peak shape at the detector.
Curves b and c show what happens if the diffusion and convection mechanism both influence the dispersion. Curves b and c show that the response curve gets lower and has a lot more tailing. When the influence of the convection gets even larger (curve d) we see that a so-called double humped peak [5] appears at the detector. In the extreme case (not shown in Figure (2.8)) with no diffusion taking place, a response curve with a sharp peak in front and very long tailing section shall appear at the detector.
Figure (2.10) shows the representation of a slice along z and y with two different diffusion coefficients. This slice is scaled to give the pictures in Figure (2.10). The ratio between length (along the z-axis) and height (along the y-axis) is changed (see Figure (2.9)) to give the pictures in Figure (2.10). The concentrations are presented with a greyscale spectrum that ranges from black (a low concentration) to white (a high concentration). The corresponding time is given at the left (in seconds).

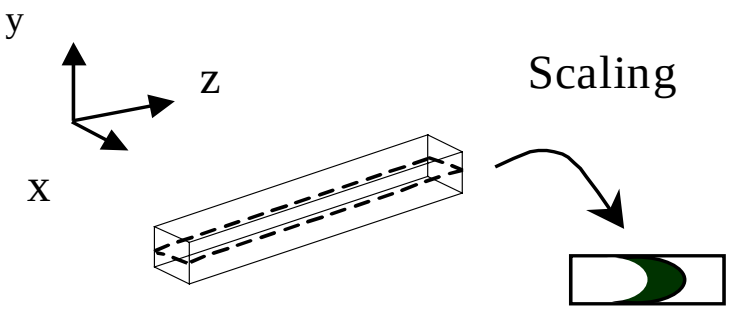

Figure (2.9) Slice representation

The pictures on the right (diffusion coefficient is $1*10^{-10}$ m^2/s) show clearly that the sample is breaking apart. This explains the double humped response curve in Figure (2.8). The pictures on the left show what happens if the diffusion coefficient is $1*10^{-7}$ m^2/s.

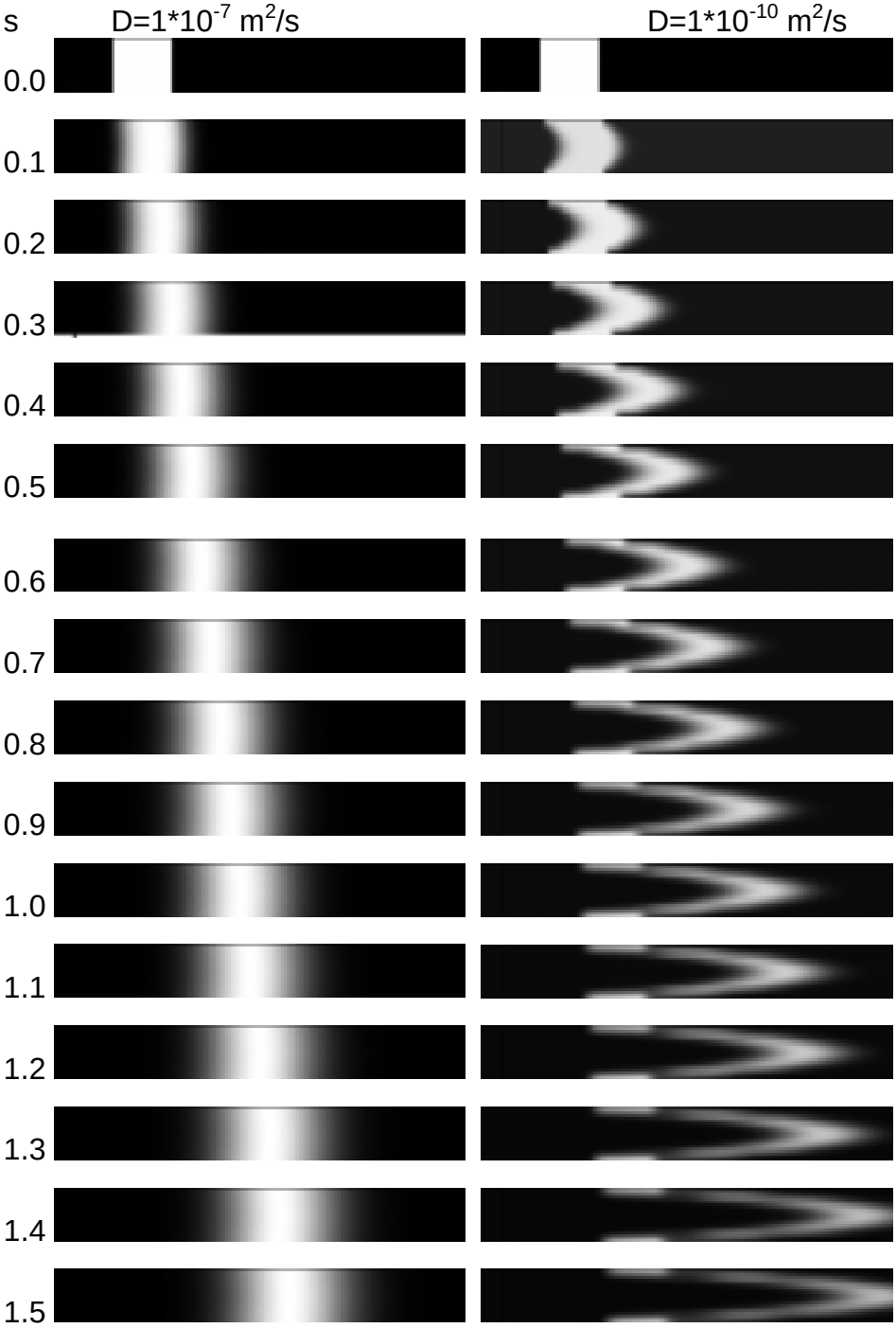

Figure (2.10) Slice view of the channel

2.4 Conclusions

In this chapter the theory behind convection and diffusion was explained. This explanation included molecular and convective transport and resulted in the Navier Stokes equations. These equations describe flow, heat and mass transport. Furthermore, the basic response curves were explained, taking into account both convection and diffusion. From these numerical calculated examples it can be concluded that convection and diffusion do not necessarily result in a larger dispersion (or work in the same direction). In combination with convection, diffusion keeps the dispersion of a sample in a flow system less then it would be without diffusion. On the other hand, if convection is not present the diffusion causes an increase in dispersion.

2.5 References

[1] J. Kuipers, W.P.M. van Swaaij, ‘Fysische transport verschijnselen 1 (deel SL)’, 1996
[2] R.B. Bird, W.E. Stewart, E.N. Lightfoot, ‘Transport phenomena’, John Wiley & Sons Inc, New York, 1963
[3] L.E. Sissom, D.R. Pitts, ‘ Elements of transport phenomena’, Mcgraw-Hill book company, New York, 1972
[4] AEA technology, ‘CFX 4.2 : solver manual’, 1997
[5] J.T. Vanderslice, A.G. Rosenfeld, G.R. Beecher, ‘Laminar-flow bolus shapes in flow injection analysis’, Anal. Chim. Acta, 179(1986)119-129

Chapter 3

An introduction to computational fluid dynamics and problems related to flow injection systems

3.1 Introduction

Computational fluid dynamics has a long history. The Navier-Stokes equations were first developed by Navier in 1822 based on molecular arguments [1]. Since then people have tried to solve these equations. First simple problems with paper and pen, but with the introduction of the computer more difficult problems could be tackled. One of the first to present a mathematical analysis of the transient convective-diffusion equation in a flow system was Taylor [2]. Since Taylor's publications a lot of work has been done on this subject. For some of the older work we refer to [3, 4, 5, 6] and for some of the more recent work to [7, 8, 9]. In these papers all the studies are being done on two dimensional cases. This is extended to a cylindrical tube by assuming symmetry. This can be seen as calculating a slice and then rotating it to get the three-dimensional picture. This is not possible for the simulation of the sample dispersion in the type of micro flow system used in this thesis. The calculations have to be three-dimensional, because in the fabrication of the micro flow systems straight walls are produced.
In recent years, the computer (calculation) power has reached a point where fluid dynamics problems can be solved not only for two-dimensional structures but also for three-dimensional structures.
In this chapter, an introduction shall be given on solving fluid dynamics problems by means of computation. Some essential choices shall be explained that will be used in later chapters.

3.2 Problem solving with the use of a numerical computation.

The next sections are taken mainly from [10] but adapted to our needs to give the reader a basic insight in the numerical solving of problems.

3.2.1 Discretization methods

The numerical solution of a differential equation consists of a set of numbers from which the distribution of the dependent variable ϕ can be constructed. We

shall assume that the variable ϕ is a function of only one independent variable x. The idea is, however, not restricted to one independent variable. The unknown values of the dependent variable are defined at a finite number of locations (called grid points) in the calculation domain. All the grid points together are known as a mesh. The continuous information, contained in the exact solution of the differential equation, is replaced with discrete values at the grid points. This replacement process is referred to as a **discretization method**. The discretization of the distribution of ϕ allows us to replace the governing differential equations with algebraic equations. These algebraic equations, referred to as the **discretization equations,** can now be solved. The use of standard equation solvers allows us to solve the algebraic equations and thereby calculating the distribution of ϕ.

3.2.2 Discretization equations

A discretization equation is an algebraic equation that specifies the relation between the values of ϕ, at the different grid points. Since this equation is derived from the differential equation governing ϕ, it contains the same physical information as the differential equation. In this derivation, we must employ some assumption about the variation of ϕ between grid points. Normally a profile (a description of how ϕ varies between grid points) is used that describes the variation of ϕ in a small region. The influence of the local value of ϕ is now restricted to this small region. With a very large increase in the number of grid points, the solution of the discretization equations is expected to approach the exact solution of the corresponding differential equation.

There are different ways of deriving the discretization equations. For example: the Taylor series approach, the variational formulation, the method of weighted residuals and the control-volume formulation. In this thesis, only the control-volume formulation will be used.

3.2.3 The control-volume (finite volume) approach

In section 3.2.1 and 3.2.2 the partial differential equations (PDE's) were discretized and replaced by the discretization equations. The control volume method takes a slightly different approach. The conservation principle is applied to a finite control volume fixed in space instead of a point (as with the PDE). The calculation domain is divided into a number of non-overlapping volumes. Such a volume surrounds each grid point. Different profiles describe the variation of ϕ between the control volumes (or grid points). The (control volume) discretization equations (derived in this manner) express the conservation principle for a finite volume, just as the PDE expresses it for an infinitesimal control volume.

One of the main advantages of the control-volume approach is that it enforces conservation across a certain volume. This volume ranges from one control-volume to the whole calculation domain (adding up the different control-volumes). It is likely that the discretisation developed by the control-volume approach has the conservative property [11].

The usual starting point for the derivation of the conservation law for a finite volume (control-volume) would be to write out the different integrals over the control-volume and its surfaces for the different variables (heat, mass or momentum).

$$\iiint_{\Omega} \frac{\partial \phi}{\partial t}\, d\Omega + \oiint_{S} q \cdot n dS + \iiint_{\Omega} R\, d\Omega = 0 \qquad \text{Equation (3.1)}$$

where the left term represents the time rate of increase of the dependent variable ϕ in the control-volume (Ω) and the second term represent the fluxes (q) through the surface (S) of the control-volume. The third term represents the source term.
Since we have derived the partial differential equations in chapter two we can work backwards by integrating the PDE over the control-volume and after applying the divergence theorem this results in Equation (3.1). This is the appropriate integral form for a finite volume.

To illustrate the control-volume approach and the method to obtain the discretization equation, and to introduce the terms that will be used when solving the Navier Stokes equations, two examples will be given. In these examples the starting point will be the appropriate PDE. The step(s) from the PDE to the discretization equation for the control-volume won't be thoroughly explained but the different fluxes in and out of the control-volume should be recognizable.

3.2.3.1 Steady state diffusion.

The governing one-dimensional differential equation of diffusion shall be taken (with constant density of the medium and c_i (in Equation (3.2)) denoted as C).

$$\frac{\partial}{\partial x}\left(D \frac{\partial C}{\partial x} \right) + S = 0 \qquad \text{Equation (3.2)}$$

where D is the diffusion coefficient (m^2/s), C the concentration of species i (kg/m^3) and S the rate of mass generation per unit volume.

A grid-point cluster shown in Figure (3.1) will be used during the derivation.

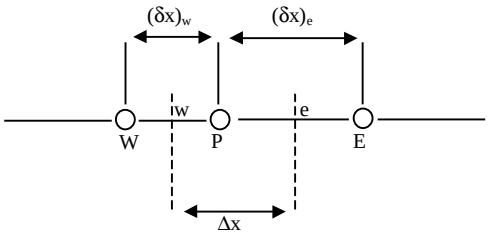

Figure (3.1) Grid-point cluster for the one-dimensional problem. (taken from [10])

The center grid point P, which has the grid points E (east, positive x) and W (west, negative x) as its neighbours, will be our working point. The control-volume is marked with dashed lines (the letters e and w denote the faces of the control-volume). Since we are interested in only one dimension but a volume approach implies multiple dimensions, we shall assume unit thickness in the y and z directions. Thus, the control-volume shown is $\Delta x \cdot 1 \cdot 1$.
Integration of differential Equation (3.2) over the control-volume results in Equation (3.3):

$$\left(D\frac{dC}{dx}\right)_e - \left(D\frac{dC}{dx}\right)_w + \int_w^e S dx = 0 \qquad \text{Equation (3.3)}$$

Two fluxes now can be seen in Equation (3.3): two versions of Fick's first law (east and west). The third term in Equation (3.3) is the source term. A profile is now needed to relate point P with its neighbouring points. Two simple profiles are shown in (Figure (3.2)a represents a stepwise profile and Figure (3.2)b represents a piecewise-linear profile).

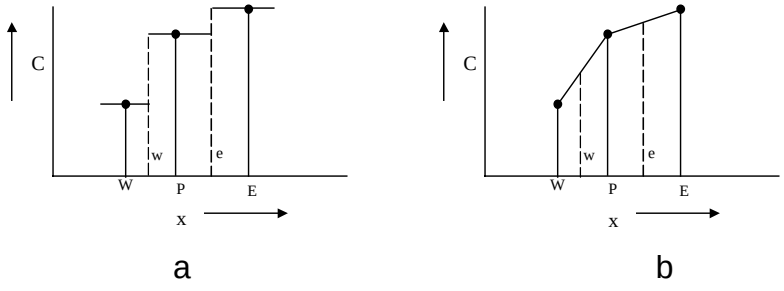

Figure (3.2) Assumed profiles (taken from [10])

We can now derive the discretization equation by evaluating the derivative dC/dx in Equation (3.3) from the piecewise-linear profile (Figure (3.2)b, also know as the central difference scheme)

$$\frac{D_e(C_E - C_P)}{(\delta x)_e} - \frac{D_w(C_P - C_W)}{(\delta x)_w} + \bar{S}\Delta x = 0 \qquad \text{Equation (3.4)}$$

where $\bar{S}$ is the average value of S in the control-volume.

Writing Equation (3.4) in the standard form [10] results in Equation (3.5)

$$a_p C_p = a_E C_E + a_W C_W + b \qquad \text{Equation (3.5)}$$

where

$$a_E = \frac{D_e}{(\delta x)_e},\ a_W = \frac{D_w}{(\delta x)_w},\ a_p = a_E + a_W \text{ and } b = \bar{S}\Delta x \qquad \text{Equation (3.6)}$$

A more general discretization equation, that includes multiple dimensions, is :

$$a_p C_p = \sum a_{nb} C_{nb} + b \qquad \text{Equation (3.7)}$$

where the subscript nb stands for neighbouring point.

The situation at the boundaries of the calculation domain was not discussed yet. Equation (3.7) only describes what happens at an internal point. A possible situation is shown Figure (3.3). In this figure, we have two grid points specified on a boundary and four ‘internal’ points.

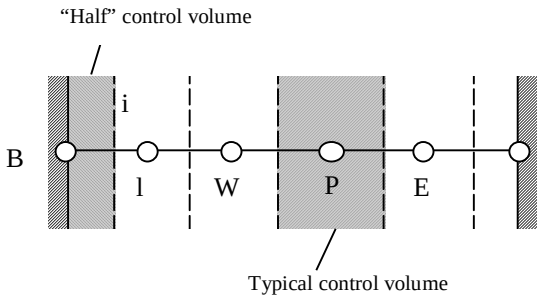

Figure (3.3) Control-volumes for the internal boundary points (taken from [10])

The discussion for the two boundary points is similar, so only the left (point B) will be explained. Typically, two kinds of boundary conditions are encountered: Dirichlet and Neumann. A Dirichlet boundary condition means that the dependent variable is specified, in this case the concentration. A Neumann boundary condition means that the gradient of the dependent variable is specified, rather than the value of the variable itself.
In case of a Dirichlet boundary condition, the boundary value (C_B) is given and no particular difficulty arises, and no additional equations are required.
In case of a Neumann boundary condition, the boundary condition is introduced by integrating the differential equation over the “half” control-volume as shown

in the left hand side of Figure (3.3). A detailed picture of the boundary control-volume can be seen in Figure (3.4).

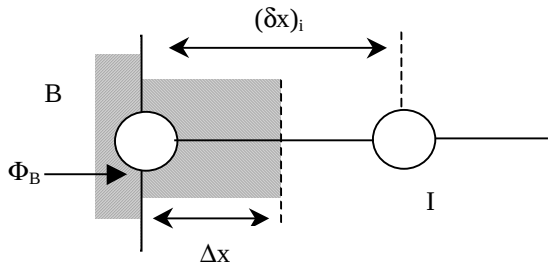

Figure (3.4) Half control-volume near the boundary (taken from [10])

Integrating Equation (3.2) over this control-volume and noting that the mass flux Φ represents Equation (2.5) and Φ_B is the flux from the Neumann boundary, we get

$$\Phi_B - \frac{D_i (C_B - C_I)}{(\delta x)_i} + \bar{S}\Delta x = 0 \qquad \text{Equation (3.8)}$$

If the value Φ_B is given, for point B, the equation becomes

$$a_B C_B = a_I C_I + b \qquad \text{Equation (3.9)}$$

where $a_I = \frac{D_i}{(\delta x)_i}$, $b = \bar{S}\Delta x + \Phi_B$ and $a_B = a_I$.

Now we are able to construct the required number of equations for solving the unknown concentrations (C) at the different grid points.

3.2.3.2 Explicit, implicit and Crank-Nicolson time schemes.

In the previous section a one-dimensional case was treated where the diffusion and source term were handled. The problem was independent of time (steady state). Another sort of differential equations is time dependent (transient). In this section the source term is dropped because the implementation would be the same as in the previous section. To show the different ways to handle these differential equations, we introduce Fick's second law, the unsteady state one-dimensional diffusion differential equation (see equation (2.17)) with constant density of the medium and c_i denoted as C.

$$\frac{\partial}{\partial x}\left(D \frac{\partial C}{\partial x} \right) = \frac{\partial C}{\partial t} \qquad \text{Equation (3.10)}$$

Given an initial distribution of C, at time t, we can calculate the distribution of C, at time t+Δt, with the use of Equation (3.10). The solution at t+Δt can be taken as a new initial distribution and the process can be repeated. The problem is now reduced to a 'time marching' problem. Following the same procedure as with the steady-state one-dimensional diffusion differential equation, and using a generalized assumption about how C_P, C_W and C_E will vary with time (time profile), we get (in accordance with Figure (3.1)):

$$a_P C_P^1 = a_E\left[fC_E^1 + (1-f)C_E^0\right] + a_W\left[fC_W^1 + (1-f)C_W^0\right] + \left[a_P^0 - (1-f)a_E - (1-f)a_W\right]C_P^0 \qquad \text{Equation (3.11)}$$

where f is a weighting factor between 0 and 1 and $a_E = \frac{D_e}{(\delta x)_e}$, $a_W = \frac{D_w}{(\delta x)_w}$, $a_P^0 = \frac{\Delta x}{\Delta t}$, $a_P = fa_E + fa_W + a_P^0$.

The use of the generalized assumption on how the different C values vary with time allows us to investigate three different time schemes using Equation (3.11) and changing the weighting factor f.
Different values of the factor f result in different relations between C_P^0 and C_P^1: f=0 gives an explicit scheme, f=0.5 gives the Crank-Nicolson (CN) scheme and f=1.0 gives a (fully) implicite scheme.

- In case of f=0 (the explicit scheme) C_P^1 is is only related to C's from the previous time step. The problem with this scheme is that the time step taken (Δt) should be relatively small. If this condition is violated unrealistic results could emerge.
- In case of f=0.5 there is a linear relation between the two C_P's from the different time steps. The Crank-Nicolson scheme is said to be unconditionally stable. This, however, is only mathematically true. For larger time steps oscillatory solutions [12] can occur.
- The (fully) implicit scheme (f=1.0) gives a satisfactory physically correct solution even with larger time steps. The disadvantage of the implicit scheme (and the CN scheme) is that it is complicated, takes more computer storage and executes slower compared to an explicit scheme. The advantages prevail over the disadvantages.

For small time steps the implicit scheme is not as accurate as the CN scheme [12].

3.3 Solving the Navier Stokes equations

In the previous sections we introduced several concepts such as: discretization methods, discretization equations, grid points (and control-volumes), profiles (relating the different grid points), sources, time schemes (explicit, CN and

implicit). In this section, we will explore the different concepts, when they are applied to the Navier Stokes equations.

In chapter 2 we saw that the Navier Stokes equations contained a set of (differential) equations. The linear equations (for example Equation (3.7)) are derived by integrating the Navier Stokes equations (equations (2.22), (2.25) and (2.27)) over the different control-volumes. The method is similar to the one used in the steady state (section 3.2.3.1) and the unsteady state (section 3.2.3.2) examples.

For the remainder of this section we make a distinction between the flow profile calculation (steady state) and the sample transport calculation (transient).

3.3.1 Calculation of the flow

The flow in our test system should be calculated with the use of the momentum equation (Equation (3.12) /(2.25)) and the continuity equation (Equation (3.13)/(2.23)) (for constant ρ and constant ν).

Continuity:

$$(\nabla \cdot U) = 0 \qquad \text{Equation (3.12)}$$

Momentum:

$$\frac{\partial U}{\partial t} = -(U \cdot \nabla) U - \frac{1}{\rho} \nabla p + \nu \nabla^2 U \qquad \text{Equation (3.13)}$$

The problem, however, is the pressure term in the momentum equation. The pressure is not directly specified by means of an equation, but it is indirectly specified through the continuity equation. A correct pressure profile substituted in the momentum equation would result in a flow profile that satisfies the continuity equation.

3.3.1.1 The pressure-correction approach

One of the ways to handle this indirect specification of the pressure is the pressure-correction approach. With an estimated pressure field the velocity is calculated by solving the momentum equation. This velocity field will not satisfy the continuity equation, unless a correct pressure field is used. If mass sources exist the pressure is corrected in a way that will eliminate these mass sources (satisfy continuity). The velocity field is again calculated with use of the momentum equation and the corrected pressure field. This procedure is repeated iteratively until the correct velocity and pressure profile is obtained.

In this thesis the SIMPLE (Semi-Implicit Method for Pressure Linked Equations) scheme is used [10,11].

$$p = p_0 + p' \qquad \text{Equation (3.14)}$$

$$u = u_0 + u' \qquad \text{Equation (3.15)}$$

where p is pressure, u velocity, the $_0$ subscript denotes the intermediate term and the superscript denotes the correction term.

With the use of a simplified momentum equation

$$\rho \frac{\partial u'}{\partial t} = -\frac{\partial p'}{\partial x} \qquad \text{Equation (3.16)}$$

the pressure correction can be linked to the velocity correction

$$u' = -A \frac{\partial p'}{\partial x} \qquad \text{Equation (3.17)}$$

where A is a constant. Combining Equation (3.15) and Equation (3.17), and substituting the result in the continuity equation, a pressure correction equation linking the estimated (intermediate) velocity field to a pressure correction can be obtained

$$\nabla^2 p' = \frac{1}{A}(\nabla \cdot V_0) \qquad \text{Equation (3.18)}$$

The basic SIMPLE procedure can be described by the following steps

1) Guess the pressure field (p_0)
2) Solve the momentum equation to obtain the velocity field
3) Solve Equation (3.18) to obtain the pressure correction
4) Adjust the pressure and velocity according to

$$p = p_0 + p'$$

$$u = u_0 - A\frac{\partial p'}{\partial x}$$

5) Replace the intermediate values (p_0,u_0) with the new corrected values and return to step 2. Repeat this process until the solution has converged.

For the different solvers see section 3.3.2.5.

3.3.1.2 Stopping the SIMPLE iteration

A method of monitoring the convergence of the SIMPLE iteration, and determining the number of iterations that are needed, is to examine how perfectly the discretization equations are satisfied by the current values of the

dependent variables. A standard way of looking at the convergence is the source residual. The source residual is the sum of the absolute values of the nett variable (ϕ) fluxes into or out of every cell in the flow domain (subsequently referred to as R_{sum} or residual). The R_{sum}, for the dependent variable ϕ, will become smaller (if the solution converges) with a greater number of iterations. After a certain number of iterations the solution does not change anymore. The required number of iterations can be set to a fixed number or determined on basis of the value of R_{sum}. This stop criterion should be determined separately for each problem.
Normally the mass residual is used for checking the convergence of the flow calculation. The iteration could be stopped according to a minimum residual value reached or a maximum number of iterations.

3.3.1.3 Staggered grids vs collocated grid

The grid where all the variables are located at the center of the control volumes (at the different grid points) is the so-called collocated grid. The use of a collocated grid can cause problems for the calculation of the flow profile.

For example,

$$\frac{du}{dx} = 0 \qquad \text{Equation (3.19)}$$

integrating this over the control-volume (see Figure (3.1)) results in

$$u_e - u_w = 0 \qquad \text{Equation (3.20)}$$

Using the piecewise-linear (central difference) profile and using midway location for the different faces the following equation can be determined

$$u_E - u_W = 0 \qquad \text{Equation (3.21)}$$

The problem is that these equations demand equality of the velocities at alternating grid points.

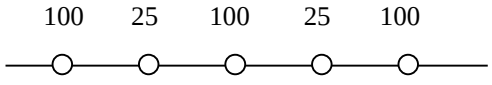

Figure (3.5) Incorrect velocity profile

Figure (3.5) shows a one-dimensional velocity profile that fits Equation (3.21) but is incorrect.

Equivalent problems arise with the pressure term in the momentum equation.

$$-\frac{dp}{dx} \rightarrow p_e - p_w = \frac{p_W + p_P}{2} - \frac{p_P + p_W}{2} = \frac{p_W - p_E}{2} \qquad \text{Equation (3.22)}$$

One solution to these problems is to use a staggered grid. In a staggered grid the velocities are calculated for the points that lie on the faces of the control-volume. The earlier mentioned problems disappear. It is, however, not straightforward to implement this for three-dimensional curvilinear coordinate systems (these coordinate systems are characterized by curves).

The second solution is to use (effectively) fourth-order pressure smoothing (or dissipation) to the continuity equations using for example Rhie-Chow interpolation [21]. The method attempts to estimate the cell-face velocity that would have been computed if the resulting pressure gradient influencing the cell-face velocity was based on adjacent nodes instead of alternating nodes. In this thesis the Rhie-Cow interpolation method is used.

3.3.1.4 The error in the flow calculations

Apart from the error in the model itself, there are basically two errors. The discretization error and the convergence error.

3.3.1.4.1 The convergence error

The convergence error is established by the stop criterion used for the iteration. The limiting situation (apart from zero iterations) is the machine accuracy. There is no need to iterate further, once the machine accuracy is reached. If the iteration is stopped before machine accuracy is reached, an error is introduced. Another error is introduced by the discretization process.

3.3.1.4.2 The discretization error

The discretization error should be zero if the control-volumes were infinitely small. In reality, this is of course not possible. The standard way of checking the grid independency, is to recalculate the same problem with twice as many control-volumes and if the solution does not change much the discretization error is probably small. The true (with no discretization error) solution could be calculated if the order of the error was known. Introduction of (for example) a piecewise linear profile introduces an error that can be made clear with the introduction of the Taylor expression for the first derivative

$$\left.\frac{\partial u}{\partial x}\right)_{i,j} = \frac{u_{i+1,j} + u_{i-1,j}}{2\Delta x} + O[(\Delta x)^2] \qquad \text{Equation (3.23)}$$

According to this equation the error should be 4 times smaller each time Δx is taken twice as small. The approximation is said to be second order in x.

Since in the flow calculation each profile used is second order or higher, the behavior of the error should also be second order. This is the case if Δx is taken small enough so that higher orders can be neglected and only second order behavior is observed.

In Table (3.1) an example is shown where the error behavior is second order. The 'true' value can be extrapolated on the basis of the error behavior. In the example this would result in 1. Now the third column of Table (3.1) can be calculated and an error can be calculated with each Δx .

Δx	Y	Error	Relative Error (%)
0.2	0.6	0.4	40
0.1	0.9	0.1	10
0.05	0.975	0.025	2.5
0.025	0.99375	0.00625	0.625
0	*1*	*0*	*0*

Table (3.1) Second order error test function

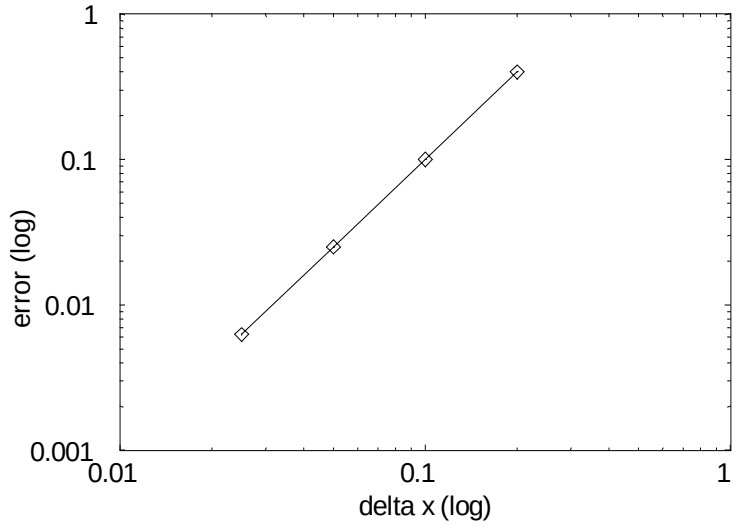

Figure (3.6) Second order log figure

In case of a second order behavior of the error the log(error) against log(Δx) should be a straight line with a slope of 2.0.

For an error that shows first order behavior:

Δx	Y	Error	Relative Error (%)
0.2	0.8	0.2	20
0.1	0.9	0.1	10
0.05	0.95	0.05	5
0.025	0.975	0.025	2.5
0	*1*	*0*	*0*

Table (3.2) First order error test function

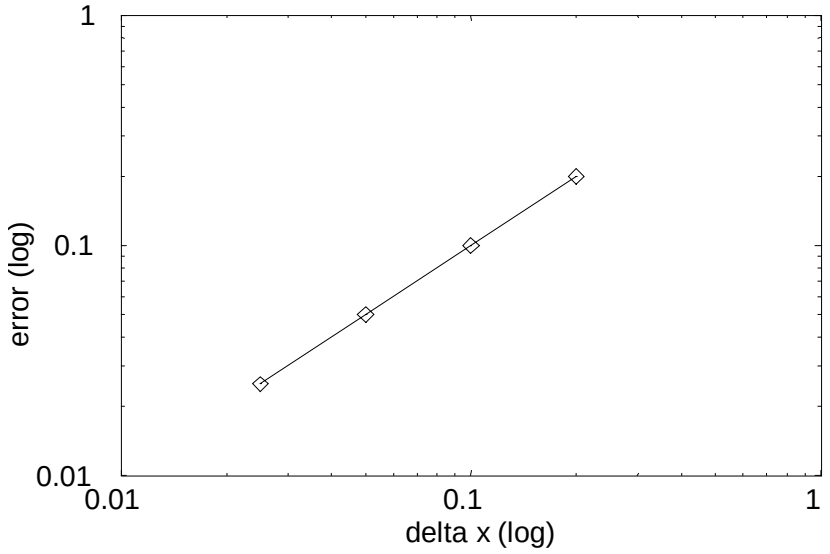

Figure (3.7) First order log figure

In case of a first order behavior of the error the log(error) against log(Δx) should be a straight line with a slope of 1.0.

The procedure mentioned above is analogous to the Richardson error estimate [13].

3.3.2 The convection-diffusion equation.

The convection-diffusion equation describes the transport of the sample through the flow injection system. In section 3.2 we only discussed the diffusion

mechanism. When convection is included special profiles have to be used to solve the equations. If we look at equation (2.27) and rewrite (while dropping the source term) this for a steady state one-dimensional convection-diffusion equation we get

$$\frac{d}{dx}(\rho u\phi) = \frac{d}{dx}(\Gamma\frac{d\phi}{dx}) \qquad \text{Equation (3.24)}$$

where u is the x component of the velocity, ϕ the dependent variable and Γ the diffusion coefficient. The symbols are different from those used in chapter two to indicate that this is a general equation and not limited to diffusion of a species. It could also be used for the heat equation and even for the momentum equation except for the pressure term.
Following the same process, outlined in the previous section, we integrate Equation (3.24) over the control-volume.

$$(\rho u\phi)_e - (\rho u\phi)_w = \left(\Gamma\frac{d\phi}{dx}\right)_e - \left(\Gamma\frac{d\phi}{dx}\right)_w \qquad \text{Equation (3.25)}$$

The different symbols and directions are given in Figure (3.1).
The piecewise-linear profile (also known as the central-difference scheme) is applied to both the diffusion term (see section 3.2.2.1) and the convection. The result for the convection is

$$\phi_e = \frac{1}{2}(\phi_E + \phi_P) \qquad and \qquad \phi_w = \frac{1}{2}(\phi_P + \phi_W) \qquad \text{Equation (3.26)}$$

where the factor ½ results from the assumption that the interfaces are midway between the grid points.

Equation (3.25) becomes

$$\frac{1}{2}(\rho u)_e(\phi_E + \phi_P) - \frac{1}{2}(\rho u)_w(\phi_P + \phi_W) = \left(\Gamma\frac{(\phi_E - \phi_P)}{\delta x}\right)_e - \left(\Gamma\frac{(\phi_P - \phi_W)}{\delta x}\right)_w \qquad \text{Equation (3.27)}$$

Rewriting this in the standard form :

$$a_P\phi_P = a_E\phi_E + a_W\phi_W \qquad \text{Equation (3.28)}$$

where

$a_E = D_E - F_E/2$,

$a_W = D_W + F_W/2$,

$a_P = a_E + a_W + (F_E - F_W)$

with $F \equiv \rho u$ and $D \equiv \frac{\Gamma}{\delta x}$.

The grid point cluster shown in Figure (3.1) is used, and the faces of the control-volume are assumed to be located midway between two grid points. Using the continuity equation we can see that in fact $a_P = a_E + a_W$.

A problem is that, under certain conditions, the solution to Equation (3.28) gives, with the central difference scheme for the convection, unrealistic results. This is dependent on the cell Péclet number (P=F/D).

To illustrate this a realistic example, for the situation in this thesis, is chosen:

D	=	$1*10^{-10}$	m^2/s
u	=	$1*10^{-4}$	m/s
ϕ_E	=	$1*10^{-4}$	kg/m^2s
ϕ_W	=	$2*10^{-4}$	kg/m^2s
δx	=	$10*10^{-6}$	m

Fe=Fw=	$998*1*10^{-4}$	=	0.0998 kg/m^2s
$D_e=D_w$=	$1*10^{-10}/10*10^{-6}$	=	$1*10^{-5}$ m/s

(P= F/D = 9980)

and a_E= -0.04989, a_W = 0.04991, a_P = $2*10^{-5}$ → ϕ_P = 0.2497

This would mean that ϕ_P lies outside the range specified by ϕ_E, ϕ_W and is an unrealistic result. The piecewise-linear profile is, in this case (convection dominant on cell level), clearly not the correct scheme to be used for the convection term. The central scheme could produce physically realistic solutions but at the cost of excessively fine grids and time steps. The solution for this problem is to adjust the profiles used in the derivation. This way solutions can be produced that give realistic results even on coarse grids.

Simpler schemes for this purpose are available [10].

3.3.2.1 Different profiles

The different schemes that can be used for solving the problems introduced by the convection term in Equation (3.24) all have in common that they try to construct a profile based on the underlying physics. The problem with the central scheme is that it calculates an average value for the convected property at a control-volume face on the basis of the neigbouring volumes. The simplest way to get a better model for the transport properties is to use an upwind scheme. In words such a scheme states that “the fluid does not know anything

about toward where it is flowing but carries the full legacy from where it is coming". Some of the schemes mentioned below use more points (upwind and/or downwind) to construct the profile. The advantage is that these schemes have a better accuracy (or higher order) at the other hand these higher order schemes sometimes lack stability.
To explain the different profiles used for calculation of the convection term in Equation (3.25), Figure (3.8) will be used. In this figure, P is the central point and the west side is defined as upwind. All the interfaces are assumed to be located midway between the different points.

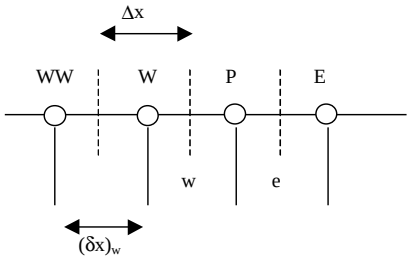

Figure (3.8) Grid point cluster for the convection term

The discussion for the different schemes is done for the west side (the upwind side), but of course a similar discussion can be held for the east side, if that was the upwind side.

The problem with the convection term focuses on the calculation of ϕ_w (the transported property at the w interface).

the "central" scheme

The central scheme was already used. The convection term at the west interface is calculated with

$$\phi_w = \frac{1}{2}(\phi_P + \phi_W) \qquad \text{Equation (3.29)}$$

The result from the example is ϕ_P = 0.2497.

the "upwind" scheme

The first profile used to tackle the problems with convection is the "upwind" scheme [14, 15, 16 and 17]. The diffusion term is left unchanged but the convection term is calculated according to

$$\phi_w = \phi_W \quad if \quad F_w > 0$$
$$and \qquad \text{Equation (3.30)}$$
$$\phi_w = \phi_P \quad if \quad F_w < 0$$

$$\phi_e = \phi_P \quad if \quad F_e > 0$$
$$and \qquad \text{Equation (3.31)}$$
$$\phi_e = \phi_E \quad if \quad F_e < 0$$

or in words

> "The value of ϕ at an interface is equal to the value of ϕ at the grid point on the 'upwind' side of the interface." (cit. [10])

This would mean for Equation (3.28) that

$$a_E = D_E + \max(-F_E, 0),$$
$$a_W = D_W + \max(F_W, 0),$$
$$a_P = a_E + a_W + (F_E - F_W)$$

with $F \equiv \rho u$ and $D \equiv \frac{\Gamma}{\delta x}$ and max(x,y) will return the greater of x and y.

If the example is worked out for this scheme ϕ_P, would be $2.0*10^{-4}$. Compared to the central difference scheme this result is realistic.

the "hybrid" scheme

The hybrid scheme [18] includes a modification of the upwind scheme. Central differencing is used if the mesh Péclet number ($P_e = \frac{(\rho u)_e (\delta x)_e}{\Gamma_e} = \frac{F_e}{D_e}$) is less then 2, and upwind differencing (of the convection term) if the mesh Péclet number is greater than 2.

This would mean for Equation (3.28) that

$$a_E = \max(-F_E, D_E - \frac{F_E}{2}, 0),$$
$$a_W = \max(F_W, D_W + \frac{F_W}{2}, 0),$$
$$a_P = a_E + a_W + (F_E - F_W)$$

with $F \equiv \rho u$ and $D \equiv \frac{\Gamma}{\delta x}$ and max(x,y,z) will return the greater of x, y and z.

If the example is worked out for this scheme ϕ_P, would be $2.0*10^{-4}$ (the Péclet number >> 2). Compared to the central difference scheme this result is realistic.

the "higher upwind" scheme

The "higher" upwind scheme uses two upwind points to calculate the value of ϕ at the interface [19] (w is upwind).

$$\phi_w = \frac{3}{2}\phi_W - \frac{1}{2}\phi_{WW} \qquad \text{Equation (3.32)}$$

the "QUICK" scheme

The "quick" scheme uses two upwind points and one downstream point to calculate the value of ϕ at the interface (w is upwind).

$$\phi_w = \frac{3}{8}\phi_P + \frac{3}{4}\phi_W - \frac{1}{8}\phi_{WW} \qquad \text{Equation (3.33)}$$

the "CCCT" scheme

The higher order upwind schemes can suffer from non-physical overshoots in their solutions. "CCCT" is a modification of the "quick" scheme eliminating these overshoots by restricting the extrapolation [21].

There are more schemes for solving the problems introduced by the convection term [20], but we will restrict ourselves to the five mentioned above.

The example used for some of the schemes is one-dimensional. The problem that has to be solved is however three-dimensional. For this purpose the schemes have to be investigated through three-dimensional calculations.

3.3.2.2 Different grid spacing

In general, an accurate solution is only obtained with a sufficiently fine grid. There are reasons for limiting the number of control-volumes (or grid points). The first is computer memory. All the information about the different control-volumes (concentration, velocity etc) takes up a fair amount of computer memory. For a three-dimensional calculation a doubling of the grid means 8

times the number of control-volumes and of course a lot of computer memory. It is clear that the total number of control-volumes is bound by an upper limit. The second reason for limiting the number of control-volumes is calculation time. More control-volumes mean more calculations to be performed and therefore a longer calculation time.

3.3.2.3 Different time steps

In the previous section(s), we neglected the effect of the time step size on the calculations of the response curve. We assumed that it was taken small enough to guarantee physical correct and accurate results. The black box method of checking if the time step size is small enough is to gradually decrease the time step size. When the response curve doesn't change significantly the correct time step size is reached.

3.3.2.4 Solving the convection-diffusion equation

For each dependent variable and for each control-volume an equation (Equation (3.28)) can be written down (where the velocity profile is fixed). These equations describe the influence on that particular variable in that control-volume of

1) other variables in the same cell; and
2) values of the same variable in neighbouring cells.
3) values of other variables in neighbouring cells.

There are several reasons for not solving the equations directly. The computational work would be excessive and the non-linearity of the underlying differential equations would be ignored (with the use of lineair solvers). Therefore, iteration is carried out at two levels. The inner level is used to solve the spatial coupling of each variable. The outer level solves the coupling of the various variables. Thus each variable is taken successively, regarding all other variables as fixed, a discrete 'transport' equation for that variable is formed for every control-volume in the flow domain and the problem is submitted to a linear solver which returns the updated values of the variable. The coupling of the original equations is simulated by reforming the coefficients of the discrete equations, using the most recently calculated values of the variables, for each outer iteration. [21]

To illustrate the previous section, consider the two following equations.

$$f(\phi_1) = a\phi_1^2 + b\phi_1 + c = 0 \qquad \text{Equation (3.34)}$$

$$g(\phi_2) = p\phi_2^2 + q\phi_2 + r = 0 \qquad \text{Equation (3.35)}$$

There are two dependent variables ϕ_1 and ϕ_2. The problem is now that the coefficients a, b and c are functions of ϕ_2 and p, q and r are functions of ϕ_1. The iteration scheme to solve this system of equations is given in Figure (3.9). The blocks where the two functions are solved are part of the inner level.

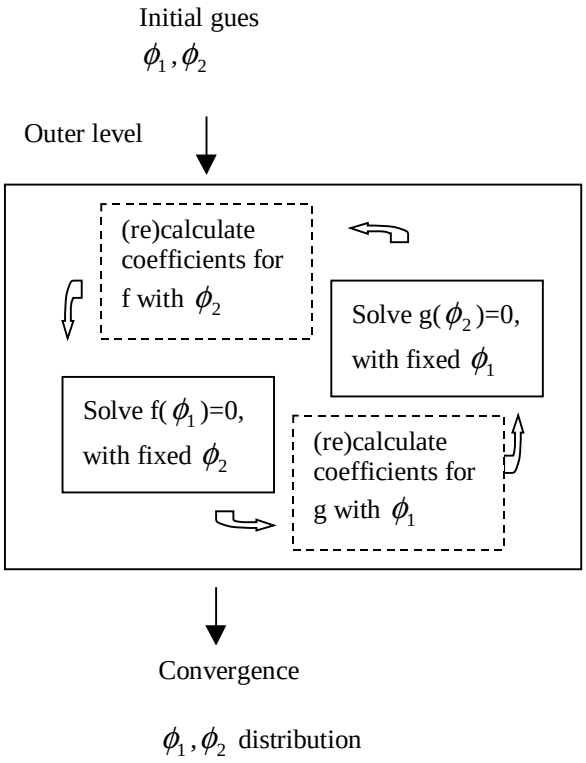

Figure (3.9) Iteration scheme

The solution to the discretization equations is found with so-called lineair equation solvers.

3.3.2.5 Linear equations solvers

A set of linear equations for a particular variable (for example ϕ_1 or ϕ_2), one equation for each control-volume, is passed to a simultaneous linear equations solver (the inner level). At this inner level an iterative solution method is used. There are several different solvers available : Line relaxation, preconditioned conjugate gradients (ICCG), full field Stone's method, algebraic multi-grid and a general version of the algebraic multi-grid method.
It is not in the scope of this thesis to explain these solvers. We refer to [21] for a detailed explanation of the different solvers.

3.3.2.6 The error in the sample transport calculations

As with the flow calculations there is a stopping error and a discretization error, but since the calculations are transient there is also an error that will result from the time stepping. The idea is to calculate each error while keeping the contribution of the other errors as small as possible.
The error introduced by the time stepping can best be established with an element length that is as small as possible. This way the discretization error is minimized. The time step can now be varied to obtain the order of the time stepping scheme and the error of the different calculations. There are two time stepping schemes: backward implicit (first order) and Crank-Nicolson (second order).

The discretization error (and order) should be obtained with a fixed time step. This time step should be as small as possible. This way the discretization error will be the dominant error. As with the flow calculations the discretization will be second order in space. The fact that the flow calculations at each grid also have a discretization error will influence the error behavior. The slope of the log-log figure should be higher than 2. The same procedure as with the flow calculation can be followed.

3.3.2.7 Decoupling the flow calculation from the convection-diffusion transport

The flow profile calculation can be done separately from the calculation of the transport of the sample. The idea behind this is to save time in calculating the response curve. In the decoupled situation the flow profile has to be calculated once and is used as a fixed profile in the convection-diffusion calculations. In the coupled case, the flow profile calculation must be done for each time step. After the first time steps, the flow profile should already be converged to a stable solution. After that, each time step a few iterations are used to update the flow field. The fact that each calculation consists of a considerable number of time steps results in a considerable increase in calculation time to solve the coupled problem. The assumption that decoupling is allowed, has to be checked.

3.3.2.8 The injection

The replacement of an injection simulation with inserting a sample plug in the channel could also save some valuable calculation time. In a flow system the sample is injected through a side channel. This is done by means of a so-called time based injection. The sample is injected for a certain time through the injection channel. During this injection we have convection and diffusion established by the (injection) inlet flow profile. After the injection, the sample still diffuses from the side channel into the main channel.

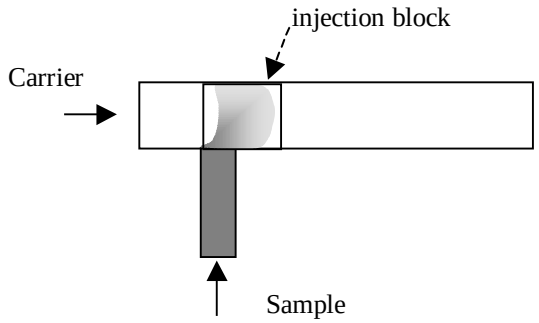

Figure (3.10) Time based injection

It is clear that this inserted plug is not the block shape we shall adopt in our block injection calculations, but an approximation Figure (3.10) shows an artist's impression of this phenomenon.

The simulation of the injection adds a step to the calculation:
- a simulation of the injection and subsequently
- the normal simulation of the transport through the main channel.

There are three ways to solve this combined problem.

1) The first method is to solve the injection and the transport directly in one process. This can be done by switching at a certain time the inlet velocities from injection to the carrier. In this case the flow and sample transport calculation should be solved at the same time. As far as the calculation is concerned this is the most expensive, but also the most accurate one.
2) The second method is to decouple the flow calculation from the convection-diffusion, and still solve the injection. This means that we would have to calculate two flow profiles. One calculation for the carrier and one for the injection. This should be done before the convection-diffusion calculations. Depending on the state (injection or carrier transport) one of the profiles should be selected. This is possible but we would prefer the third method.
3) This means that we set the injection block (an approximation) in combination with the decoupled carrier calculation (mentioned in 3.3.3). The length of the injection block would be calculated from the flow through the injection channel.

3.3.3 Calculating the flow and transport in our test system.

In chapter 2 we used a test system to show the basic working of convection and diffusion in a test system. This test system will now be used to investigate the different available options discussed in sections 3.2 and 3.3. In short, we are going to solve Navier Stokes equation in three-dimensions and transient for

our test micro system, used at the end of Chapter 2 . The flow rate and geometric sizes are given in Chapter 2 .

3.3.3.1 Calculation of the flow

An example of the residuals (of the flow calculation) for the three different velocities and the mass during the iteration process is shown in Figure (3.11). Only the mass and z-velocity have considerable residual values at the beginning of the calculation. This, of course, results from the fact that the velocity in the x and y direction is very small.

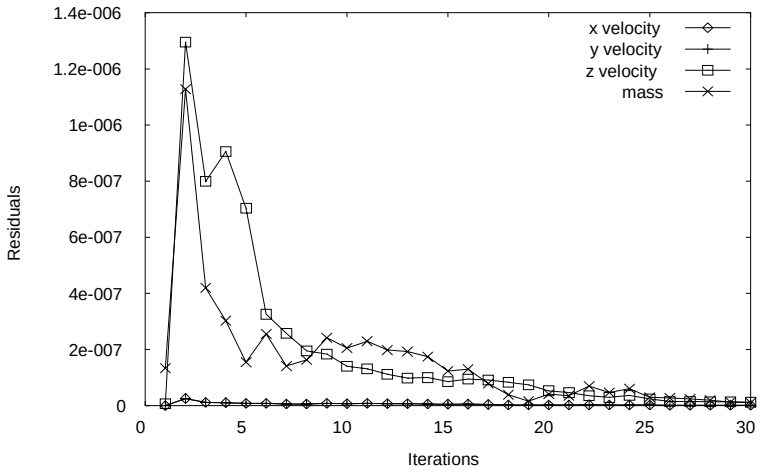

Figure (3.11) Residuals for a flow calculation

In section 3.3.1.4 the different errors were explained. In this section the maximum flow velocity (in the detection block) in the z direction was taken as the fixed parameter.

3.3.3.1.1 The convergence error

Figure (3.11) shows the residuals for the first 30 iterations. The relative convergence error versus the number of iterations is shown in Figure (3.12). The relative convergence error is defined as

$$relative\ convergence\ error = abs\left(\frac{m_{z,300} - m_{z,i}}{m_{z,300}}\right) * 100 \qquad \text{Equation (3.36)}$$

where m_z is the maximum velocity in the z direction in the detection block and 300 or i is the number of iterations.

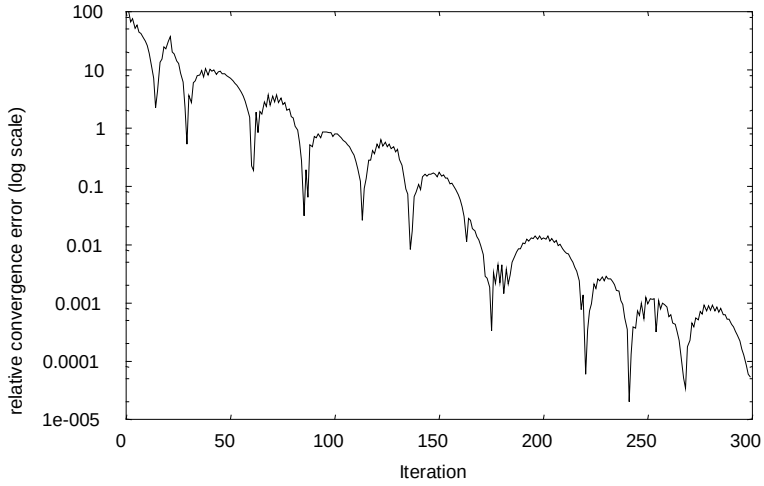

Figure (3.12) The convergence error for the flow calculation

After 100 iterations the relative error is less than 0.8 % and the residual value for the mass is $0.42*10^{-7}$. The element length in these calculations is 9.52 µm.

3.3.3.1.2 The discretization error

The maximum z velocity was calculated for different element lengths (EL). The iterations were done to machine level accuracy. Figure (3.13) shows the results. The points are the results from the flow calculations and the line is the result from a fitted function (see Equation (3.37)).

$$f(x) = 3.49720769*10^{-3} - 1.2610963510^{-7}\,x^2 \qquad R^2 = 0.999953 \qquad \text{Equation (3.37)}$$

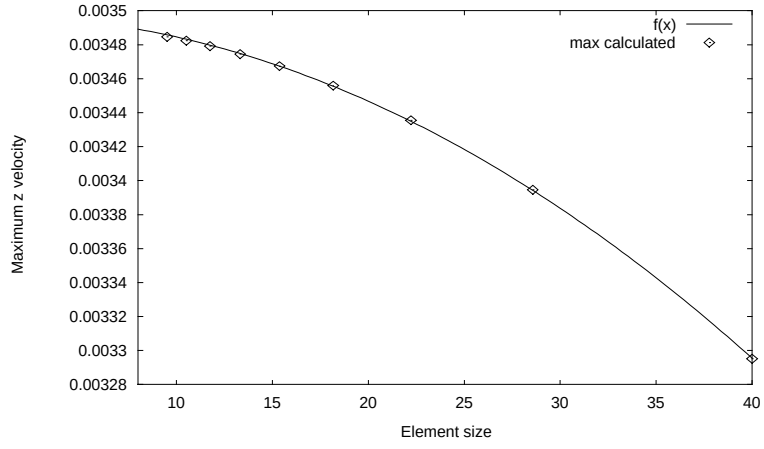

Figure (3.13) The maximum z velocity vs the element length

According to this fit-function the ‘true’ maximum z velocity in the detection block should be 0.0034972.

EL	Z velocity	Error	Rel Error (%)
40	0.32951150E-02	2.0209269e-4	5.78
28.57	0.33945430E-02	1.0266469e-4	2.94
22.22	0.34355444E-02	6.166329e-5	1.76
18.18	0.34559253E-02	4.128239e-5	1.18
15.38	0.34674017E-02	2.980599e-5	0.85
13.33	0.34744726E-02	2.273509e-5	0.65
11.76	0.34791159E-02	1.809179e-5	0.52
10.52	0.34823185E-02	1.488919e-5	0.43
9.52	0.34846193E-02	1.25884e-5	0.36
0	*0.34972000E-02*	*0*	*0*

Table (3.3) Flow error table

The relative error in the maximum z velocity in the detection block is less than 1 % if the element length is taken 15 or smaller. To check if the flow calculation is indeed second order in space the log from the element length vs the log from the error should result in a straight line with a slope of 2 (see Figure (3.14)). The slope in Figure (3.14) is 1.93.

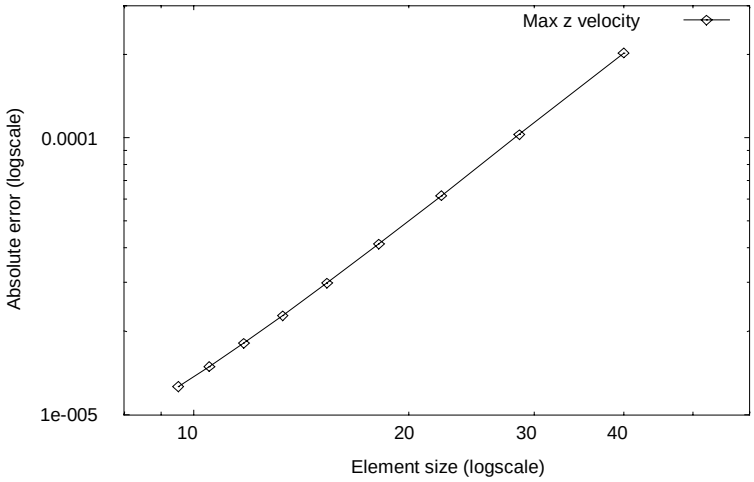

Figure (3.14) The EL vs error (logscale) for the flow calculation

3.3.3.2 Calculation of the sample transport.

For the next section all the iterations were done until machine accuracy. (For the convergence error see the end of this section)

3.3.3.2.1 The error in the sample transport calculation

In section 3.3.3.2.2 the effect of the different convection profiles will be investigated. In this section the 'quick' scheme is used for the convection term.

The error introduced by the time stepping scheme

To minimize the discretization error the grid with an element length of 9.52 was used (see section 3.3.1.4.2). The error in the flow calculations was 0.36 % (for the maximum z velocity in the detection block) so the flow is taken as the correct flow. The (first) maximum value (peak height) of the response curve was taken as the fixed parameter. Since it is possible to calculate the peak height for very small time steps, the peak height calculated with a time step of 0.001 second was taken as the 'true' solution.

Cranck-Nicolson

Δt (s)	Peak height (*1e^{-4})	Error	Relative Error (%)
0.5	1.32848159	5.52795e-5	29.4
0.1	2.03759482	1.56318e-5	8.3
0.05	1.94529304	6.40417e-6	3.4
0.04	1.91784857	3.65722e-6	1.9
0.03	1.88921810	7.94170e-7	0.42
0.02	1.88541642	7.14002e-7	0.38
0.01	1.88268372	1.40732e-7	0.07
0.001	*1.88127640*	*0*	*0*

Table (3.4) The time step error with Crank-Nicolson scheme

From Table (3.4) it can be seen that a time step of 0.01 produces a peak height with a relative error of 0.07 %. This will be small enough for investigation of the discretization error independent of the time step. The slope (see Figure (3.15)), (log(1.56e-5)-log(1.407e-7))/ (log(0.1)-log(0.01)), is 2.05.

Backward fully implicit

Δt (s)	Peak height ($*1e^{-4}$)	Error	Relative Error (%)
0.5	1.15757793	7.29253e-5	38.6
0.1	1.45779311	4.29037e-5	22.7
0.05	1.58090828	3.05922e-5	16.2
0.04	1.61614298	2.70687e-5	14.3
0.03	1.65771096	2.29119e-5	12.1
0.02	1.70876679	1.78064e-5	9.44
0.01	1.77629844	1.10532e-5	5.86
0.001	*1.88683044*	*0*	*0*

Table (3.5) The time step error with backward fully implicit scheme

From Table (3.5) it can be seen that the backward fully implicit scheme performs a lot worse than the Crank-Nicolson scheme. The slope (see Figure (3.15)), (log(4.29e-5)-log(1.105e-7) / (log(0.1)-log(0.01)) is 0.59.

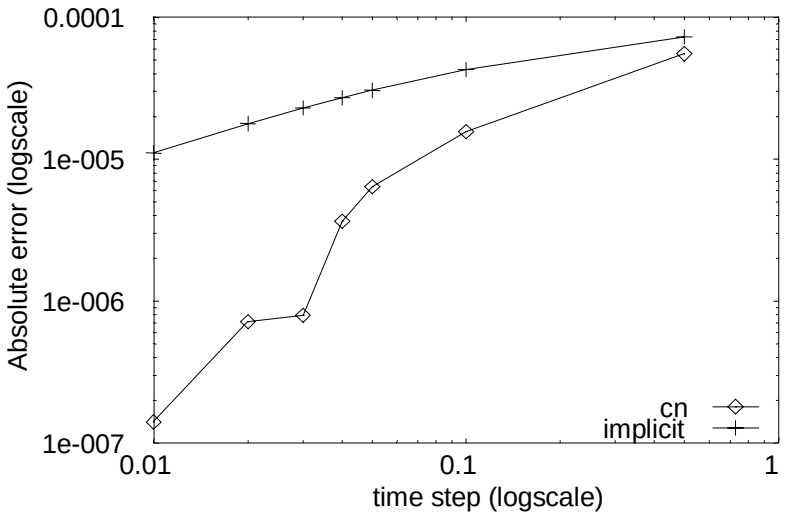

Figure (3.15) log figure for the backward implicit and CN scheme

The discretization error

To investigate the discretization error the Crank-Nicolson scheme is used with a time step of 0.01. The results for the different element lengths are shown in Table (3.6). The results do not follow (nicely) a second order function. For this reason the estimate of the 'true' value is difficult. In this case the peak height with an element length of 9.52 μm was taken as the 'true' solution.
From Table (3.6) we can see that the relative error in the peak height is smaller than 0.5% when the element length is smaller than 15 μm.

Δx (μm)	Peak height ($*1e^{-4}$)	Relative Error	Relative Error (%)
40	2.343568	4.60884E-05	24.5
28.57	1.988173	1.05489E-05	5.60
22.22	1.906773	2.40895E-06	1.28
18.18	1.898649	1.59653E-06	0.85
15.38	1.880346	2.33806E-07	0.124
13.33	1.888734	6.05054E-07	0.321
11.76	1.884949	2.26515E-07	0.120
10.52	1.883397	7.12898E-08	0.038
9.52	1.882684	*0.0*	*0.0*

Table (3.6) Discretization error in the sample transport

Since all the profiles used are second order or higher the slope in the log-log figure should be 2.0, with a decreasing element length. The slope is 4.85 (see Figure (3.16)).

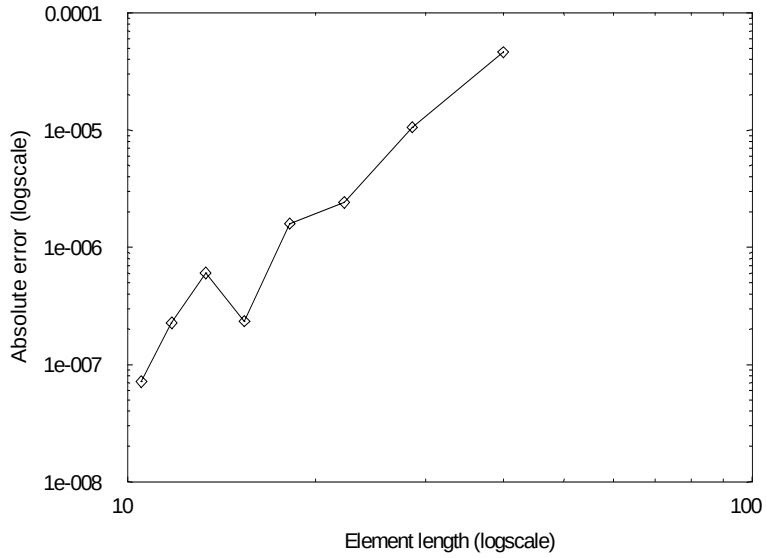

Figure (3.16) The EL vs error (logscale) for the sample transport calculation

The reason for this is that the influence of the flow calculation with the different element lengths is contributing to the faster decrease of the error. Ideal, for investigating the sample transport error, independent of the flow, would be to use the flow calculations from the finest grid in the coarser grid calculations. This is not necessary for the determination of the discretization error.

The convergence error

Until now the iterations were carried out until machine accuracy. Now that the 'true' solution is known the effect of the residual limit can be studied.
Since we are solving the convection-diffusion equation, only for one sample the convergence has to be checked against the source residual of this sample, for each time step.

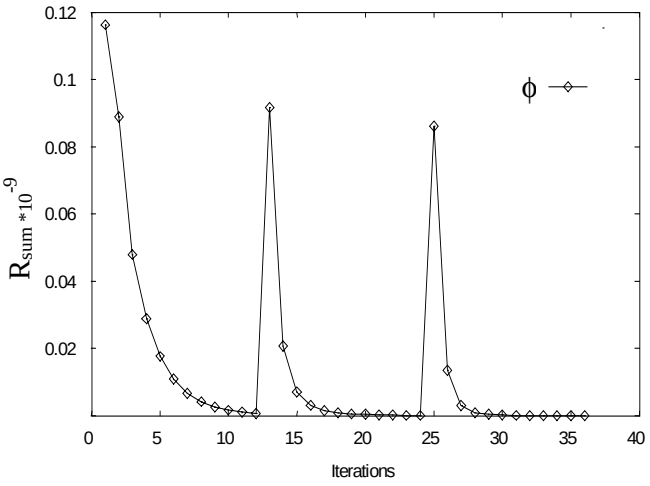

Figure (3.17) Convergence of ϕ for the first three time steps

The data needed to produce Figure (3.17) was taken from the calculation of the test micro flow system in chapter 2. The first three time steps, for the transport of ϕ (the sample), are shown. The stop criterion is 12 iterations or a (in this case) R_{sum} mass below $1*10^{-15}$, which ever is reached first. After one of these conditions is true the solution doesn't change significantly. In Figure (3.17) in each of the three time steps the maximum number of iterations was reached. This final unchanging state is called the convergence of the iteration. The converged solution is actually the correct solution to the equation. Although it is arrived at by the methods for solving linear equations, the iteration scheme accounts for (possible) non-linearity of the equation.

The limiting number of iterations can be set to 300 (a high value) and the R_{sum} must be applied to establish the number of iterations at each time step.

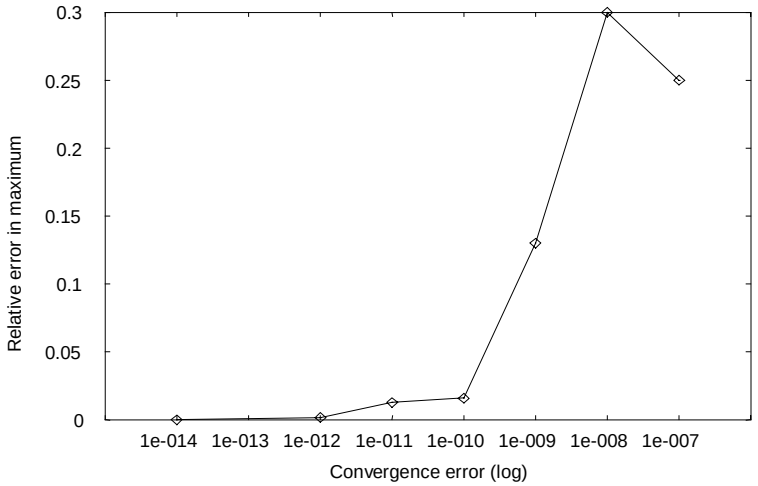

Figure (3.18) Convergence error

Figure (3.18) shows the convergence error as a function of the relative error (according to Equation (3.36)). When the R_{sum} is set to a value less then 1e-10 there are fluctuations around the (base) signal. The lower the R_{sum} the larger the fluctuations. The values larger than 1e-7 produce a non-converged solution. As mentioned before the R_{sum} value is problem dependent. From Figure (3.18) the conclusion can be drawn that a R_{sum} value of 1e-12 should give optimal results in this test case. A value of 1e-15 should suffice as R_{sum} in all of the problems calculated in this thesis.

3.3.3.2.2 Different convection profiles

We shall now discuss the different schemes used in the calculation of the sample transport and the assumption that we are allowed to decouple the flow and sample concentration calculation at a later stage. For the moment, the flow profile is assumed given and the decoupling is assumed valid.
First we will take a look at the convergence of the different schemes, introduced in section 3.3.1.2, at the first time step, which is taken relatively large. Figure (3.19) shows the sum of residuals (R_{sum}), over the whole domain, of ϕ for the first ten iterations for the convection-diffusion transport in our test system.

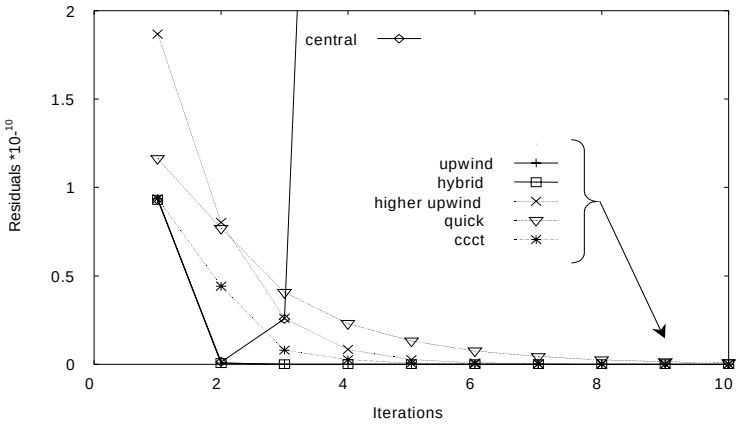

Figure (3.19) Residuals for the different schemes and the first time step (0.5 s)

The R_{sum} for the central differencing scheme decreases with the second iteration, but after that it increases and becomes very large. Indeed, if we look at the simulation results we can conclude that the solution is unrealistic. The concentrations, seen at the detector, are out of bound. We see, for example, a concentration of $1*10^{23}$ mol/l and this is clearly impossible. The central scheme could be used in such a calculation but the time step should be adjusted. Figure (3.20) shows what happens to the R_{sum} if the time step is taken smaller. Only for the time steps of 0.02 and 0.01 seconds, the solution seems to converge for the first time step.

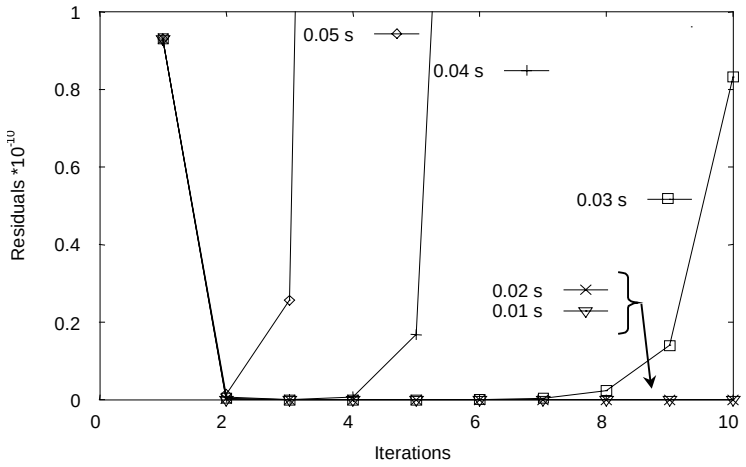

Figure (3.20) Different time steps for the central scheme

The trend in Figure (3.20) is that after more iterations the solution becomes unstable, despite the smaller time step. So the central differencing scheme is not recommended for the convection term in Equation (3.24).

All the other schemes presented in Figure (3.19) seem to be converged after 10 iterations. In Figure (3.21) the calculated response curves for the different convection schemes are shown.

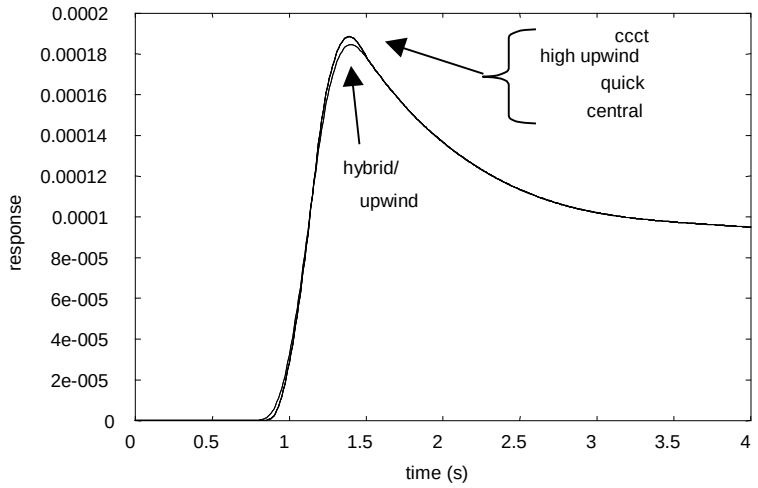

Figure (3.21) Response curves for the different convection schemes

From this figure it can be seen that for this example there is not much difference between the various schemes, except for the upwind and hybrid scheme. The results can be subdivided in two groups.

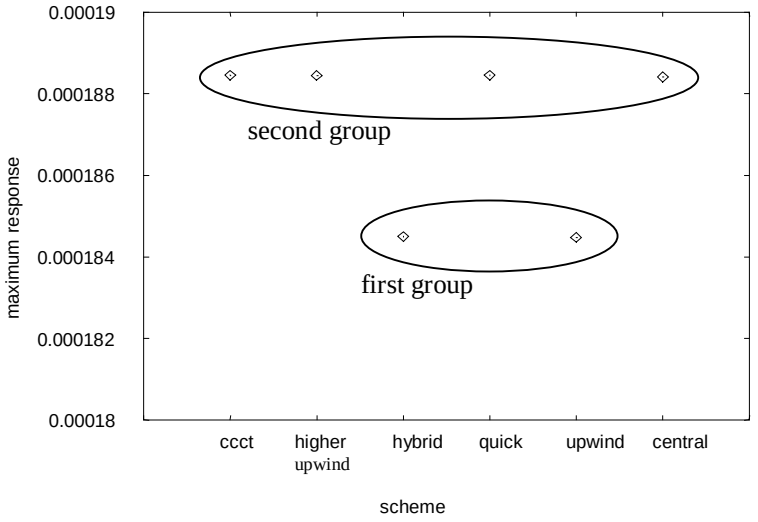

Figure (3.22) Peak heights for the different convection schemes

The first group contains the upwind and hybrid scheme. The second group contains the higher order upwind schemes and the central scheme. According to literature the higher order upwind schemes should give better results than the first order upwind schemes. The disadvantage is that they can produce a physical overshoot. Figure (3.23) shows that the higher upwind schemes can give negative results at the beginning of the peak with a ‘larger’ time step. The quick and ccct scheme also produce negative values but these are

considerably smaller. The results of the latter two schemes are exactly the same. In Figure (3.23) the time step is 0.05 seconds with the backward implicit time scheme, the negative values disappear with a time step of 0.01 seconds.

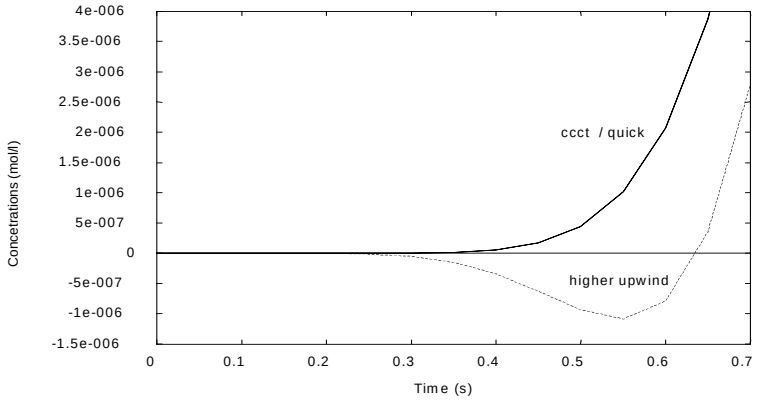

Figure (3.23) Physical overshoot of higher order upwind schemes

The central scheme can become unstable with a larger time step (or not dense enough grid). The logical choice would be one of the higher upwind schemes, for example quick.

3.3.3.2.3 Different grid spacing

In section 3.3.1.4 and section 3.3.2.6 the need for a dense grid was explained. The number of elements that can be used is limited. Figure (3.24) shows the relation between the number of elements in the error calculations and the element length.

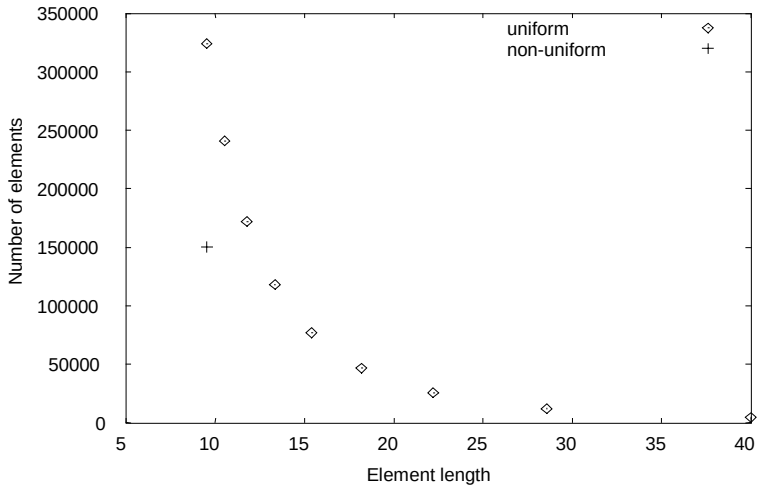

Figure (3.24) Number of elements vs element length

It can be seen from the uniform points (uniform grid) that the number of control-volumes needed indeed increases with a factor 8, each time the element length is divided by 2.

The second thing that increases, with a decrease in element length, is the calculation time. Figure (3.25) shows the calculation time (for the sample) versus the element length. We see a substantial increase of calculation time with a smaller element length.

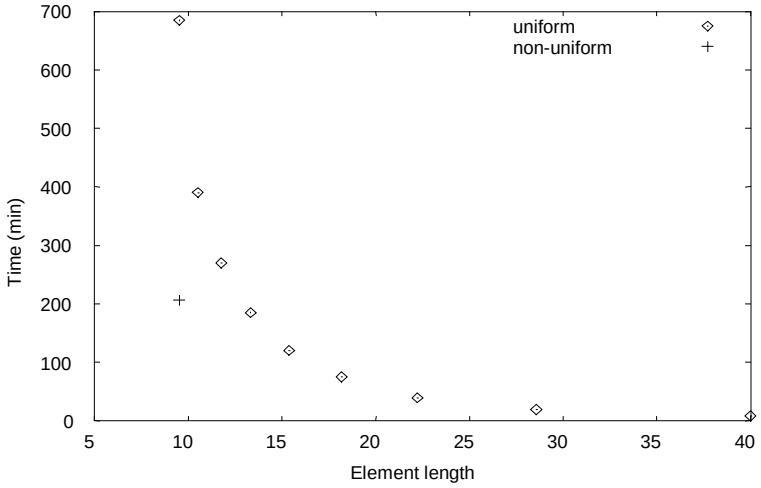

Figure (3.25) Calculation time vs element length

If we need more grid resolution, and don't have that much memory or time, the solution could be the use a non-uniform grid. The guiding principle is, that there is no need to employ a fine grid in regions where the dependent variable ϕ changes rather slowly with the independent variable (x, y or z).

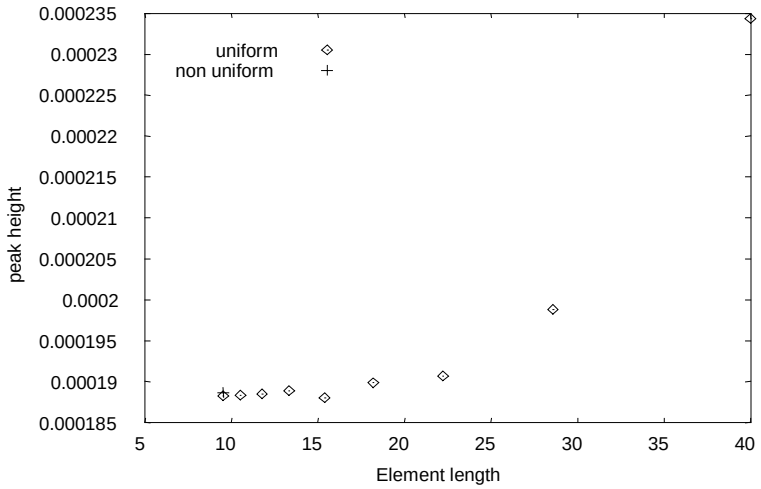

Figure (3.26) Peak height vs element length

On the other hand, a fine grid is required where the $\phi \sim x$ variation is steep. Non-uniform grid spacing can be used to minimize the control-volumes needed in solving a problem. In our test flow system, the variation around the injection block would be the steepest. A non-uniform grid, with an element length of 9.52 μm at the steepest variation, was made and the problem was calculated again.

In Figure (3.24) and Figure (3.25), we can see that this method saves memory and time. In Figure (3.26) it can be seen that this reduction is without significant loss in accuracy.

3.3.3.3 Decoupling of the flow from the sample transport.

Up till now the assumption was made, that we could decouple the flow calculation from the convection-diffusion transport of the sample. To check this assumption two response curves were calculated. One with the flow profile calculation decoupled from the convection-diffusion calculation and one where they were solved as a coupled system.
With the use of the fixed flow profile (residuals in Figure (3.11)) the convection-diffusion was solved for our test system (quick scheme) and the backward implicit time scheme and a time step of 0.05 seconds. The decoupled calculation took 3 hours and 22 minutes.
A coupled calculation was also done with the “quick” scheme and the backward implicit time scheme with a time step of 0.05 seconds. It took 11 hours and 25 minutes. The results are virtually the same. Figure (3.27) shows part of the response curve for both cases. Only in a small range minor differences between the two can be observed. If the full range was taken into account they would be indistinguishable.

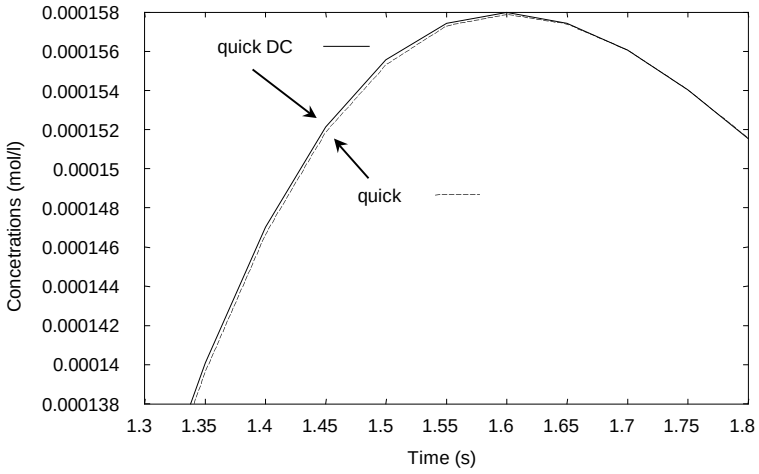

Figure (3.27) Coupled versus decoupled

3.3.3.4 The injection

The difference between options 1 and 3 mentioned in section 3.3.2.8 are shown in Figure (3.28). Option 1 is the calculation of the injection and sample transport in one process. Option 3 is the use of the injection block and a decoupled flow and sample transport calculation. The time scheme used is Cranck-Nicolson with a time step of 0.01 second and a QUICK differencing scheme for the convection terms. The (coupled) injection reaches the detection earlier and in Figure (3.28) we see that after 20 seconds the concentration at the detector is a bit higher compared to the decoupled calculation.

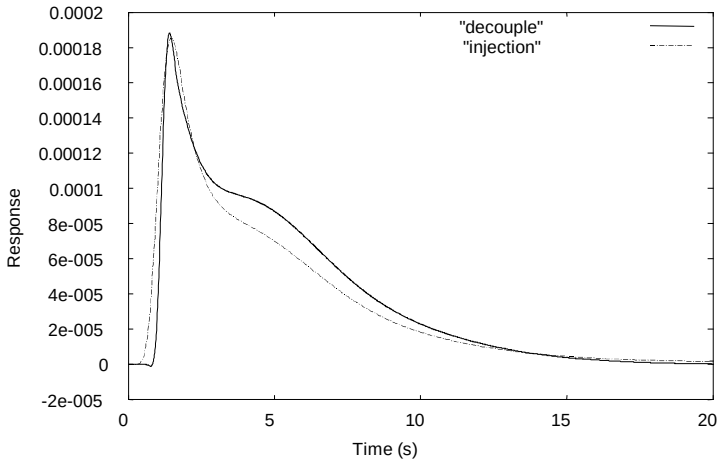

Figure (3.28) Coupled injection vs block injection

Figure (3.29) shows different slices of the sample transport during the injection. Between each picture is a time period of two seconds (0, 2, 4, 6, 8, 10, 12, 14, 16, 18 and 20 seconds). It should be remembered that these pictures show a distorted view caused by the scaling.

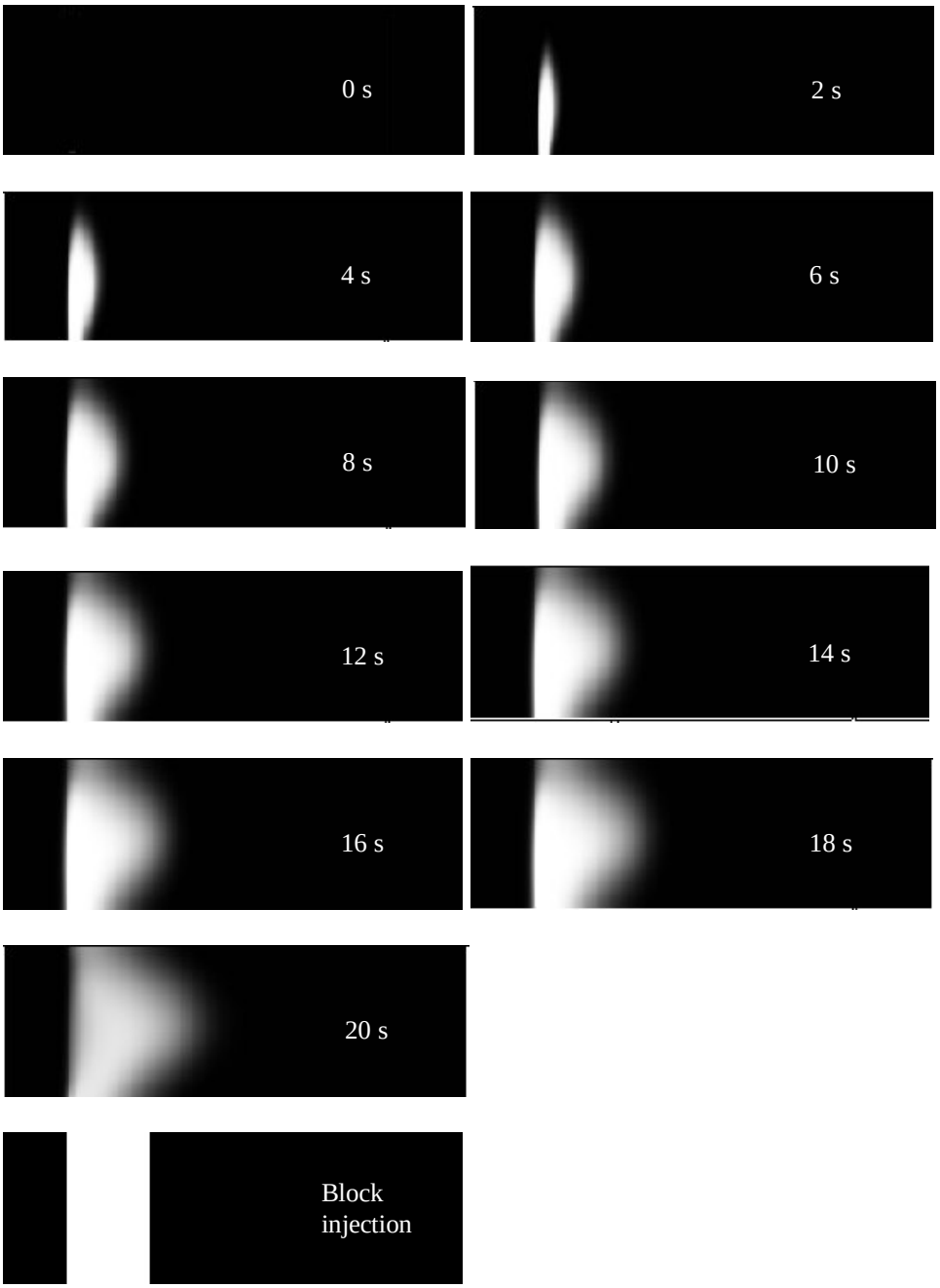

Figure (3.29) Different slices of the injection

At the end of the injection period (20 s), the left side of the injected plug is straight and the right side is parabolic. The last picture is the injected block. This is the block that is used in the decoupled case.

Figure (3.30) shows the carrier transport after 21, 22 and 23 seconds.

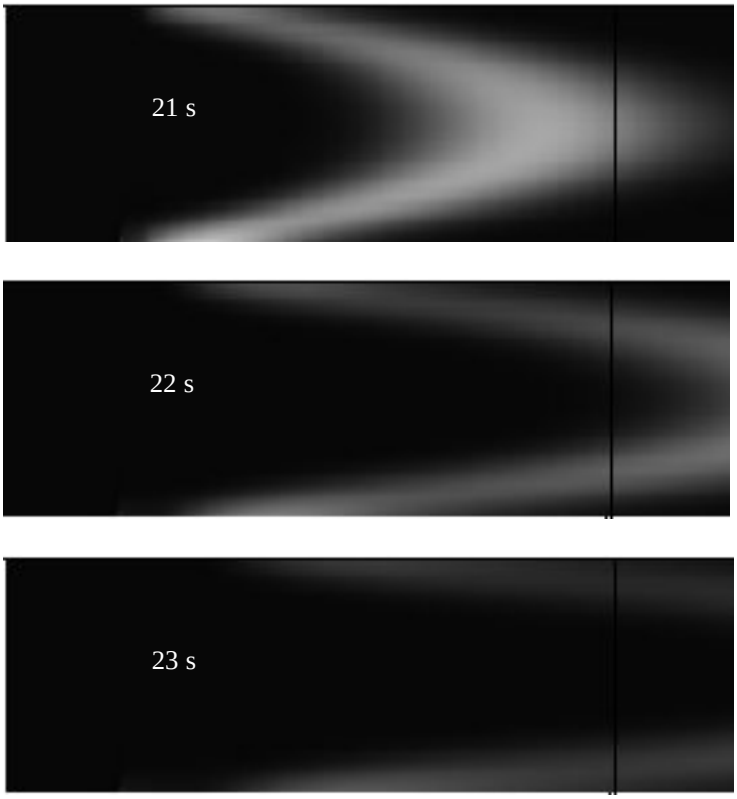

Figure (3.30) Different slice of the carrier transport

The last two pictures in Figure (3.29) explain the differences in the response curves made for both situations. The picture at 20 seconds shows a parabolic profile that should reach the detector earlier than the defined block. The response curve for the case with simulation of injection shows a peak that arrives a bit earlier (than the block injection) at the detector and returns quicker to the base line (the zero concentration line) but it doesn't reach it. Through diffusion from the injection channel, a small concentration of sample introduces a longer tail.

3.4 Conclusions

In this chapter, an introduction was given on how to solve a fluid dynamics problem by means of numerical computation. The terms discretization methods and discretization equations were introduced. Two examples explained the two terms, and introduced boundary points and time stepping. The problems with solving the convection-diffusion equation were explained. The problems with the convection term can best be solved by the use of the "quick" or "ccct" scheme. The element length of a control-volume, in the neighbourhood of a steep variation of the dependent variable with one of the space coordinates, should be smaller than 15 μm.

The largest time step that produces realistic and accurate results, in this test example, is about 0.01 second. The best time stepping scheme for this test case was Crank-Nicolson.
The application of a non-uniform grid was recommended to solve the problem, because it saves considerable calculation time and does not result in an excessive amount of memory needed. A well constructed non-uniform grid can give the same accuracy as a uniform grid.
To further save calculation time, it was shown that it is allowed to decouple the flow calculation from the convection-diffusion calculation. Further more it could be seen that the time based injection can be replaced with an injection block. This procedure allows elimination of the injection calculation, thereby reducing also the calculation time.

3.5 References

[1] H. Rouse, S. Ince, 'History of hydraulics', Dover Publ.,1963
[2] G.I. Taylor, ' Disperson of Soluble Matter in Solvent Flowing Slowly through a Tube' ,Proc. Roy. Soc., London, 219 A (1953) 186
[3] R. Aris, 'On the dispersion of Solute in a Fluid in laminar Flow Through a Tube', Proc. Roy. Soc.,London, 235 A(1956)67
[4] H.R. Bayley, W.B. Gogarty, 'Numerical and Experimental Results on the Dispersion of a Solute in a Fluid in Laminar Flow Through a Tube', Proc. Roy. Soc., London, 269 A(1962)352
[5] V. Ananthakrishnan, W.N. Gill, A.J. Barduhn, AIChE J., 11(1965)1063
[6] W.N. Gill, V. Ananthakrisnan, 'Laminar Dispersion in Capillaries : Part IV. The Slug Stimulus', AIChe J., 13(1967)801
[7] C.C. Painton, H.A. Mottola, 'Dispersion in Continuous-Flow Sample Processing', ACA, 154(1983)1-16
[8] J.T. Vanderslice, A.G. Rosenfeld, G.R. Beecher, 'Laminar-Flow Bolus Shapes in Flow Injection Analysis', ACA, 179(1986)119-129
[9] S.D. Kolev, E. Pungor, 'Mathematical Modeling of Single-Line Flow-Injection Analysis Systems without Chemical Reaction', Anal. Chem. 60(1988)1700-1709
[10] S.V. Patankar, 'Numerical Heat Transfer and Fluid flow', Hemisphere, 1980
[11] J.C. Tannehill, D.A. Anderson, R.H. Pletcher, 'Computational Fluid Mechanics and Heat Transfer', Taylor & Francis, 1997
[12] S.V. Patankar, D. K. Baliga, 'A New Finite Difference Scheme for Parabolic Differential Equations', Num. Heat Transfer, 1(1978)27
[13] M. Lesieur, P. Comte, J. Zinn-Justin, (editors) "computational fluid dynamics", Les Houches 1993, Elsevier Science B.V., Amsterdam

[14] R. Courant, E. Isaacson, M. Rees, ‘On the Solution of Non-Linear Hyperbolic Differential Equations by Finite Differences’, Comm. Pure Appl. Math., 5(1952)243
[15] R.A. Gentry, R.E. Martin,B. J. Dalby, ‘An Eulerian Differencing Method for Unsteady Compressible Flow Problems’, J. Phys., 1(1966)87
[16] H.Z. Barakat, J.A. Clark, ‘Analytical an Experimental Study of Transient Laminar Natural Convection Flows in Partially Filled Containers’, Proc 3d Int. Heat Transfer Conf. Chicago, 2(1966)152
[17] A.K. Runchal, M. Wolfshtein, ‘Numerical Integration Procedure for the Steady State Navier-Stokes Equations, J. Mech. Eng. Sci., 11(1969)445
[18] D.B. Spalding, ‘A Novel Finite Difference Formulation for Differential Expressions Involving Both First and Second Derivatives’, Int. J. Num. Methods Eng., 4(1972)551-559
[19] C.P. Thompson, N.S. Wilkes, ‘Experiments with Higher-Order Finite Difference Formulae’, 1982, AERE-R 10493
[20] J.H. Alderton, N.S. Wilkes, ‘Some applications of new finite difference schemes for fluid flow problems, 1988, AERE-R 13234
[21] AEA technology, ‘CFX 4.2 : solver manual’, 1997

Chapter 4

The effect of different basic building blocks of a micro flow system on the dispersion of a sample[#]

4.1 Introduction

Miniaturization of a normal Flow Injection Analysis-System (FIA-System) has a number of great advantages. The most important ones are: economy of material consumption, high efficiency of radial mixing in conduits of sub millimeter dimensions, portability and speed of analysis [1].
With the current micro fabrication technologies it is possible to construct a manifold with a volume of a few micro liter, which is a thousand fold volume reduction compared to a normal FIA manifold. The construction and development of such a micro-FIA system is, at this moment, expensive and time consuming. Some general design rules would be very useful in the development of a micro-FIA system. The use of numerical simulations could be helpful in developing these rules and speedup the development of such a system in general.
The research, found in the literature, about numerical modeling of the dispersion of a dye injected in a carrier stream flowing through micro manifolds isn't very extensive. Although a lot of research is done in the field of CFD (Computational Fluid Dynamics), the modeling done in the field of Flow Injection Analysis (FIA) is restricted to straight macro-tubes [2,3], as was mentioned in chapter 3. A lot has been written about the construction of µ-devices [4] but numerical modeling and experimental validation of micro manifolds is still in its infancy. It seems that CFD is a valid technique to model accurately the fluid dynamics within complex microstructures down to a scale of 25 µm [5]. At this moment several CFD-packages are commercially available for modeling fluid dynamics. The numerical modeling in this chapter is done with the commercially available CFX-F3D suite version 4.1 from AEA (originally FLOW3D).
The basic idea of this chapter is to validate the numerical modeling of the basic structures in micro scale manifolds with experimental results. In this way the numerical results obtained for the simulated micro manifolds can help to optimize a micro-FIA system without the earlier mentioned drawbacks of developing a micro-FIA system experimentally. The numerical model (used in

[#] Published in Analytica Chemica Acta, ACA 373(1998)227-239

this chapter and explained in chapter 3) provides advantages compared to the equations used in FIA to predict the dispersion. These advantages are: an arbitrary manifold can be used, the flow profile is available, the pressure distribution is available and the concentration distribution of the sample throughout the channel is available (all three-dimensional time-dependent). The trial and error approach of developing a (micro) FIA system could be replaced by a numerical pre-analysis of the problem and the fluid dynamics involved.

To study the transport of the injected sample, five structures have been constructed (See Figure (4.1)).

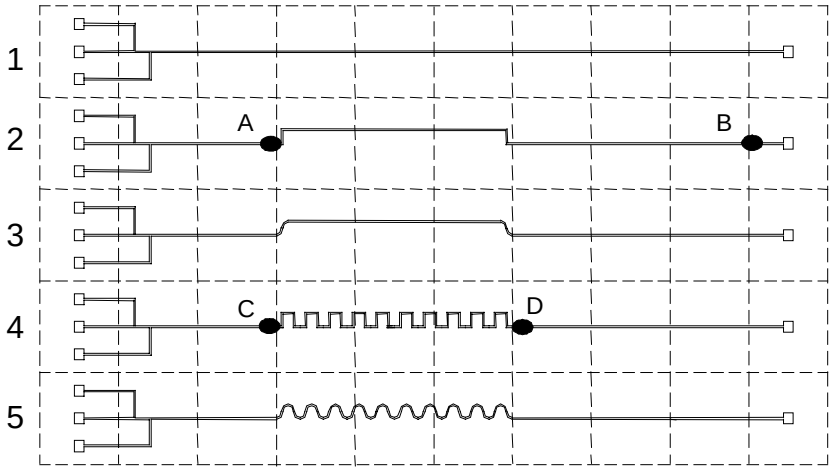

Figure (4.1) The five manifolds. One grid block is 5 mm by 5 mm. The channels have a 200 µm by 200 µm cross-section. A, B, C and D show the different measurements points.

In the geometry of these structures the basic elements, from which micro manifolds can be built, were represented, i.e. curved and straight bends.

4.2 Theory

The dynamic behavior of fluids can be modeled with the Navier-Stokes equations. Knowledge about of the flow regime can simplify the work to get an accurate solution of the fluid dynamics problem. The fluids used in this thesis are incompressible, the fluid density is constant, and the assumption was made that all the cases studied were in the laminar flow regime at 20 °C. The assessment of the prevailing type of flow regime can be based on the Reynolds number [6].

$$\mathrm{Re} = \frac{U * l}{\nu} \qquad \text{Equation (4.1)}$$

where Re is the dimensionless Reynolds number, U the velocity of the fluid, l the characteristic length for the flow under consideration (diameter of the

channel) and ν the kinematic viscosity. The flows in this thesis have a Reynolds number of less then 2.0. This places them well into the laminar flow region [7]. The basic mathematical model equations for fluid dynamics (fluid flow and mass transfer) were given in chapter two. Specified with the previous assumptions in mind :

Continuity equation

$$\nabla \cdot (U) = 0$$ Equation (2.23)/Equation (4.2)

Momentum equation

$$\frac{\partial U}{\partial t} = -(U \cdot \nabla)U - \frac{1}{\rho}\nabla P + \nu \nabla^2 U$$ Equation (2.25)/Equation (4.3)

Scalar equation

$$\frac{\partial \phi}{\partial t} + \nabla(U\phi - D_\phi \nabla \phi) = \frac{S}{\rho}$$ Equation (4.4)

where t, is time, ρ is the mass density, U the velocity of the fluid, P the pressure and ν the kinematic viscosity of the fluid and D_ϕ the diffusion coefficient of the sample. In this paper the scalar ϕ represents the concentration of the sample in the system and S represents the concentration of the sample at the injection point at the beginning of the simulation (this value is provided by the user: user source).
The full set Navier Stokes equations contains several other equations but in particular the three equations mentioned above are important for the modeling of an incompressible fluid with mass transfer (no heat transfer). Equation (4.4) is also known as the convection-diffusion equation.
The general Navier Stokes equations are valid for laminar and turbulent flow. Turbulent flows are just very complex unsteady laminar flows. Usually flows with high Reynolds numbers are solved with special turbulent models [8]. In this thesis no such special models are necessary.

4.2.1 Moment analysis

To study the dispersion of a dye injected in a carrier stream flowing through micro manifolds, the following procedure is adopted. At the beginning of a micro manifold a sample is introduced (as a finite volume) into a carrier stream. The sample travels through the system undergoing dispersion. Along the flow systems detection points can be setup where the sample concentration can be recorded as a function of time. Such a recording results in a response curve. The shape of this response curve can be characterized with the use of moment analysis.

The formulae to describe the moments:

General moment

$$M_p = \int_{-\infty}^{\infty} F(t) * t^p \, dt \qquad \text{Equation (4.5)}$$

Normalized moment

$$m_p = \frac{M_p}{M_0} \qquad \text{Equation (4.6)}$$

Centralized (and normalized) moment

$$u_p = \frac{1}{M_0} \int_{-\infty}^{\infty} F(t) * (t - m_1)^p \, dt \qquad \text{Equation (4.7)}$$

where F(t) represents the response curve. The zero-th moment (M_0) represents the peak area. The first moment (m_1) represents the center of gravity of the response curve (or the residence time). The second moment (u_2) represents the variance of the response curve.
Moments higher than the zero-th one are normalized (the normalized zero-th moment will always be 1) (see Equation (4.6)). Normalized moments are given a small letter m_p. Moment higher than the first moment are also centralized (see Equation (4.7)). Normalized and centralized moments are described by the symbol u_p.

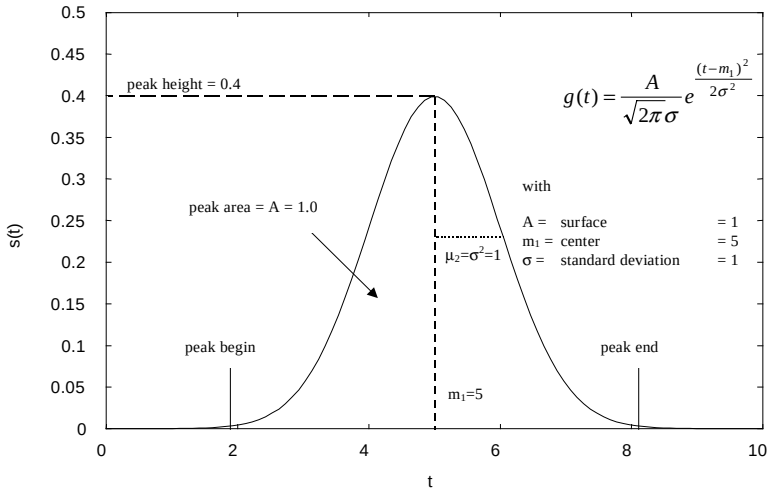

Figure (4.2) Graphical representation of the moments

A peak can be described by M_0, m_1 and u_2. The higher moments can also contain interesting information, but these higher moments become also more inaccurate. Since the value of the zero-th moment (the surface, M_0) is used in the calculations of the higher moments, an error in M_0 results in inaccurate higher moments.

Figure (4.2) shows the moments for a gaussian curve.

To generate Figure (4.2) Equation (4.8) was used. The factor A represents the surface area and was defined as 1.0. The center of gravity was defined as 5 and the standard deviation was defined as 1.0.

$$s(t) = \frac{A}{\sqrt{2\pi}\sigma} e^{\frac{(t-m_1)^2}{2\sigma^2}} \qquad \text{Equation (4.8)}$$

From Equation (4.5) can be concluded that values that have a ‘great’ distance from m_1 contribute significantly to the calculation of u_2. In experimental curves there is always noise present. The contribution of noise (far from the center of the curve) would influence the calculation of the moments. For this reason it is necessary to integrate the moment equations only over a certain peak area. This means that a peak begin and a peak end have to be determined (see Figure (4.2)).

4.2.2 Deconvolution

The method to compare the numerical and experimental results was based on deconvolution. The advantage of this method is that the results are independent of the injected sample volume. Response curves measured before and after the structure under consideration were taken and a transfer curve was calculated using deconvolution [9] together with the Hunt filter [10] to decrease the effect of noise on the determination of the transfer curve. The mathematical procedure can be depicted as follows [11]:

$$\begin{aligned} f(t) &\xrightarrow{FFT} F(f) \\ &\longrightarrow \quad \frac{G(f) * F^*(f)}{F(f) * F^*(f) + h} = H(f) \quad \xrightarrow{inv.\,FFT} \quad h(t) \\ g(t) &\xrightarrow{FFT} G(f) \end{aligned} \qquad \text{Equation (4.9)}$$

The two input functions are f(t) and g(t). f(t) is the response curve before the structures and g(t) is the response curve after the structure. FFT denotes the use of a Fast Fourier Transform algorithm, F(f) and G(f) are the transformed curves, $F^*(f)$ is the complex conjugate of F(f), H(f) is the transfer function, inv. FFT denotes the transformation back to the time domain and h(t) is the resulting transfer curve. The constant h is used to set the filtering effect of the Hunt filter.

The effect of the transfer curve can best be explained with the following picture

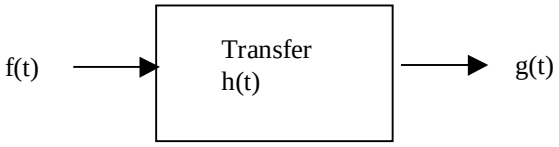

Figure (4.3) The transfer curve principle

The structure under consideration is represented with the transfer block in Figure (4.3).

4.3 Experimental

4.3.1 Moment analysis

A program was written in C to calculate the moments. The program implemented the moment analysis equations. This program was tested with the use of Equation (4.8). A random (white) noise was added to Equation (4.8) to simulate experimental values. The (maximum) noise is defined as a percentage of the maximum peak height. For example, with signal to noise ratio (S/N) of 33.3 (or 3 % noise) the N is defined as N=(Maximum signal) / 100 * 3. This means that there is a maximum variation of 1.5 % around the normal signal. First sharp spikes are removed from the data. The program then calculates the standard deviation of the begin base line and mean value of the base line itself from 10 values at the beginning of the curve (and the same procedure at the end). The place of the top on the x-axis is then determined. From this top the begin of the peak is calculated with the use of the begin base line deviation. This is done by going from the top to the left (along the response curve), when the value of the curve is smaller than the begin base line deviation the peak begin is reached. The same procedure is repeated for the peak end (of course now stepping to the right).

The effect of the noise can be seen in Table (4.1). The effect is clearly visible with the variance moment (u_2).

	No noise	33.3 (S/N)	33.3 (S/N) + filter	16.7 (S/N)	16.7 (S/N) + filter
Peak height	0.4	0.397	0.388	0.398	0.3878
Surface (M_0)	1.0	0.973	0.997	0.968	0.994
Center (m_1)	5.0	4.994	4.99	4.998	5.00
Variance (u_2)	1.0	0.746	1.049	0.694	1.045

Table (4.1) The effect of noice on the moment analysis

After the use of a moving average filter (30 points or 0.3 seconds) the peak height decreases but the surface (M_0) increases to the correct value of 1. The effect of M_0 on the other moments is also very clear. A change from 1.0 to 0.973 for M_0 results in a change from 1.0 to 0.746 in the u_2 value (for 16.7 (S/N)).

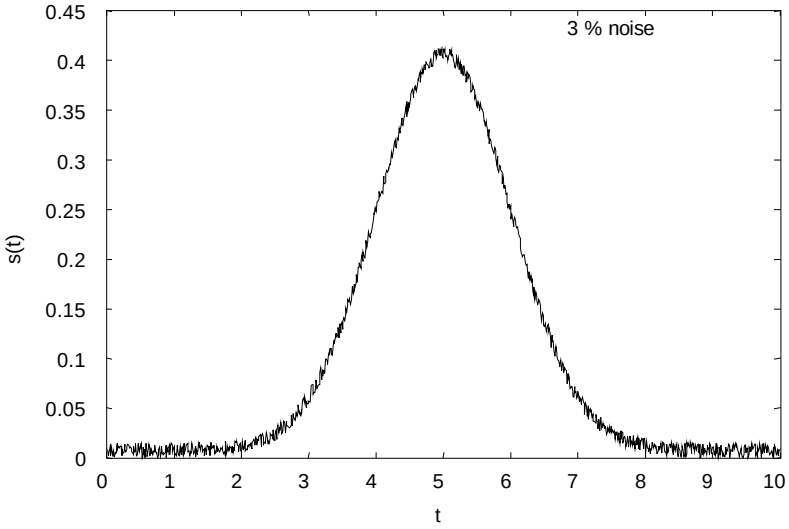

Figure (4.4) 33.3 (S/N)

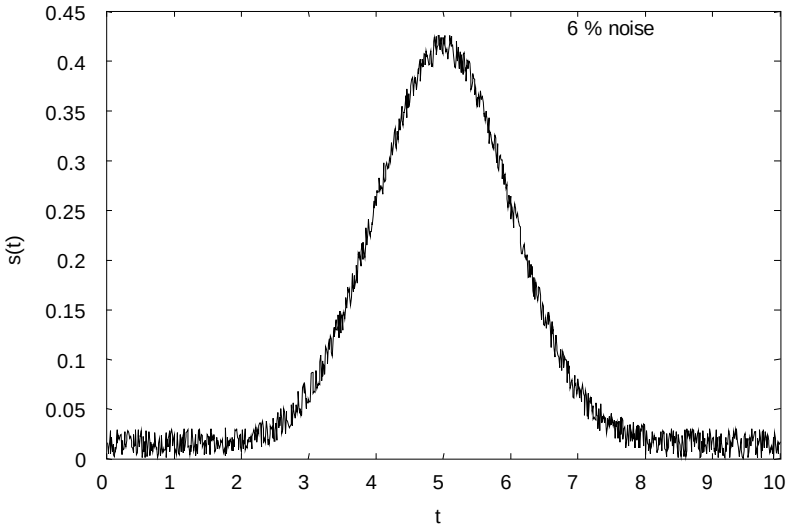

Figure (4.5) 16.7 (S/N)

From these results it can be concluded that filtering is necessary.

Another phenomenon that needs to be corrected is base line drift. An exaggerated base line drift is shown in Figure (4.6).

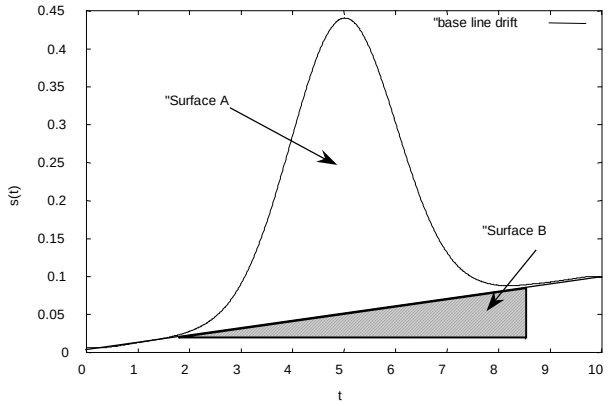

Figure (4.6) base line drift

If there was no correction, surface B would be added to the calculations of the moments. The moments are calculated with surface B removed.

4.3.2 Deconvolution

A program was written in C to deconvolute two peak shapes. To test this program two peaks were generated using Equation (4.8) with a S/N ratio of 33.3 for the noise component (see Figure (4.7)).

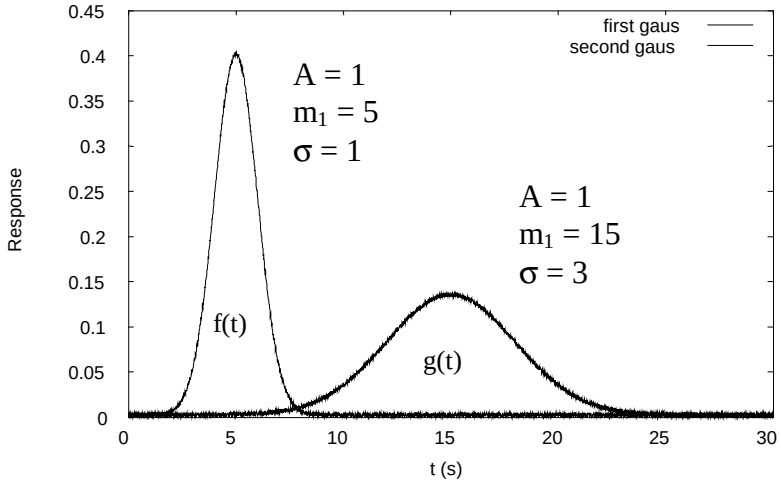

Figure (4.7) The two gaus peaks for deconvolution

Deconvolution was done according to scheme Equation (4.9). The Hunt filter constant has to be carefully established. A small Hunt filter constant will also calculate the transference of noise (high frequent signals). Figure (4.8) shows the transfer curve with a Hunt filter constant of 1.0. Figure (4.9) shows the transfer curve with a Hunt filter constant of 10.0. The correct Hunt filter constant is a trade off between two conflicting criteria. Convolution of f(t) with h(t) should result in g(t) (as accurate as possible) and h(t) should not contain

the information to transfer higher frequencies. This last criterion will keep the transfer function smooth and will allow comparison with other transfer functions.

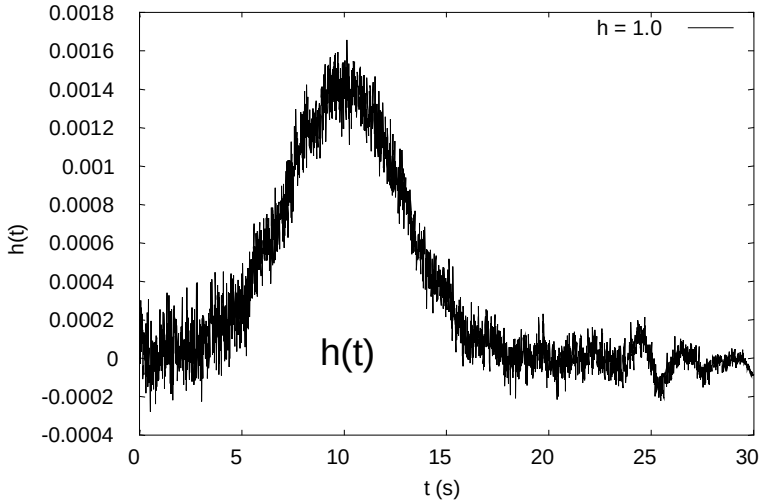

Figure (4.8) The transfer function h=1.0

Figure (4.8) shows that a low Hunt filter constant results in a rapidly fluctuating transfer curve. The rapid fluctuation can be removed from the transfer curve by setting the Hunt filter constant to a larger value. The back transformation according to Figure (4.9) results in a smoother g(t) curve. If the Hunt filter constant is taken too large the low frequencies (the signal itself) disappear.

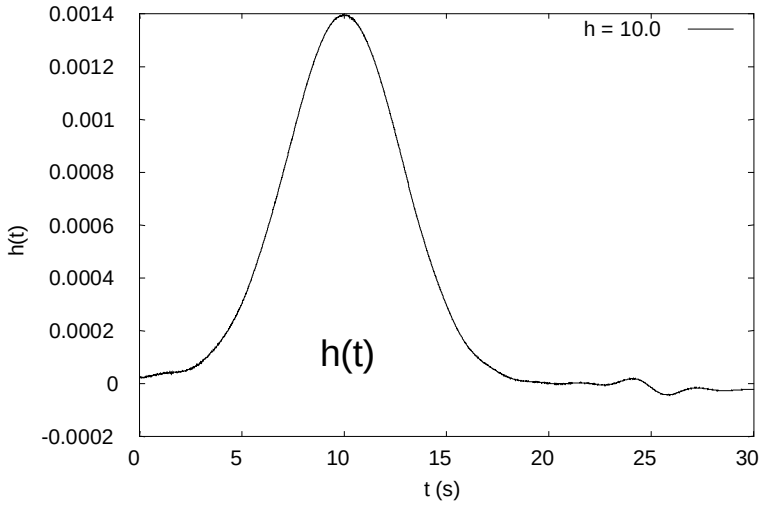

Figure (4.9) The transfer function h=10.0

A optimal Hunt filter constant of 10.0 was determined.

4.3.3 Computational fluid dynamics tools

At the initial stage of the research a computer program was written for the calculation of the flow and the two-dimensional distribution of an injected sample in a FIA-system [12]. To avoid the time consuming development of a 3d solver, the CFX-F3D package is used to model the five manifolds. This package was chosen for its good reputation and good customer support. The results from a self-written 2d solver agreed with the results obtained from the commercial CFD package.
The CFX-F3D package (or suite) consists of three main parts: a builder, a solver and a postprocessor.

4.3.3.1 The builder

The builder is called CFX-BUILD. The problem geometry is divided into several blocks. In the default situation, the boundary regions of such blocks are the walls assuming no slip conditions. No slip means that the fluid doesn't move at the walls. Defining inputs and outputs gives the user the option to define the flow through the structure. The user can mark planes (2d) and blocks (3d) that need special treatment in the solver. These planes and blocks can be accessed in the solver with the help of a self-written code (user functions). In this case two such user-blocks were applied: one for injecting the sample and one for the simulation of a detector. The software is capable of setting up different geometries. Standard blocks were used to build manifolds 1, 2 and 4 (See Figure (4.1) and Figure (4.10)). Sliding a surface over a curve to build a curved block ('slide'-option) was used together with the normal blocks to build manifolds 3 and 5 (See Figure (4.1) and Figure (4.10)).

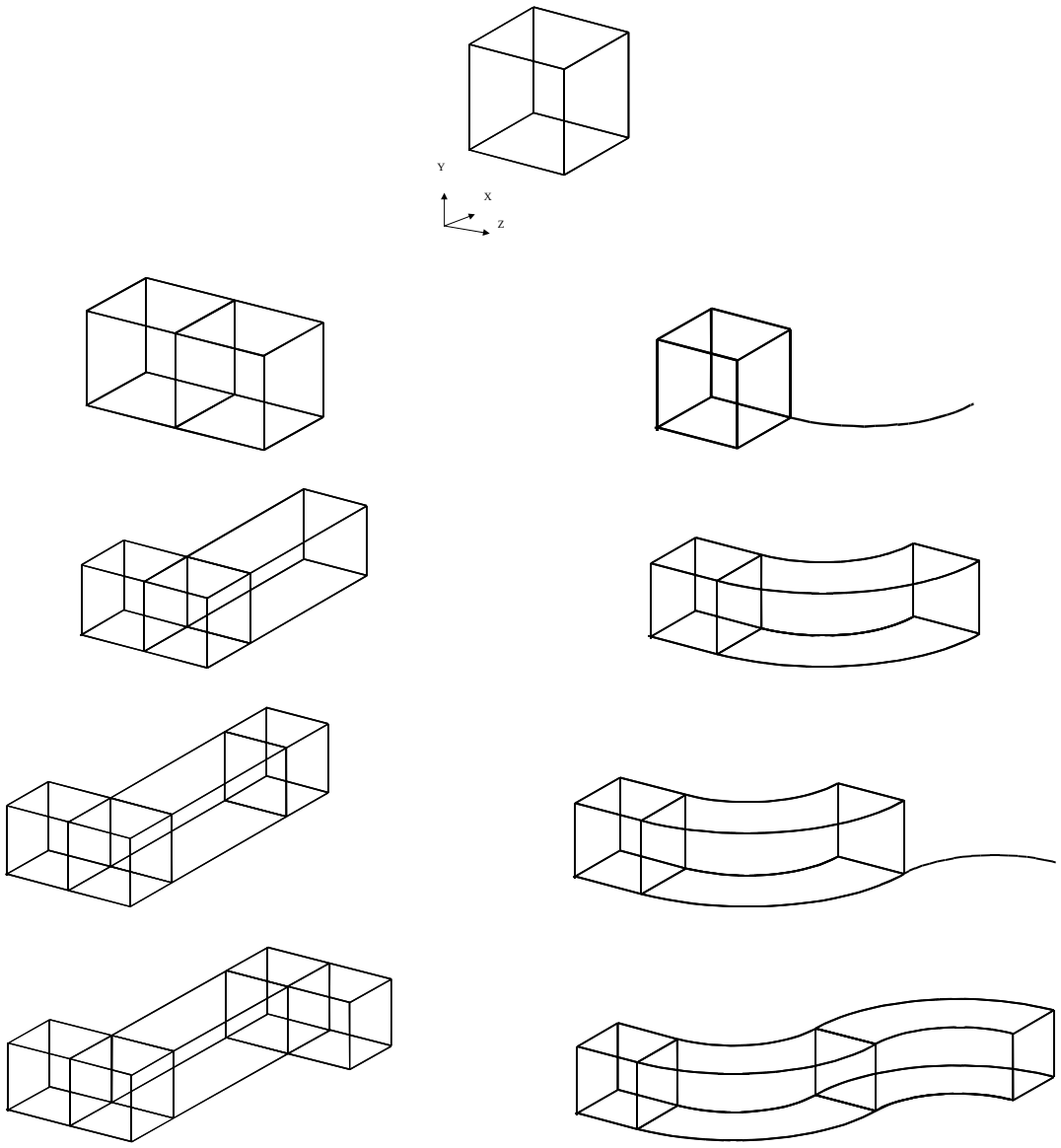

Figure (4.10) The different building blocks

Arbitrary units were used to create these structures. At the end of the building stage the arbitrary units were converted to meters. The conversion from arbitrary units to meters was done to allow the development of the manifolds, in the builder, with integer values. One arbitrary unit corresponds to one µm. The structures were 200 (x) by 200 (y) by about 40000 (z) arbitrary units. In Figure (4.1) the top view (normal to y) of the structures can be seen.
To setup the problem for the solver the structure must be divided into small elements (see chapter 3 section 3.2.3), where the Navier-Stokes equations are solved. This division is done by creating a mesh for the structure. The mesh

used for the five structures was made with an element length of 15 arbitrary units. This would lead to the use of 13*13*26666 elements. To minimize memory use, the mesh distribution can be changed in area's where there are no sudden changes in the structure geometry (see chapter 3 section 3.3.4.2.3). The adjustment of the mesh distribution is called seeding and was used mainly in the z-direction. Figure (4.11) shows seeding of one of the building blocks. The seeding used in this thesis is actually different, but if the seeding from the calculations was used the mesh picture (Figure (4.12)) would be mostly black.

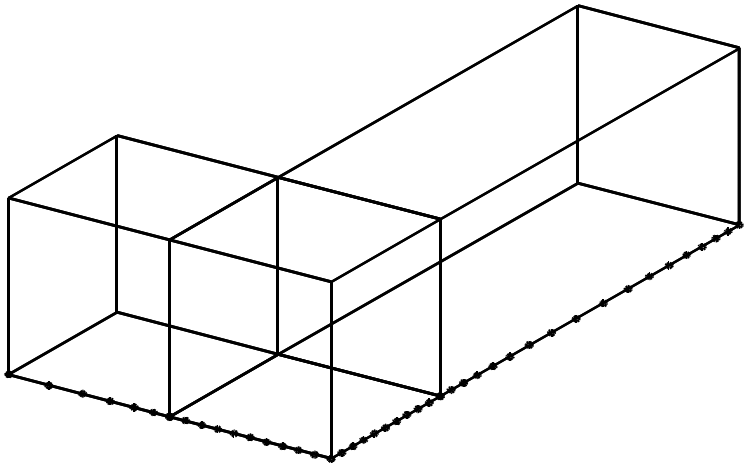

Figure (4.11) Seeding

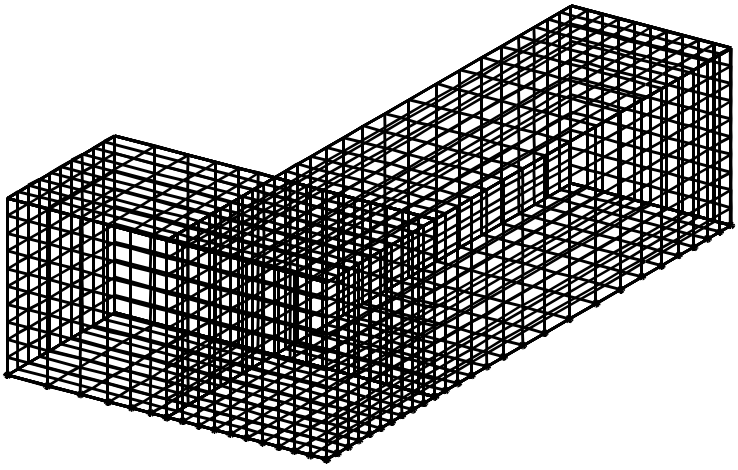

Figure (4.12) Meshing

4.3.3.2 The Solver

The solver reads the input from the builder. The solver makes use of two other files containing information on how to solve the problem. There is a command file where information about the fluids, discretisation, iteration, output, user-functions etc. is stored. In the simulations, of the five manifolds, water at 20 °C

was used as carrier and the entrance flow rate was 1 µl/min. There is also a file where the user-functions are stored. Through these user-functions it is possible to write output to file during a simulation run. For all the five manifolds a steady state solution was calculated for the fluid flow (see appendix 1-3 for the command file and user functions file for structure 1). After the flow was available the distribution of the injected sample in time (transient) was simulated and output was written to disk at each time step (see appendix 2 for the command file and user functions file).
The user-functions for the simulations of the five manifolds included the following features: the injection block was filled with the scalar at the beginning of the simulation run (only with the transient run) and at each time step the results from the detection blocks were written to file (only with the transient run). We refer to chapter 3 for all the different options that can be chosen for the steady state and transient calculations. The convection terms were discretised using the quick differencing scheme (see 3.3.3.2.2). The fully implicit backward difference time stepping procedure was used to simulate the sample dispersion from 0 to 250 seconds.

4.3.3.3 The post processor

The post processor is used to view the results obtained from the solver. It's possible to view the structure and variables in three dimensions with iso plots, slice plots, vector plots, stream plots etc. A color scale is used to represent the value of the variable under consideration.

4.3.4 Equipment and procedures

In this chapter a hybrid system, containing macro and µ-parts, was used (See Figure (4.13)) to study two of the five earlier mentioned manifolds.

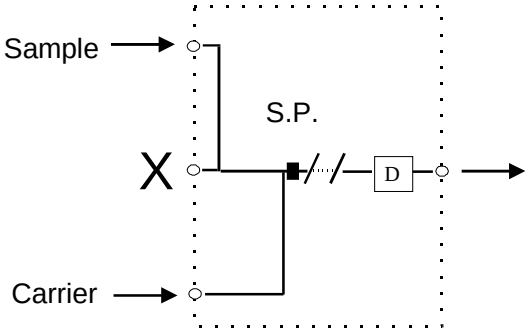

Figure (4.13) Principle of the measurement system. S.P. Sample Plug and D Detector. The X shows that the channel is blocked.

A syringe pump (CMA/102 Microdialysis Pump) established the flow. One syringe (Hamilton 250 µl) was used for propelling the carrier stream and one (Hamilton 10 µl) for injection of the sample. The carrier solution was borax $1.0*10^{-2}$ mol/l (Millipore Q2 water was used as solvent). The sample solution

was 4.26*10^{-3} mol/l bromocresolgreen (the carrier solution was used as solvent). In the default situation the carrier is passed through the system. The injection consists of stopping the syringe for pumping the carrier, and starting the syringe for propelling the sample. After the injection the syringe for propelling the sample is stopped and the syringe for propelling the carrier is started.

A measurement consists of the following procedure:

- 10 seconds of propelling the carrier stream with 1 µl/min
- stopping the carrier syringe and starting the sample syringe
- 20 seconds of samples injection with 0.2 µl/min
- stopping the sample syringe and starting the carrier syringe

A program written in C was used to control the syringe handling and the data acquisition (up to 100 Hz). The computer hardware consisted of an IBM compatible PC (386), a Keithley interface card (DAS-1600) and a home-made passive DA/AD interface.

4.3.4.1 Macro parts

The tubes in the macro part of the system had an internal diameter of 0.8 mm. The connections from the tubes to the micro system were made with the use of a Pyrex block glued to the device and several interconnections (metal tube, flexible tubing).
To allow accurate positioning of the LED photometric detector a construction was built (See Figure (4.14)). The u-shape in Figure (4.14) could be positioned in x, y and z direction. The LED (Honeywell HFE4000-013) and the silicon photodiode (UDT PIN-6DP) could be positioned in the z direction with micrometers (Mitutoya Nr153-204 0-25 mm). The accuracy in the placement of u-shape in the y direction was about 0.01 mm and the accuracy in the z direction was about 0.01 mm.

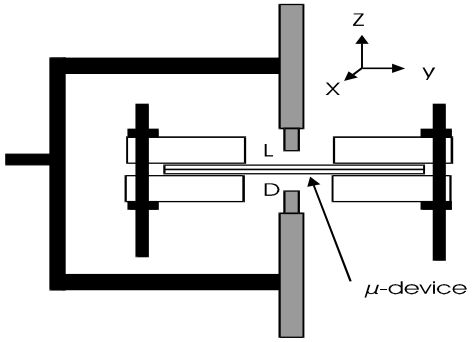

Figure (4.14) Positioning tool. The u-shape can be moved in x, y and z direction. The LED and detector are (accurately) positioned in the z direction with a micrometer. L Light Emitting Diode, D Detector.

An (shaped) aluminium block, with a hole of 1 mm, was placed over the LED the get a well-defined light spot. Before each measurement the LED and the photodiode were placed as close to the device as possible.
A Toellner function generator (Toe 7706) was connected to the LED (with the use of a 0.908 Ω resistor) and to the reference input of a lock-in amplifier (PAR^{tm} model 122). A sine wave with 5 kHz was used as input signal. The signal from the photodiode was fed back to the lock-in amplifier. The output signal from the lock-in amplifier was used as data signal.

4.3.4.2 Micro parts

Five micro manifolds were constructed. The manifolds were created by etching through a 200 µm silicon plate. The outlines of the structure are represented in Figure (4.1). The silicon plate was then sandwiched between 2 glass plates of 0.5 mm. In the top glass plate holes were drilled at the input and output connections of the structure etched in the silicium plate. These holes had a diameter of 0.9 mm and were made with an ultrasonic drilling device. Figure (4.15) shows a picture of the µ-device and a zoomed view of interesting parts.

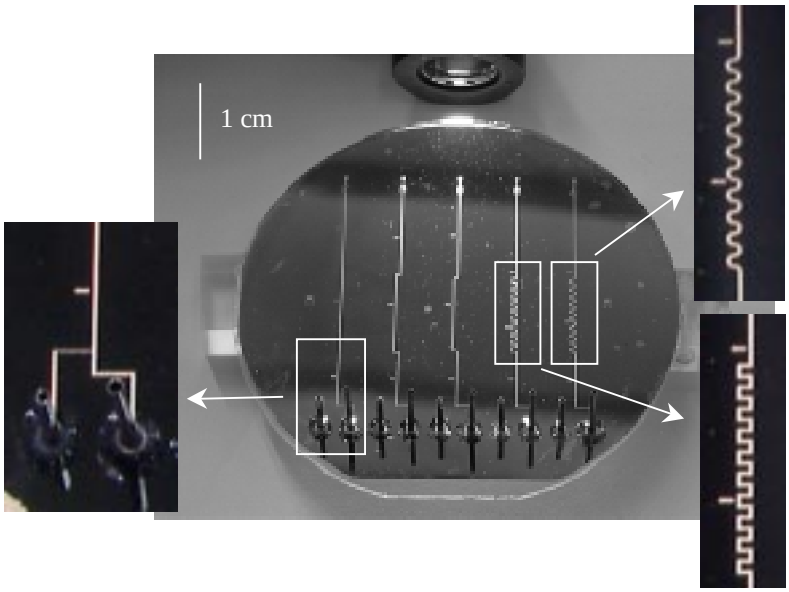

Figure (4.15) A picture of the µ-device.

Measurements were performed at two points per structure. Figure (4.1) shows the different measurement points. Point A and C are located at 8400 µm from the point of injection and B and D are at 39650 µm from the point of injection.

4.3.5 The numerical setup

4.3.5.1 The manifolds

The injection plug in the five simulation structures was 1660 µm x 200 µm x 200 µm.
The simulated detection was done at two points for each of the 5 structures. The first simulated detection took place after 8400 µm and the second after 39650 µm. For structure 2 and 4 these simulated detection places correspond to points A, B, C and D.
Two basic elements were used to construct the manifolds: a rectangular (See Figure (4.16)) and a curved bend (See Figure (4.17)). To be able to position the simulated detector correctly the estimated travelled length through the bends was 750 and 1178 µm, respectively.

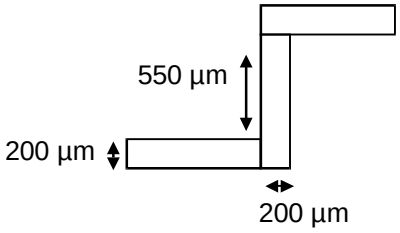

Figure (4.16) Size of the straight bend used in the µ-manifolds

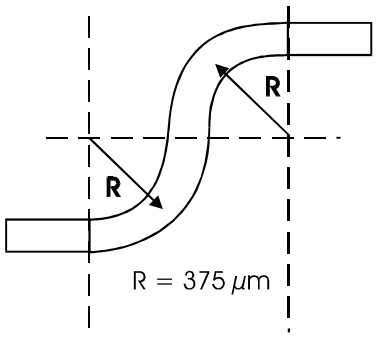

Figure (4.17) Size of the curved bend used in the µ-manifolds

For the numerical study, blocks were introduced before and after the structure to make sure there were no entrance or exit effects (1000 µm * 200 µm * 200 µm).

4.3.5.2 Grid dependency

The solution of a numerical algorithm always has to be checked for grid independency (see chapter 3 section 3.3.1.4 and section 3.3.2.6). A denser grid (more elements) will result in a solution that better represents the ‘true’

solution. The default action is to check if the same numerical solution is obtained with twice as many elements. To check the different effects of grid density, seeding and differencing schemes a straight channel was simulated in several different numerical situations. The straight channel used was build with arbitrary units 200 (x) * 200 (y) about 5000 (z). The injection and detection block were 200 (x) * 200 (y) * 200 (z) arbitrary units. To make sure there were no entrance or exit effects blocks were introduced before and after the structure (500 (x) * 200 (y) * 200 (z) arbitrary units). The element length was varied between 100 and 8. The effect of seeding, differencing scheme (upwind vs. quick) and the effect of double vs. single precision were studied.

4.3.5.3 Time dependency

The transient calculations (the sample travels through the system) should also be checked to ensure that the time step is taken small enough (see chapter 3 section 3.3.2.3). The problem is to find a time step that represents the 'true' solutions and isn't too small. A very small time step results in a very long simulation time. Four different time steps 0.5, 0.25, 0.1, and 0.01 seconds were used to study the effect of the time step on the numerical solution.

4.3.5.4 The diffusion coefficient

The diffusion coefficient of the dye in the carrier solution influences the dispersion of the dye in the flow system. The diffusion coefficient of a dye in a solvent (water based) has generally values in the range from$1*10^{-9}$ m^2/s – $1*10^{-10}$ m^2/s.
To study the effect of the diffusion coefficient on the numerical response curve the results from calculations with a diffusion coefficient of $1*10^{-9}$ m^2/s and $5*10^{-10}$ m^2/s were compared to an experimental response curve.

4.4 Results and discussion

4.4.1 Grid dependence of the numerical solution

In Table (4.2) the different situations are given with the values for the various statistical moments. The situation with the element length of 8 is taken as the best solution.

	Situation	Peak area (* 10^{-6})	Residence time	Variance
1	EL 100	2.0000	0.536	0.007
2	EL 50	2.0962	0.640	0.044
3	EL 25	2.0965	0.695	0.088
4	EL 12	2.0961	0.707	0.098
5	EL 8	2.0963	0.705	0.099
6	EL 10 / Se	2.0999	0.706	0.107
7	EL 10 / Se + Q	2.0959	0.693	0.097
8	EL 25 / S	2.0965	0.695	0.086

Table (4.2) Grid dependence. EL element length, S single precision, Se seeding and Q quick differencing scheme. The default situation is with double precision and upwind differencing

From Table (4.2) it can be concluded that the element length has to be around 15 to get accurate results. This is in agreement with the results in chapter 3 section 3.3.4.2. Applying a non-uniform grid (seeding) doesn't seem to have much effect on the solution (see also chapter 3 section 3.3.2.6) and the quick differencing scheme gives better results. There seems to be not much difference between the single and double precision calculations. The single precision calculations cost less memory and thus are preferred. Table (4.2) shows that with a decreasing element length (more elements) the variance seems to reach a stable value.

4.4.2 Time dependency of the numerical solution

From the results of the simulations with the different time steps it can be concluded that 0.1 seconds is a reasonable time step. The time it takes to simulate the response curve with 0.01 seconds to the end of the time range (250 s) is not acceptable. The solution with the 0.01 seconds time step is virtually the same as the solution with the 0.1 time step.

Time step	Peak height (*1e-5)	Error (*1e-6)	Relative Error
0.5	8.0465	5.6966	6.61
0.25	8.3201	2.9602	3.44
0.1	8.4973	1.1881	1.38
0.01	8.6122	3.8878E-02	4.5e-2
0.0	*8.6161*	*0*	*0*

Table (4.3) The time step error with the backward fully implicit scheme

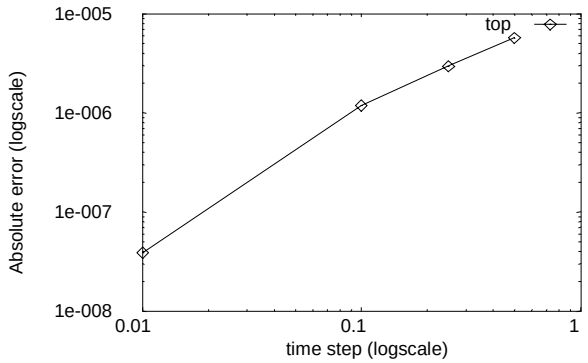

Figure (4.18) log figure for the backward implicit scheme

Table (4.3) shows that the relative error in the peak height is 1.38 % if the time step is taken 0.1. Figure (4.18) shows the absolute error versus the time step on a logscale. Section 3.3.1.4.2 in chapter 3 states that the slope of the log(Δt) against log(error) should be 1.0. The slope in Figure (4.18) for the three points on the right is 0.97.

4.4.3 The diffusion coefficient

The diffusion coefficient of the dye was measured with the use of polarography using the Ilkovic equation [13,14].

$$I_d = (7.08*10^4)\, n\, C\, D^{1/2}\, m^{2/3}\, t^{1/6}$$ Equation (4.10)

where

I_d diffusion current, in μA
n Number of electrons per molecule involved in the oxidation or reduction of the electroractive species.
C concentration of the electroactive species, in mmol/L
D diffusion coefficient of electroactive species, in m^2/s
m rate of flow of Hg, in mg/s
t drop interval, in s

The rate of flow of Hg (with the base solution) was 1.31 mg/s. The drop time was set to 1 second. The number of electrons involved in the process was 2 [14].

The diffusion current was measured for several different concentrations.

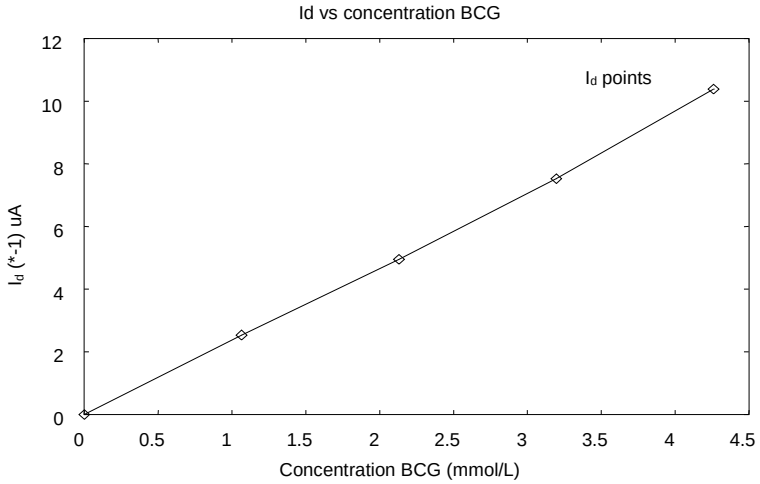

Figure (4.19) Diffusion current against [BCG]

Equation (4.10) can be rewritten (with a constant background, represented with B) as

$$I_d = A*C + B \qquad \text{Equation (4.11)}$$

with $A = (7.08*10^4)\, n\, D^{1/2}\, m^{2/3}\, t^{1/6}$

From Figure (4.19) (with the use of regression analysis) it can be seen that A is –2.4182 μA /mmol/l and B is +0.0741 μA.

So

$$D = \left(\frac{A}{(7.08*10^4)*n*m^{2/3}*t^{1/6})} \right)^2$$

This results in D = 2.03 * 10^{-10} m^2/s

The experimental result obtained from structure 2 at point A was used for the comparison with the calculations containing the two different diffusion coefficients. The numerical results (compared to the experimental result) show that the diffusion coefficient of the dye has to be less then 5*10^{-10} m^2/s. The numerical model shows a result that agrees with the experimentally determined diffusion coefficient.

4.4.4 Experimental results

The injection volume is 0.067µl. The detection volume (on the basis of a channel with a cross section of 200 µm * 200 µm and a detector length of 1 mm) was 0.04 µl. The volume of the manifolds was calculated to be 1.6 µl, using 39650 µm as the length of the manifolds.
Due to technical difficulties with the fabrication of the device only structure 2 and 4 could be measured. In Figure (4.20), Table (4.4) and Table (4.5) the measurement results are presented. The values found in Table (4.4) and Table (4.5) are only corrected for the baseline. The curves in Figure (4.20) are corrected for the base line and normalized to an area value, under the curve, of 10. For each point (A, B, C and D) 25 measurements were done. A sample was discarded if it had a peak height that deviates more than 1 standard deviation of the average peak height. The moments were calculated without these samples and can be seen in Table (4.4) and Table (4.5). From the curves and the various statistical moments it can be concluded that there is no difference between the results measured at point A and C. The results for point B and D are not that clear. It seems that the sample plug in structure 2 undergoes less dispersion than the sample plug in structure 4.

		Average	SD	Average SD	RSD
Structure 2 begin (point A)					
	Peak height	**0.653**	**0.0138**	**0.0034**	**2.12**
	Peak area	**11.99**	**0.636**	**0.154**	**5.31**
	Residence	**53.62**	**0.898**	**0.218**	**1.68**
	Variance	**53.97**	**10.41**	**2.53**	**19.30**
Structure 4 begin (point C)					
	Peak height	**0.705**	**0.0067**	**0.0017**	**0.95**
	Peak area	**13.15**	**0.502**	**0.13**	**3.82**
	Residence	**53.52**	**0.562**	**0.15**	**1.05**
	Variance	**55.87**	**4.93**	**1.27**	**8.82**

Table (4.4) The Peak height, peak area, residence time and the variance for the measuring points A and C

		Average	SD	Average SD	RSD
Structure 2 end (point B)					
	Peak height	**0.161**	**0.0073**	**0.0018**	**4.54**
	Peak area	**6.31**	**0.339**	**0.082**	**5.37**
	Residence	**138.15**	**0.696**	**0.169**	**0.50**
	Variance	**229.82**	**12.82**	**3.11**	**5.58**
Structure 4 end (point D)					
	Peak height	**0.26**	**0.017**	**0.0036**	**6.55**
	Peak area	**12.09**	**1.09**	**0.227**	**9.01**
	Residence	**138.78**	**1.52**	**0.316**	**1.09**
	Variance	**370.58**	**52.40**	**10.93**	**14.14**

Table (4.5) The Peak height, peak area, residence time and the variance for the different measuring points B and D

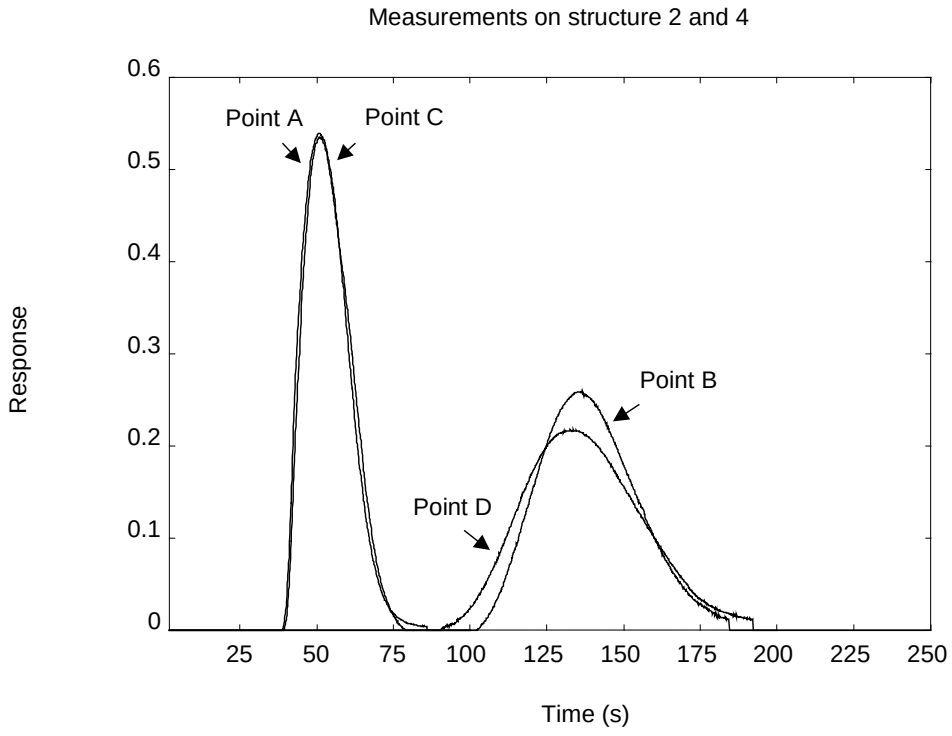

Figure (4.20) The measured response curves for the different points A, B, C and D

4.4.5 Numerical results

The calculations in this section were done with a diffusion coefficient of $2.03*10^{-10}$ m^2/s. The results from the numerical calculations are presented in Figure (4.21) and Table (4.6). The values found in Table (4.6) are only corrected for baseline. The curves in Figure (4.21) are corrected for the base line and normalized to an area value, under the curve, of 10.

Structure :	**Peak height (* 10^{-4})**	**Peak area (* 10^{-3})**	**Residence**	**Variance**
1 begin	**2.05**	**3.87**	**49.46**	**55.94**
2 begin	**2.05**	**3.88**	**49.46**	**55.93**
3 begin	**2.05**	**3.88**	**49.46**	**55.94**
4 begin	**2.05**	**3.88**	**49.46**	**55.71**
5 begin	**2.05**	**3.88**	**49.45**	**55.66**
1 end	**0.85**	**3.84**	**129.42**	**323.30**
2 end	**0.85**	**3.84**	**127.47**	**324.32**
3 end	**0.86**	**3.84**	**127.03**	**315.90**
4 end	**0.78**	**3.84**	**126.89**	**391.52**
5 end	**0.85**	**3.84**	**126.94**	**318.73**

Table (4.6) The different calculated values for the 5 structures. The peak height, residence time and variance.

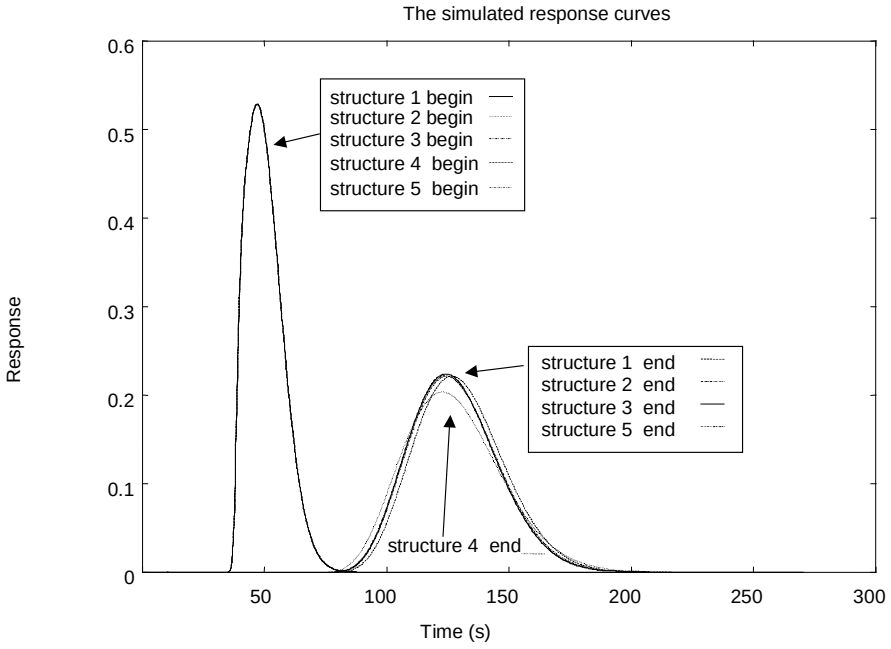

Figure (4.21) The calculated response curves for the 5 structures

From Figure (4.21) and Table (4.6) it can be seen that only structure 4 shows a different response curve at the detection point at the end of the structure. The fact that the sample plug undergoes more dispersion in structure 4 was also observed in the experimental results.

4.4.6 Numerical results compared to the experimental results

The numerical and the experimental results can not be compared directly. The numerical results should however show the same trend as the experimental results. There are several assumptions made in the numerical case that makes a direct comparison not relevant. The first assumption is that the channels are exactly 200 µm by 200 µm. This is, however, not the case. Etching downwards (12 µm) also results in a displacement sideways (2 µm). This results in a channel being 200 µm wide at the top and 234 µm wide at the bottom. The effect of the etching error will result in a higher velocity in the numerical case. The curves of the numerical flow will have a shorter residence time.
The second assumption concerns the injected sample volume. Due to the method of injection there will not be a well-defined sample plug placed in the carrier stream. Deconvolution of the curve before and after the structure under observation eliminates this problem. The resulting transfer function is independent of the injected volume. The transfer functions for the different experimental situations can be seen in Figure (4.22).

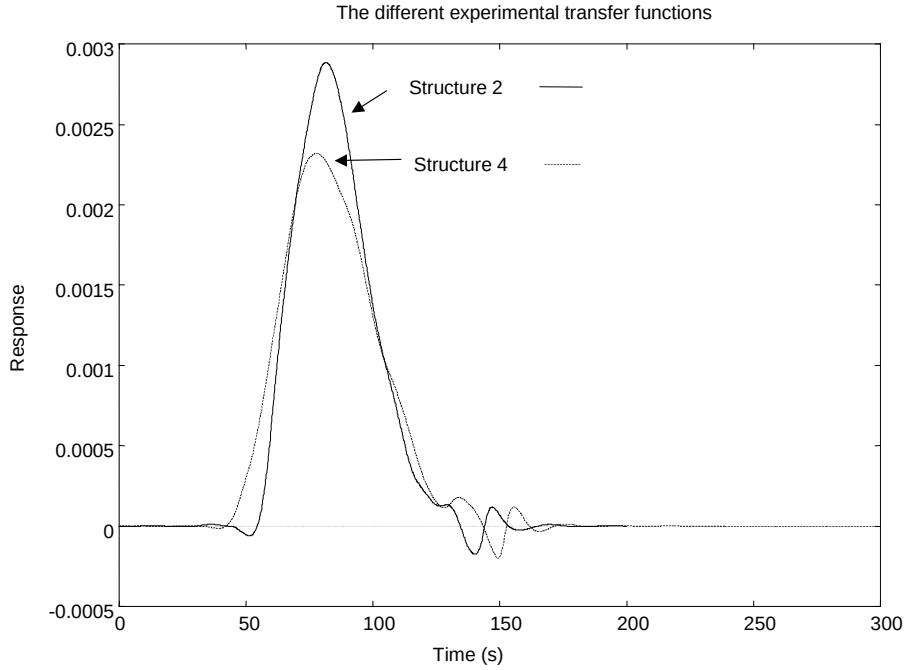

Figure (4.22) The measured transfer functions

The transfer functions for the numerical cases can be seen in Figure (4.23).

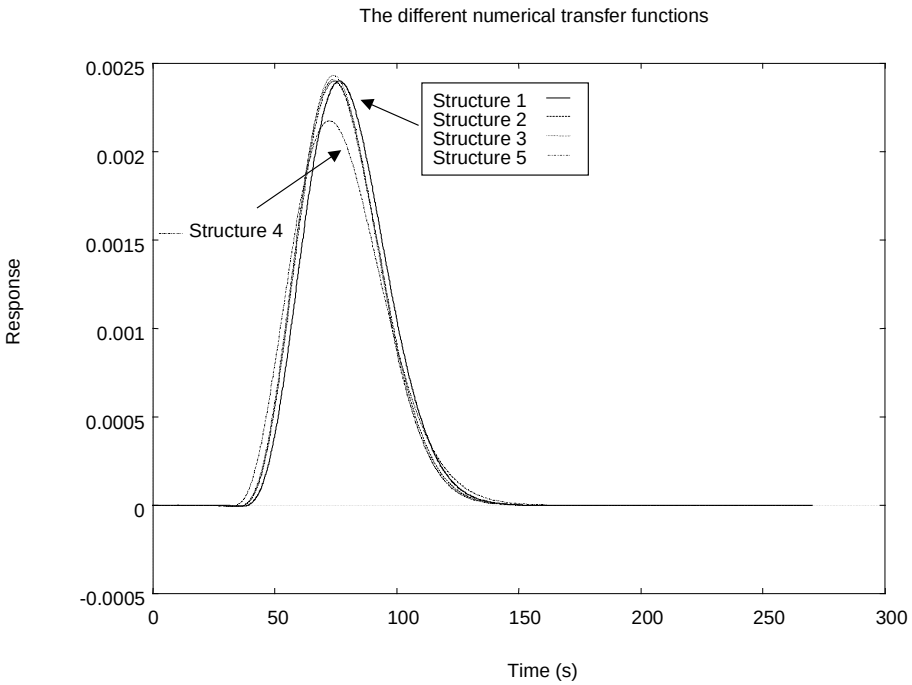

Figure (4.23) The numerical calculated transfer functions.

The constant h in the Hunt filter was optimized, in case of experimental results, using known signals composed by convolution of the input signal with the transfer function. The idea was to have the Hunt filter remove a large amount of noise without a significant difference between the output curve and the input curve convoluted with the transfer function. This resulted in a value of 10.0 for the measured curves. The value 10 of the constant h was also adopted in case of the numerical curves. Figure (4.22) and Figure (4.23) shows that only structure 4 has a different transfer function in both the numerical and experimental results.

The numerical and experimental response curves show the same effect of structure 4 on the dispersion compared to the other channels. The 40 rectangular bends in structure 4 result in more dispersion compared to the other geometrical situations. This difference, however, is not sufficient to advise a specific channel structure for future µ-structures to minimize the dispersion in a system.

The use of sharp bends to establish a flow system with a certain traveling distance within a small area has minimal effects on the dispersion of a sample under the conditions described in this chapter.

The comparison shows that the numerical model used in this chapter could be used as a numerical pre-analysis tool. The general numerical model allows the calculating of the flow profile, pressure distribution and the concentration distribution of the sample, three dimensional, throughout an arbitrary channel.

4.5 References

[1] J. Ruzicka, Micro Total Analysis Systems (Proceedings of the µTAS '94 Workshop), editors: A. van den Berg, and P Bergveld, Kluwer Academic Publishers, Dordrecht, 1994, p. 117-125
[2] J.T. Vanderslice, A.G. Rosenfeld and G.R. Beecher, Anal. Chim. Acta., 179(1986)119
[3] R.D. Hull, Flow injection dispersion phenomena : simulation and evaluation of theoretical models, UMI Dissertation Services, 1993
[4] A. van den Berg,and P Bergveld, Micro Total Analysis Systems (Proceedings of the µTAS '94 Workshop, Kluwer Academic Publishers, Dordrecht,1994
[5] M.J. Harper C.M. Turner and J.E.A. Shaw, Proceedings of the 1st International Conference on Simulation and Design of Microsystems and Microstructures MicroSIM95, editors: R.A. Adey, A. Lahrmann, and C. Lessmolman, Comp. Mech. Publications, UK 1995, p. 155-163
[6] L.D. Landau and E.M. Lifshitz, Course of theoretical Physics Volume 6 Fluid mechanics, Pergamon Press, Oxford, 1959
[7] J. Pfahler, J. Harley, H. Bau and J. Zemel, Sensors and Actuators, a21-a23(1990)431
[8] AEA, CFX 4.1 Flow solver user guide, Building 8.19, Oxfordshire, 1995
[9] W.H. Press, S.A. Teukolsky, W.T. Vetterling and B.P. Flannery, Numerical recipes in C, Cambridge University Press, Second Edition, 1995
[10] B.R. Hunt, The application of constrained least squares estimation to image restoration by digital computer, IEEE transactions on computers,c-22 no.9 (1973)805-812
[11] I.C. van Nugteren-Osinga, Optimization of flow-injection analysis for on-line in-process control, thesis,1991
[12] S.V. Patankar, Numerical heat transfer and fluid flow, Hemisphere, 1980
[13] D.C. Harris, Quantitative Chemical Analysis, Third Edition, W.H. Freeman and Company, New York, 1991
[14] H. Jain, M. Shivhare, M Singh, Indian J. Chem. 21A (1982) 198-200

Chapter 5

Continuous, pulsed and stopped flow in a micro-flow injection system[#]

5.1 Introduction

To establish a certain residence time in a flow system the flow rate can be adjusted or the carrier stream could be stopped for a while. Controlling the residence time is useful to allow reactions to take place. The basic question is what method to use for controlling the residence time while keeping the dispersion of the sample to a minimum. The two important books about 'normal' flow injection analysis (FIA) don't agree on the effect of the flow rate on the dispersion. According to Růžička [1] 'the dispersion of the sample zone decreases with decreasing flow rate'. Valcárcel [2] states the other situation, ' the dispersion increases with decreasing flow rate'. Růžička [1] also shows what happens in a FIA system when stopped flow is applied. The dispersion is practically independent of the time the flow is halted.
The dispersion of a sample in a flow system is influenced by two phenomena: diffusion and convection. See chapter 2 section 2.3 for examples of the different types of peaks with increasing effect of diffusion and a general explanation of the two phenomena. The different shapes of the signals were also described and measured by Vanderslice [3].
The assumption is that use of a smaller channel will have the effect that the diffusion predominates from the start and that the contribution of convection is negligible. One of the objectives of this paper is to investigate this assumption.
When a flow is established with a mechanical device, pulses are virtually always present. The pumps mostly used in macro flow systems are the so-called peristaltic pumps. These pumps can not be used in a µ-flow system because of the high flow rates and large dimensions. The pumps that could be (are) incorporated into µ-flow systems are membrane pumps. The basic function of a membrane pump can be seen in Figure (5.1).

[#] Published in Analytica Chemica Acta, ACA 378(1999)111-117

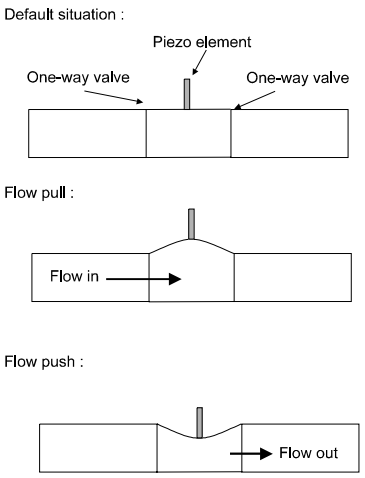

Figure (5.1) A theoretical membrane pump

A review of the different µ-pumps is given in [4]. It is clear from Figure (5.1) and [4] that the typical µ-pump produces a pulsed flow. In our theoretical pump (Figure (5.1)) the pulse depends on the vertical movement of the membrane. The maximum displacement of the membrane in combination with the frequency establishes a certain flow. A greater displacement would mean a lower frequency to maintain the same average flow. The working range of our theoretical pump is restricted at both sides of the frequency domain. Preferably a pump has to be self-priming. This means that the pump can fill itself with fluid. This requirement places a restriction on the maximum displacement of the membrane. If the maximum displacement of the membrane is taken too small, the pump looses the ability of self-priming. In this case the fluid has to be introduced into the pump with the aid of other methods, for example by pressure or by the use of a fluid with a lower viscosity. The latter examples can certainly be designed but to create a simple and robust flow system, self-priming is a desired option.
In the situation where the pump introduces a very large pulse (the displacement of the membrane is taken too large), the pump will flush the flow system with a few strokes. In this study we hope to give some insight into the effect of a pulsed flow on the dispersion of a sample in a µ-flow system.

5.2 Theory

The dynamic behavior of fluids can be modeled with the Navier-Stokes equations. The basic mathematical model equations for fluid dynamics (fluid flow and mass transfer) consist (among others) of the following equations (see chapter 2 for a detailed explanation):

Continuity equation

$$\frac{\partial \rho}{\partial t} + \nabla \cdot \left(\rho U \right) = 0$$ Equation (2.23)/Equation (5.1)

Momentum equation

$$\frac{\partial U}{\partial t} = -(U \cdot \nabla)U - \frac{1}{\rho}\nabla P + \nu \nabla^2 U$$ Equation (2.25)/Equation (5.2)

Scalar equation

$$\frac{\partial \phi}{\partial t} + \nabla(U\phi - D_\phi \nabla \phi) = \frac{S}{\rho}$$ Equation (5.3)

where t is time, ρ is the mass density, U the velocity of the fluid, P the pressure and ν the kinematic viscosity of the fluid and D_ϕ the diffusion coefficient of the sample. In this chapter the scalar ϕ represents the concentration of the sample in the system and S represents the concentration of the sample at the injection point at the beginning of the simulation (this value is provided by the user: user source).
A calculation of the dispersion of a sample through the flow system consists of two simulations. The first steady state simulation calculates the three-dimensional flow profile and the three-dimensional pressure distribution. The second transient simulation calculates the dispersion of the injected sample through the flow system. After the transient calculation the distribution of the sample (throughout the flow system) is available in a three-dimensional format and in dependence on time.

For a detailed explanation and description of the statistical moment analysis see chapter 4. The user source code that describes the continuous flow is given also in chapter 4.

The stopped flow is numerically modeled by the following procedure :

- save the flow profile generated by the steady state calculations
- for the stop period set the flow profile to zero
- after the stop period use the flow profile saved in step 1

The pulsed flow calculations use the same structure. The user source code that is needed to investigate stopped and pulsed flow will be explained in section 5.2.3.

For an explanation of the mathematical model and the basic equations used for the numerical modeling we refer to the chapter 2 and 3.

5.2.1 Equipment and procedures

For a description of the measurement system (hardware, solutions/concentrations) used in this chapter we refer to chapter 4. For the continuous flow case 3 measurements were carried out at different flow rates (0.5, 1, 2, 3, 4, 5 µl min^{-1}). For the stopped flow case 3 measurements were performed with different halting periods (10, 25, 50, 100, 200 and 400 seconds) and the different flow rates mentioned above.
A measurement consists of the following procedure:

1) 10 seconds of propelling of the carrier stream with X µl min^{-1}
2) stopping the carrier syringe and starting the sample syringe
3) 20 seconds of sample injection with 0.2 µl min^{-1}
4) stopping the sample syringe and starting the carrier syringe (X µl min^{-1})

X refers to the flow rate under investigation.

For the stopped flow measurements this procedure was updated with the following point:

5) stopping the carrier syringe during Y seconds, 10 seconds after injection (point 4)

Where Y refers to the stopped flow period.

For the pulsed flow situations the same measurement procedure as the continuous flow case was used but the carrier stream was pulsed with different frequencies (0.1, 0.3, 0.5, 0.7, 0.9, 1.0, 3.0 and 5.0 Hz). This pulse was implemented, for example for 1 Hz and 1 µl min^{-1}, by stopping the carrier syringe during 1 second and propelling the carrier with 2 µl min^{-1} during the next second.
Before and after a measurement session a calibration curve was recorded. This calibration curve consisted of a measurement with a 500 second injection time (1.67 µl). In this way the background signal and the maximum signal could easily be measured. The measured signals were converted to absorbance values according to the Lambert-Beer principle.
To visualize the dispersion process independent of the flow rate the x-axis has to be scaled according to the following equation:

$$x_{new}\,[m] = x_{old}\,[s] * \frac{flowrate}{cross-section\ of\ the\ channel} \qquad \text{Equation (5.4)}$$

5.2.2 Micro experimental setup

One manifold was used to measure all the experimental results in this chapter. This same manifold was used in the chapter 4 (structure 2) but the detector is

now placed at 21550 μm after the injection. The manifold can be seen in Figure (5.2). The channel volume was 1 μl, the injection volume was 0.067 μl and the detection volume was about 0.047 μl.

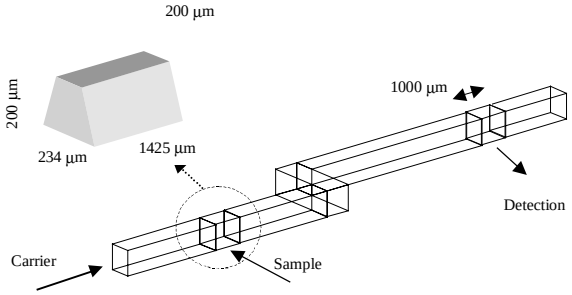

Figure (5.2) The micro-manifold.

5.2.3 The numerical setup

The injection plug in all the numerical simulations was 1425 μm x 200 μm x 200 μm. The simulated detection was done after 21550 μm and the detection block was 1000 μm (see Figure (5.2)). The diffusion coefficient was taken as 3.0 x 10^{-10} m^2s^{-1}. For the numerical study, blocks were introduced before and after the structure to make sure that there were no entrance or exit effects (1000 μm * 200 μm * 200 μm). The R_{sum} used in the flow calculations was 1e-15 (see chapter 3 section 3.3.4.1.1).
The “QUICK” scheme was used for the convection terms in the sample transport calculations. The R_{sum} used in the sample transport calculations was 1e-15 (see chapter 3 section 3.3.4.2). The time stepping scheme was backward difference with a time step of 0.1 seconds.
The experimental calibration curve was used to transform the numerical response curve to the same value range as the experiments (numerical value * ‘The maximum experimental value’ / ‘The maximum numerical value’).

5.2.3.1 Stopped flow numerical implementation.

The continuous flow case is described in chapter 4. In this chapter the command file and user Fortran file were introduced (see appendix a.1). The numerical stopped flow case needs some additions.

In the USRINT module the following Fortran code takes care of the initial saving of the steady state flow calculations.

```
C
C----- SAVE ALL FLOW VALUES TO AN OTHER WORKSPACE
C
      CALL SETPER('USRINT','WORK  ','FVEL  ',NFACE,JFVEL)
      DO 30 I=1,NFACE
       WORK(JFVEL+I-1  )= CONV(I  ,1)
 30    CONTINUE
C
```

Source (5.1) Fortran code to save the initial flow profile

The module USRSRC is added to the Fortran file to be able to set the flow profile dependent of time. The actual code that was added to this model is:

```
C SECTION WHERE THE DIFFERENT FLOW VALUES ARE SET
C
      CALL GETVAR('USRCVG','SCAL  ',ISCAL)
      IF (ISCAL.EQ.IEQN) THEN
C
C IF FLAGSIGN IS ZERO THE COPY IS SET BACK (SEE USERINT)
C STANDARD ALL IS SET TO ZERO
C
      TEMPTIME = TIME + 30.0
      FLAGSIGN=(TEMPTIME .GT. 40.0 .AND. TEMPTIME .LE. 65.0)
      CALL GETADD('USRSRC','PERMR ','FVEL  ',ILEVEL,JFVEL)
C
       DO 30 I=1,NFACE
       IF (FLAGSIGN.EQ.0) THEN
        CONV(I  ,1)=WORK(JFVEL+I-1)
       ELSE
        CONV(I  ,1)=0
       ENDIF
 30    CONTINUE
C
      ENDIF
```

Source (5.2) Fortran code to set the flow profile

A stop time of 25 seconds is implemented in the Fortran code above.

5.2.3.2 Pulsed flow numerical implementation.

The basic options (saving, and retrieving the flow profile) that are also necessary for the pulsed flow case were explained in the previous section. The only thing that is necessary is a piece of code that switches the different flow profiles (the steady state profile or the zero profile) with a certain frequency.

```
C
C IF FLAGSIGN IS ZERO THE ORIGINAL FLOW IS SET BACK (SEE USERINT)
C STANDARD ALL IS SET TO ZERO
C
      TEMPTIME = TIME + 30.0
      SETFLOW = AMOD(TIME,1.0)
      IF (NITER.EQ.1) THEN
       IF (SETFLOW .LT. 1.0e-1) THEN
         IF (FLAGSIGN .GT. 0.0)  THEN
          FLAGSIGN=0.0
         ELSE
          FLAGSIGN=1.0
         ENDIF
       ENDIF
      ENDIF
C
      CALL GETADD('USRSRC','PERMR ','FVEL  ',ILEVEL,JFVEL)
C
       DO 30 I=1,NFACE
       IF (FLAGSIGN.EQ.0) THEN
        CONV(I  ,1)=WORK(JFVEL+I-1)
       ELSE
        CONV(I  ,1)=0
       ENDIF
 30    CONTINUE
C
      ENDIF
```

Source (5.3) Fortran code to generate a pulse

A pulse is generated with a frequency of 1 Hz.

5.3 Results and discussion

5.3.1 Continuous flow.

A diffusion coefficient of 3.0 x 10^{-10} m^2 s^{-1} was adopted after several numerical calculations (with different coefficients) and comparison with the experimental 2 µl min^{-1} experiments.

The experimental curves can be seen in Figure (5.3) and the results from the numerical simulations can be seen in Figure (5.4). The x-axis in both figures is scaled (according to Figure (5.4)) to visualize the dispersion process, independent of the flow rate. It can be seen that decreasing the flow rate results in a decrease in dispersion. The results found in this paper support the statement of Růžička and Hansen [1].
Furthermore it can be concluded that convection still plays a very important role in the dispersion process. The assumption that in a µ-system the diffusion is dominant and likely to be true shortly after the injection as a result of the small dimensions is invalid for the µ-system (and sizes) used in this chapter.

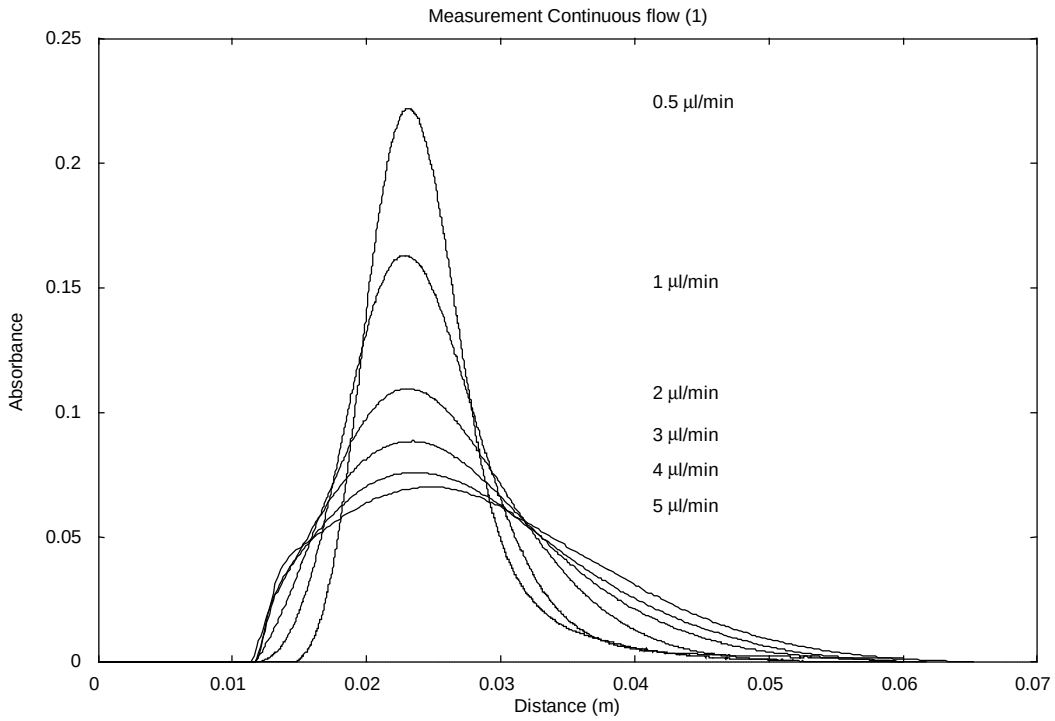

Figure (5.3) Experimental continuous flow rate measurements

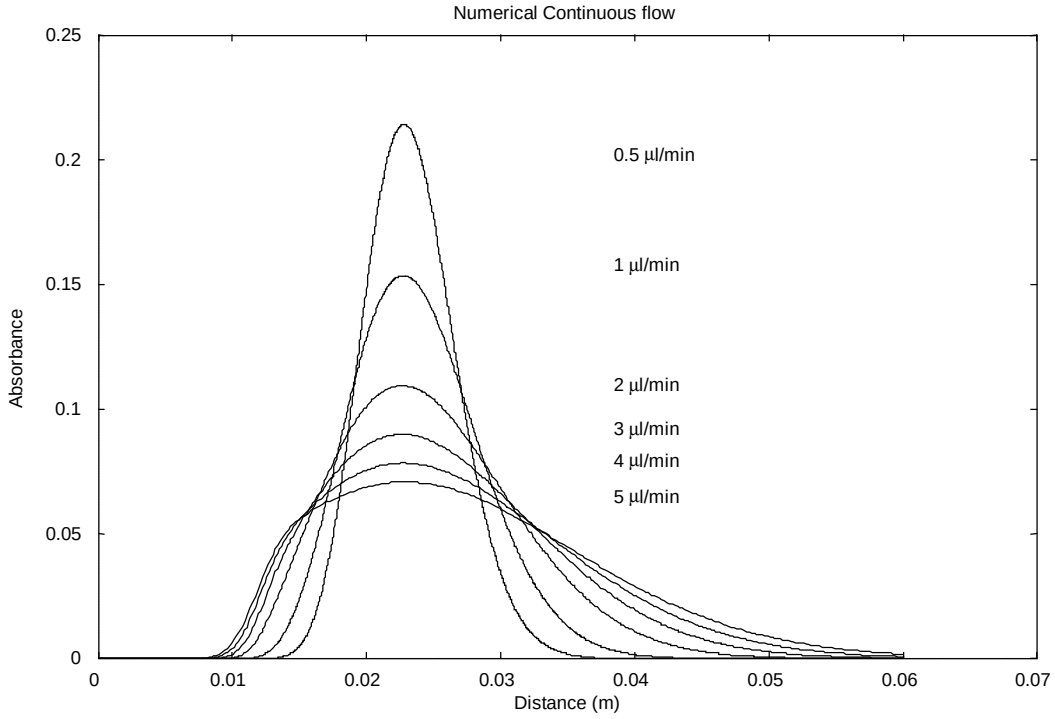

Figure (5.4) Numerical continuous flow rate measurements

A direct comparison between the experimental and numerical results can be seen for the flow rates 2, 3, 4 and 5 µl min^{-1} in Figure (5.5).
From Figure (5.3), Figure (5.4) and Figure (5.5) and, it can be concluded that the numerical approach matches the experimental values very well and that the model used is correct for this situation.

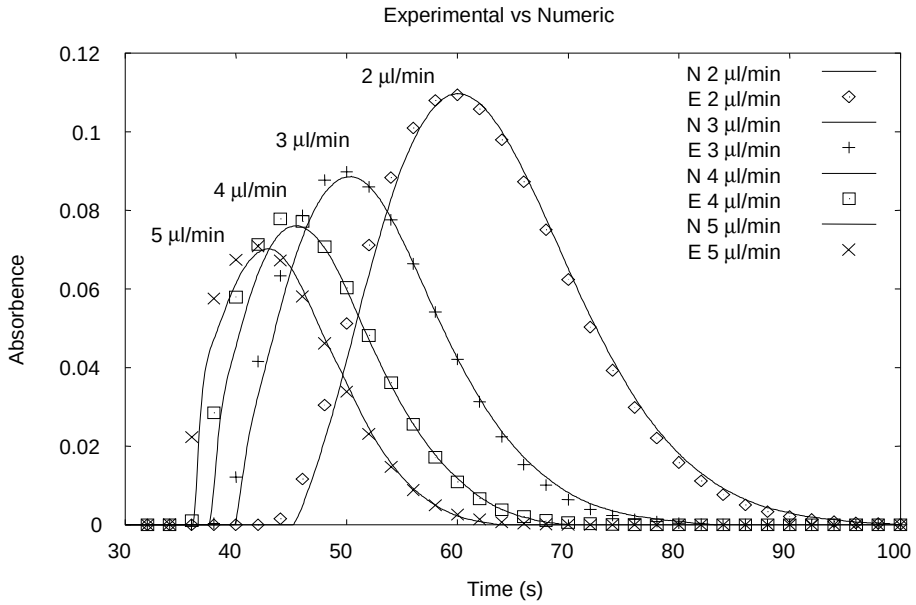

Figure (5.5) Continuous flow rate: numerical (N) vs. experimental (E)

5.3.2 Stopped flow.

Figure (5.6) shows the peak height versus the residence time with stopped flow and continuous flow. The ‘nflow’ line represents the peak height versus the residence time for the continuous flow experiments. The more horizontal lines represent the stopped flow experiments for the different flow rates.

The numerical simulations for stopped flow (2 µl min^{-1}) are also shown in Figure (5.6). The difference with the experimental values could be contributed to a numerical diffusion coefficient that is too large. The trend, however, is the same.

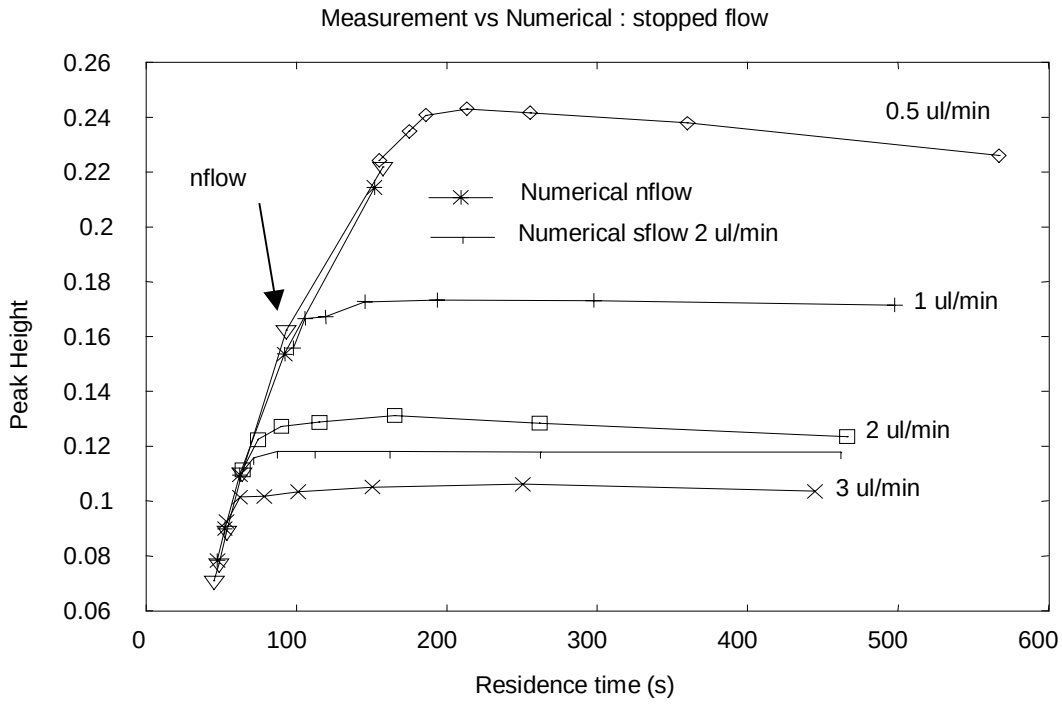

Figure (5.6) Peak height vs. residence time for stopped and continuous flow

From Figure (5.6) it can be concluded that (as in the macro case) the stopped flow period has little effect on the dispersion of the sample. The results for 4 μl min^{-1} and 5 μl min^{-1} are not shown in Figure (5.6). The measurement for these flow rates show significant smaller residence times that are caused by the way the residence time is determined. The sample has already reached the detector before the stop period begins. The residence time is the center of gravity of the signal. All the values for the residence time with 4 μl min^{-1} and 5 μl min^{-1} are therefore shorter.

5.3.3 Continuous flow vs. stopped flow.

To establish a certain residence time in a μ-FIA system, with the sizes used in this paper, the flow rate should be adapted. A decrease in flow rate shows a decrease in dispersion. If for some reason a decrease of the flow rate is not possible, stopped flow should be used with virtually no effect on the sample dispersion.
If the residence time is kept constant a smaller manifold with an accordingly lower flow rate should result in a decrease in dispersion.

5.3.4 Pulsed flow.

The numerical and experimental result can be seen in Figure (5.7) . This figure shows that in the range from 1 to 3 Hz the experimentally obtained peak

heights (the Exp line) are the same as for the ‘no pulse’ experiment (the Exp Cont line). Apparently the syringe pump has problems with frequencies above 3 Hz. The residence time of the response curves above 3 Hz is greater then the response curves below 3 Hz. These curves have a lower average flow rate and therefore a greater peak height.

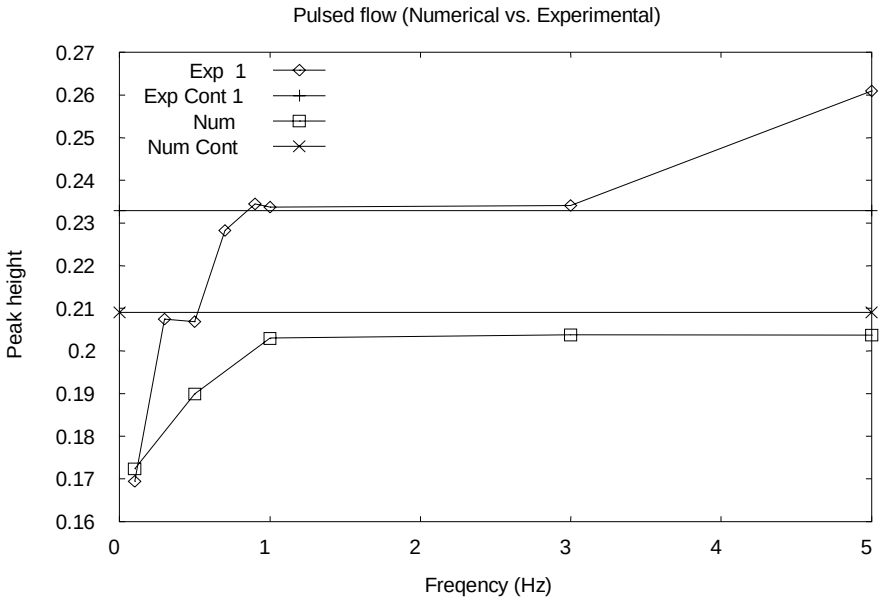

Figure (5.7) Peak height vs. frequency for pulsed flow

Frequencies below 1 Hz show a decrease in peak height. The residence time of the curves below 1 Hz are smaller and therefore the average flow rate is higher and the peak height smaller.
The ‘Num’ line and ‘Cont Num’ line show the results of the numerical simulations. The difference of the numerical result compared with the experimental values could be attributed to a numerical diffusion coefficient that is too large. The trend, however, is the same.
From these results it can be concluded that in this flow system the frequency has to be above 1 Hz and below 3 Hz to get (experimental) results that correspond with the continuous flow results.

5.4 References

[1] J. Růžička, and E.H. Hansen, Flow Injection Analysis, second edition, John Wiley & Sons, New York, 1988
[2] M. Valcárcel and M.D. Luque de Castro, Flow-Injection Analysis; principles and applications, Ellis Horwood Limited, English Edition, Chichester, 1987
[3] J.T. Vanderslice, A.G. Rosenfeld and G.R. Beecher, Anal. Chim. Acta., 179(1986)119
[4] J. van Kuijk, Numerical Modelling of Flows in Micro mechanical Devices, PhD. Thesis university of Twente, 1997

Chapter 6

Reactions in a micro flow injection system

6.1 Introduction

Often the analytes that have to be investigated, in a flow injection system, can not be detected directly. Reactions are necessary to convert the analyte to a product that can more easily be detected. It is also possible to develop a specific detector for the purpose, but this usually is accompanied by a large cost investment. It is often easier to search for a chemical solution to such a problem. The reader should realize that this is one important reason for the use of reactions in flow systems. Another reason could be, for example, that the reaction itself must be investigated.
There is a lot of literature on the use of reactions for the detection of different substances [1]. A flow system lends itself especially for the detection of substances in aqueous solutions. There are standard recipes for the detection of many metal ions, ammonia, anionic surfactants, arsenic, bicarbonate, boron etc. In Chapter 1 a flow injection system for the detection of chloride was mentioned. The measuring principle that can be used in such a system could be the reaction of chloride with mercury(II)thiocyanate. This reaction forms sparingly ionized mercury(II)chloride releasing an equivalent amount of thiocyanate. This thiocyanate forms a red complex with iron(III) that can be measured spectrophotometrically at 490 nm. This is a typical example of an indirect detection method.
Numerical simulations could be used to optimize a flow system regarding the amount of product produced. In the previous example this would be iron(III)thiocyanate. As a result of the optimization the detection limit is lowered. Another example is the investigation of the influence of a local heater on the reaction. The placement of such a heater could also be a worthwhile subject of study.
This chapter tries to check the numerical results against experimental results when a reaction is being used to convert the analyte to a measurable species.

6.2 Theory

Since the Navier-Stokes equations were explained in Chapter 2, this section will focus on the additional step, the reaction. A reaction can be described with the following equations:

For a reaction

$$a\,A + b\,B \rightarrow c\,C + d\,D \qquad \text{Equation (6.1)}$$

the rate equation is

$$r = -\frac{1}{a}\frac{d[A]}{dt} = -\frac{1}{b}\frac{d[B]}{dt} = \frac{1}{c}\frac{d[C]}{dt} = \frac{1}{d}\frac{d[D]}{dt} \quad [mol/l*s] \qquad \text{Equation (6.2)}$$

$$r = k[A]^{n1}[B]^{n2} \qquad (n1 + n2 = overall\ reaction\ \ order) \qquad \text{Equation (6.3)}$$

where A and B are the two reactants, C and D are the products, r the reaction rate and k the reaction constant (l/(mol s)). The [ ] notation specifies the concentration in mol/l.

If for example the stoichiometry of the reaction is 1:1 (1 mol A reacts with 1 mol B) and it is first order for A and B and second order overall. The reaction can be described with Equation (6.4)

$$A + B \xrightarrow{k} C \quad and \quad -\frac{d[A]}{dt} = k[A][B] \qquad \text{Equation (6.4)}$$

Once the reaction constant k, the stoichiometry and reaction orders are known, the reaction can be modeled. The reaction constant (chemical kinetics) must be determined by experiment because it can not be predicted from the stoichiometric equation [2].
The reaction constant k is dependent on the temperature. In1889, Arrhenius pointed out that this rate constant could be described with

$$k = A\,e^{-\frac{E_a}{RT}} \qquad \text{Equation (6.5)}$$

where A and E_a are constants : A is called the pre-exponential factor, E_a the activation energy, R is the gas constant and T the absolute temperature.

There are all sorts of different reactions possible. Next to second or third order reaction, competing or consecutive reactions can occur.
An example of a consecutive and competing reaction (with three first order reactions) could be

$$A + B \xrightarrow{k_1} E \qquad and \qquad -\frac{d[A]}{dt} = k_1[A][B] \qquad \text{Equation (6.6)}$$

$$A + D \xrightarrow{k_2} 2C + E \qquad and \qquad -\frac{d[A]}{dt} = k_2[A][E] \qquad \text{Equation (6.7)}$$

$$B + C \xrightarrow{k_3} D \qquad and \qquad -\frac{d[B]}{dt} = k_3[B][C] \qquad \text{Equation (6.8)}$$

The decrease of A depends directly on two reactions. The slowest reaction will be the rate determining step. The second reaction also depends on the third reaction.

Equation (6.5) is used in the numerical calculations. The production (or consumption) of species is included in the binary diffusion equation

$$\frac{\partial \rho Y_A}{\partial t} + \nabla \cdot (\rho U Y_A) - \nabla \cdot (\rho D_{AB} \nabla Y_A) = r_A \qquad \text{Equation (2.27)/ Equation (6.9)}$$

The term r_A is the production or consumption of mass of species A per volume per time. This corresponds to the reaction rate used in Equation (6.3) with a conversion to mass fraction and summation over all the different reactions and their contribution to the production or consumption of species A.
To illustrate the introduction of a reaction and the impact on the procedure to solve the problem, we refer back to an example used in chapter 3 with the following equations (a source term is added) :

$$f(\phi_1) = a\phi_1^2 + b\phi_1 + c = R \qquad \text{Equation (6.10)}$$

$$g(\phi_2) = p\phi_2^2 + q\phi_2 + r = R \qquad \text{Equation (6.11)}$$

There are two dependent variables ϕ_1 and ϕ_2. The coefficients a, b and c are functions of ϕ_2 and p, q and r are functions of ϕ_1. The iteration scheme for solving this system of equations is given in Figure (3.9). The contribution of the reaction is called R and depends (in this case) on the reaction constant and the concentration of ϕ_1 and ϕ_2.

$$R = k\phi_1\phi_2 \qquad \text{Equation (6.12)}$$

If, for example, ϕ_2 is taken as fixed b, could be rewritten as $k\phi_2$ (a similar discussion could be held for the situation with ϕ_1 fixed). The same mechanism can now be used to solve the problem with a reaction.

6.3 Experimental and numerical

Before any experimental work can be done, the reaction to be studied has to be chosen. Since BromoCresol Green (BCG) was used in the previous chapters and the detection system worked successfully, a reaction with BCG and the current detection system is preferred. BCG is an indicator that has its pH transition interval between pH=3.8 (yellow) and pH=5.4 (blue) In the previous chapter we worked with basic solutions to keep BCG in the basic (blue) form. A reaction that we can study is the bleaching (oxidation) of the basic form of BCG in a basic or neutral background solution. A phosphate buffer of pH 7.0 was selected for this purpose. Sodium hypochlorite (NaOCl) is a strong oxidator and can be used for bleaching the BCG [3].

From literature we learn that the reaction scheme, with BCG and hypochloride, is not fully known. Pickering [3] suggests two possible mechanisms:

The rate determining step will be, in either case

$$Rate = k[dye][attacking\ species] \qquad \text{Equation (6.13)}$$

One where HOCl is the attacking species according to:

$$H_2O + OCl^- \quad \Leftrightarrow \quad OH^- + HOCl \qquad \text{Equation (6.14)}$$

and

$$Rate = K_1 \frac{[OCl^-]}{[OH^-]}[Dye] = K_1'[OCl^-][Dye] \qquad \text{Equation (6.15)}$$

Since a buffer is used the OH^- concentration is constant and can be incorporated into the constant K_1'. The reaction in Equation (6.14) is assumed to be fast [4].

The second where Cl_2 is the attacking species, formed in a preceding reaction

$$H^+ + OCl^- + Cl^- \quad \Leftrightarrow \quad Cl_2 + OH^- \qquad \text{Equation (6.16)}$$

and

$$BCG(Blue) + Cl_2 \rightarrow BCG(oxidized) + 2Cl^- \qquad \text{Equation (6.17)}$$

and

$$Rate = K_2[Cl_2][Dye] = K_2'[OCl^-][Cl^-][Dye] \qquad \text{Equation (6.18)}$$

Again constant concentrations are incorporated into the constant K_2'. The reaction described in Equation (6.17) is assumed to be the rate determining reaction [5].

Pickering indeed saw a first-order hypochlorite and Cl^- dependence and suggests a second order base dependence. Since we work in a buffer solution, the base dependence can be neglected. So there are two alternative reactions schemes possible.

The second attacking species Cl_2 has to be formed according to Equation (6.16). The concentration of Cl^- needed for this reaction is probably formed from the decomposition of OCl^- in solution. This however will be not a great amount.

The previous can be summerized in the following reaction scheme:

The simple reaction scheme:

$$A + B \xrightarrow{k_1} E \qquad and \quad -\frac{d[A]}{dt} = k_1[A][B] \qquad \text{Equation (6.19)}$$

The complex reaction scheme:

$$A + D \xrightarrow{k_2} 2C + E \qquad and \quad -\frac{d[A]}{dt} = k_2[A][E] \qquad \text{Equation (6.20)}$$

$$B + C \xrightarrow{k_3} D \qquad and \quad -\frac{d[B]}{dt} = k_3[B][C] \qquad \text{Equation (6.21)}$$

with A represents BCG, B represents OCl^- (or HOCl), C represents Cl^-, D represents Cl_2 and E represents the oxidized BCG.

For the numerical calculations we shall, at first, assume that only HOCl is the attacking species (Equation (6.19).

6.3.1 Determination of the reaction constant

The reaction constant was measured on a spectrophotometer under the same conditions (equal concentrations and temperature) as with the measurements in our micro system (see section 6.3.2). A BCG and NaOCl solution of equal concentration (1e-3 mol/l) were put together and the concentration of BCG versus time was measured. Plotting the 1/[BCG] versus time should results in a straight line where the slope represents the reaction constant [2]. Different experiments showed that the (average) reaction constant is 2000 l/(mol*s).

Experiment	Reaction constant (l/(mol*s))
1	2041
2	1857
3	2100

Table (6.1) The reaction constant.

6.3.2 Experimental micro-FIA setup

The same experimental setup as in Chapter 4 and 5 was used in this chapter. The left channel in Figure (4.15) was used. Figure (6.1) shows an enlargement and the place of the detector. The detector was placed at 19 mm from the injection point. The sample was a buffer solution (pH=7.0) with a concentration of $1*10^{-3}$ mol/l BCG. The carrier was a buffer solution (pH=7.0) with a concentration of $1*10^{-3}$ mol/l NaOCl.

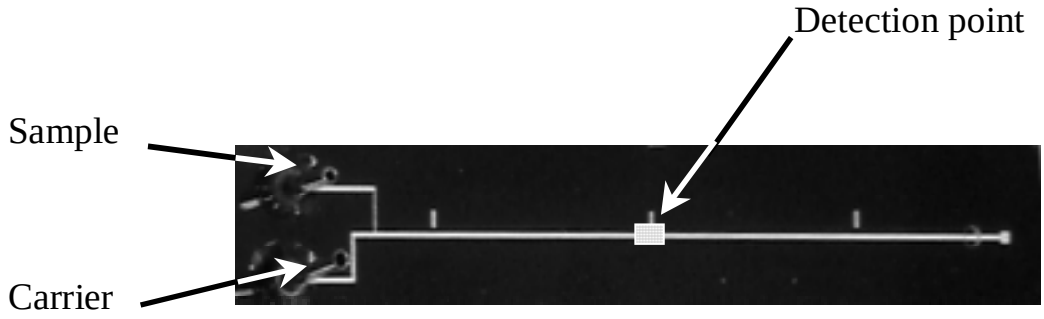

Figure (6.1) Location of the detection point.

A measurement consists of the following procedure:

1) 10 seconds of propelling of the carrier stream with X µl min^{-1}
2) stopping the carrier syringe and starting the sample syringe
3) 20 seconds of sample injection with 0.2 µl min^{-1}
4) stopping the sample syringe and starting the carrier syringe (X µl min^{1})

X refers to the flow rate under investigation.

For the stopped flow measurements this procedure was extended with the following step:

5) stopping the carrier syringe during Y seconds, 10 seconds after injection (point 4)

Measurements were made with different flow rates. The first series comprises the transport of BCG through the system without a reaction. Each experiment was repeated three times to check the reproducibility. Next NaOCl was added to the carrier and the measurements were repeated. In the last series of experiments a stopping time was added. Since the reaction should give a result that can be detected by the detector, the begin of the stop period was adjusted to the flow rate. The duration of the stop period was in each case 15 seconds.

Flow rate (µl/min)	Begin stop period (s)
2	43
3	40
5	35

Table (6.2) Stop periods for the different flow rates.

For the system shown in Figure (6.1) a calibration line was made (with only the buffer solution as carrier).

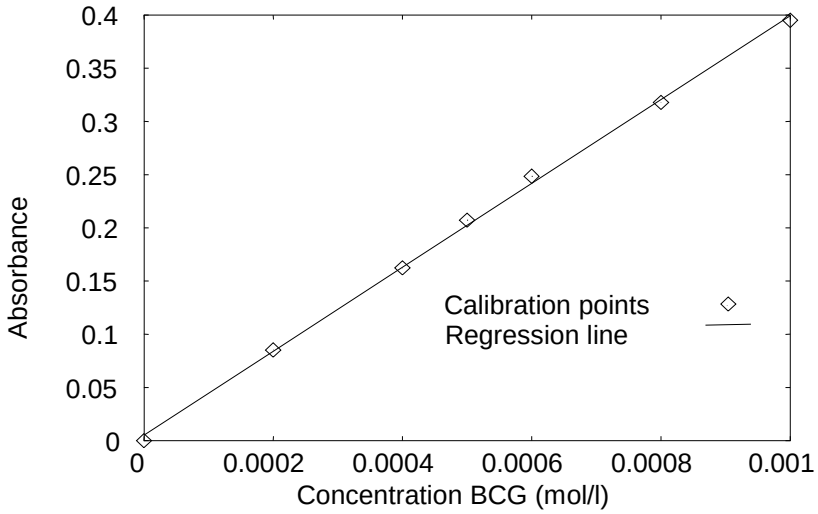

Figure (6.2) Calibration line.

The regression line is:

$$y = 394.13x + 0.0052 \quad \text{with} \quad R^2 = 0.9989 \qquad \text{Equation (6.22)}$$

where x represents the concentration BCG and y represents the measured absorbance. The measured absorbance represents the average value of

the amount of BCG present in the detector. The calibration line can now be used to convert absorbance values to (average) concentration values in the detector.

6.3.3 Numerical micro-FIA setup

The numerical setup can be seen in Figure (6.3).

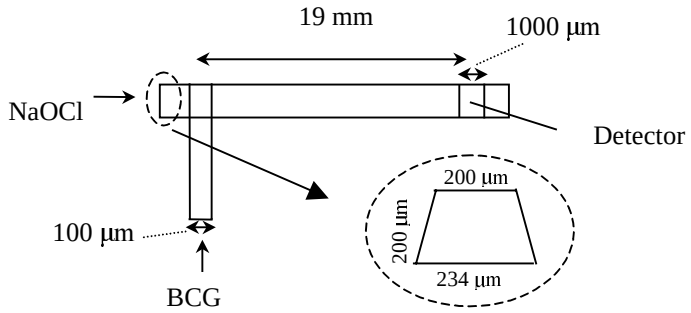

Figure (6.3) Numerical μ-system.

One of the problems (compared to the previous chapters) is the fact that the injection has to be simulated. Already during the injection the reaction will occur. This would mean that with a block injection the injection (and reaction) is not simulated correctly. We saw in chapter 3, section 3.3.2.8, that switching the inlet flow velocities and recalculations of the flow profile at each time step would take a lot of computer time. For this reason two flow profiles were calculated in two separate flow calculations. After each calculation the flow profile is written to a file (one for the injection and one for the normal carrier flow). At the appropriate times (0 second and 20 second), during the sample transport calculations, these flow profiles are read from the specific file and used to simulate the injection and the transport of the sample.

The following parameters were used in the numerical calculations :

- The time step used in the numerical calculation is 0.5 seconds (Crank Nicolson).
- The diffusion coefficient of BCG was set to 3.0e-10 m^2/s.
- The diffusion coefficient of HOCl was set to 30.0e-10 m^2/s.
- The element length was 15 μm (at steep gradients points).
- Both the flow profiles were calculated to an accuracy of R_{sum} 1e-15.
- The convection diffusion calculations were stopped at each time step when the R_{sum} of the BCG concentration was 1e-12 or lower.
- HOCl concentration 1e-3 mol/l

- BCG concentration 1e-3 mol/l
- A reaction constant of 2000 l/(mol*s) was used (Equation (6.19))

Additional information needed for the reaction scheme with Cl_2 as the attacking species.

- The initial concentration of Cl^- and Cl_2 in the carrier was estimated to be 1e-6 mol/l.
- The reaction with BCG was taken to be the rate determining step with a reaction constant of 2000 l/(mol*s) (Equation (6.20)).
- The reaction that formed Cl_2 was estimated to have a reaction constant of 5000 l/(mol*s) (Equation (6.21)).
- The diffusion coefficient of Cl_2 and Cl- was set to 1e-6 m^2/s.

6.4 Results

6.4.1 The experimental results

The results for three different experiments (at three different flow rates) can be seen in Figure (6.4), Figure (6.5) and Figure (6.6).

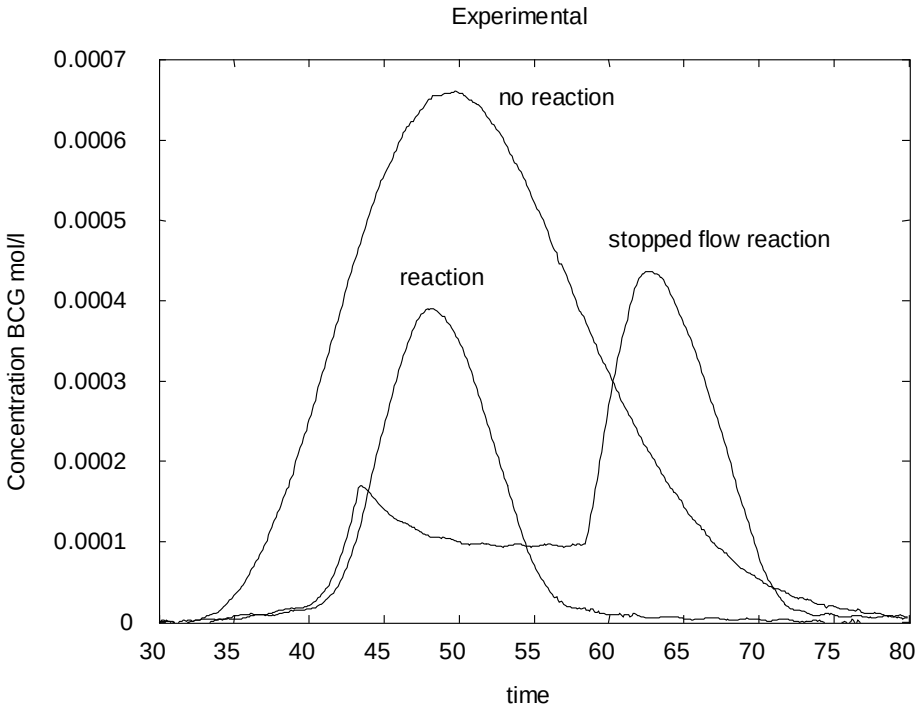

Figure (6.4) Experimental results 2 µl/min.

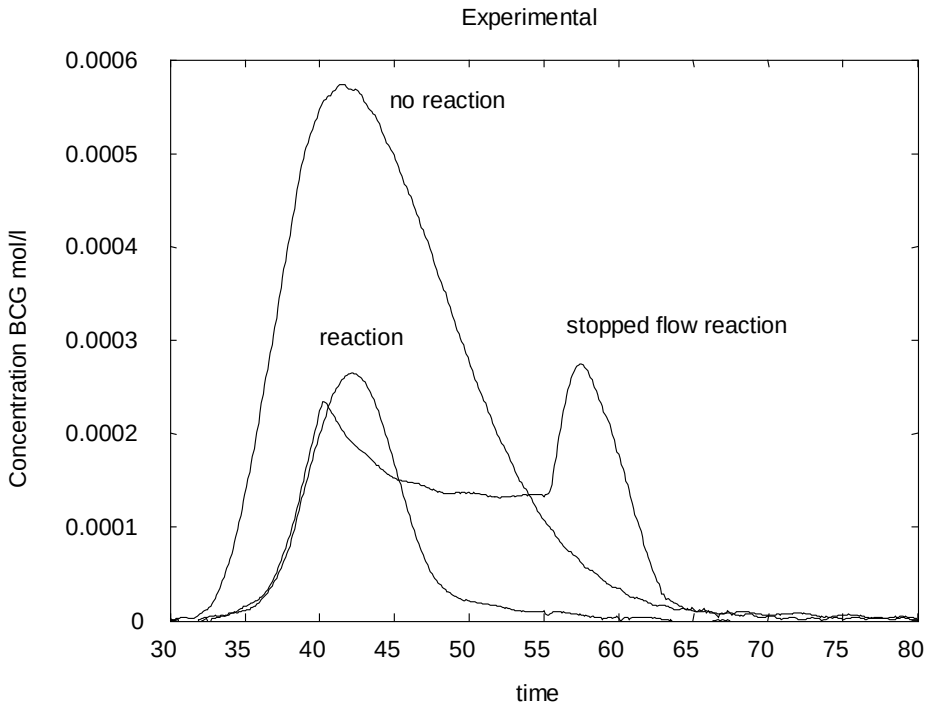

Figure (6.5) Experimental results 3 µl/min.

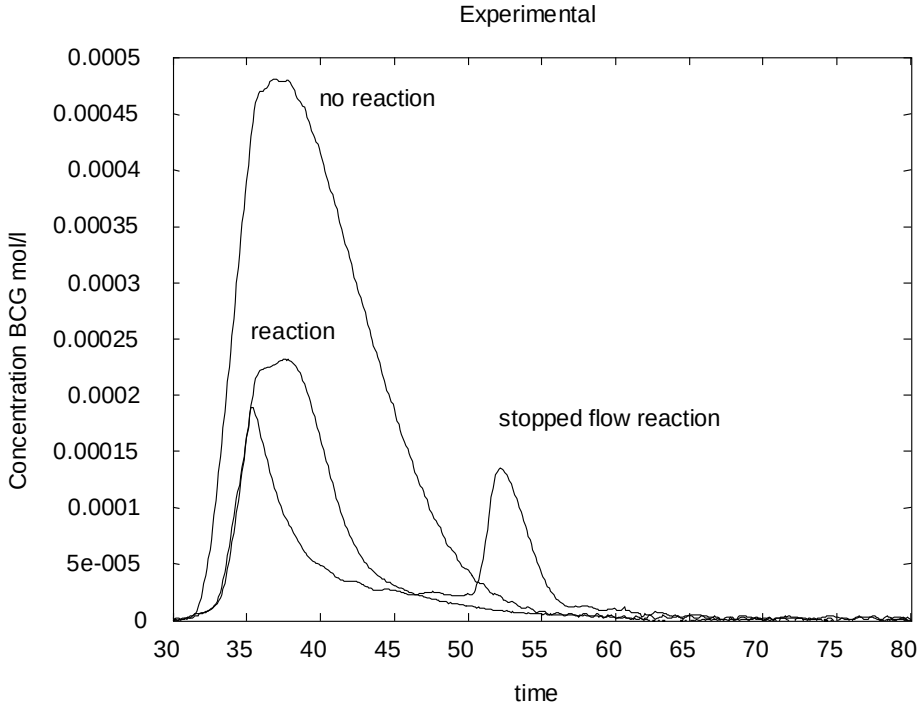

Figure (6.6) Experimental results 5 µl/min.

The experimental results show for the curve with no reaction that the residence time decreases (as expected) and the peak height also

diminishes with increasing flow velocity. The curve with reaction shows that part of the BCG has reacted. The stopped flow curve contains more information. Apparently the concentration of attacking species in the detector (with all the different flow rates) is lower than the concentration of BCG, because the BCG reacts but the curve doesn't reach zero. After the stop period (when the flow is turned on) the peak height (of the remaining BCG) becomes lower with increasing flow rate. This happens faster than for the peak height without the stopping period.

6.4.2 The numerical results

Before we can calculate the dispersion, the maximum time step has to be established. The relatively large residence time makes it impossible to calculate with a time step of 0.01 (see section 3.3.2.6), but a time step of 0.5 produces reasonable results in acceptable calculation times (see Figure (6.7)).

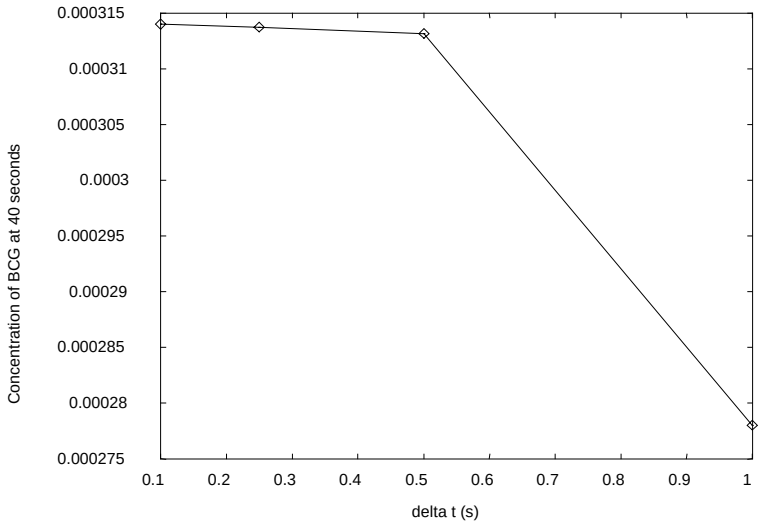

Figure (6.7) Determination of the maximum time step.

The maximum element length is taken according to the guidelines set in the earlier chapters.

6.4.2.1 The simple reaction scheme

The simple reaction scheme is the reaction scheme with HOCl as the attacking species (see Equation (6.19))
The next figures (Figure (6.8), Figure (6.9) and Figure (6.10)) show that the dispersion without a chemical reaction is predicted accurately. From these figures we can conclude that the numerical injection procedure gives excellent results.
The numerical results for the calculations with no reaction follow the same trend as can be seen in the previous chapters and from the experimental results. As the flow rate increases the residence time and the peak height decreases.
The numerical results for the reaction show that the residence time remains the same compared to the no reaction curves, but the curve gets lower and less broad. This agrees with the fact that BCG reacts.
The stopped flow results show that BCG doesn't decrease during the stop period. Only the stopped flow results for a flow rate of 5 µl/min shows a slight decrease of BCG after the beginning of the stop period. After the stop period the resulting peak is higher than the peak height without the stop period (and with reaction) for each of the different flow rates.

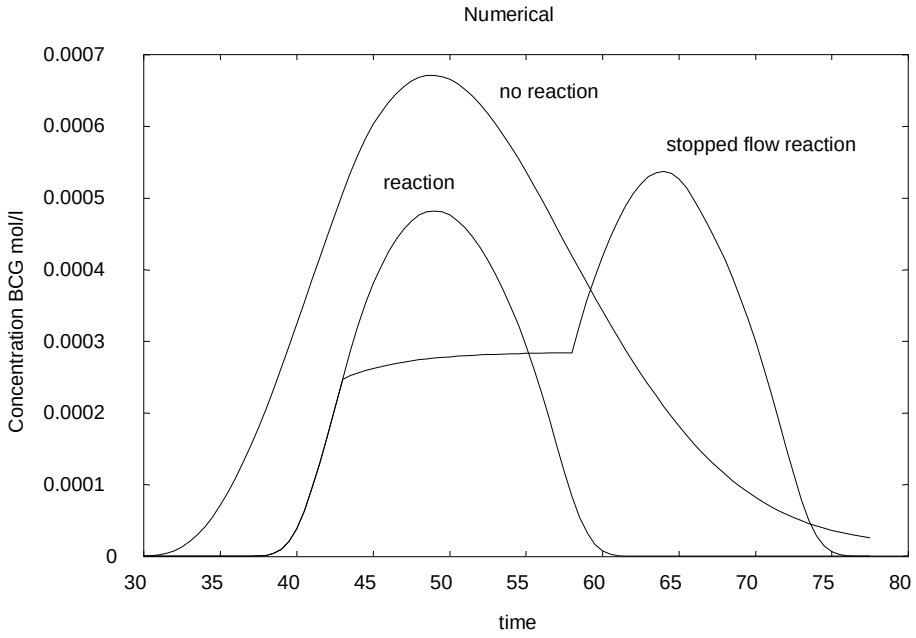

Figure (6.8) Numerical results 2 µl/min.

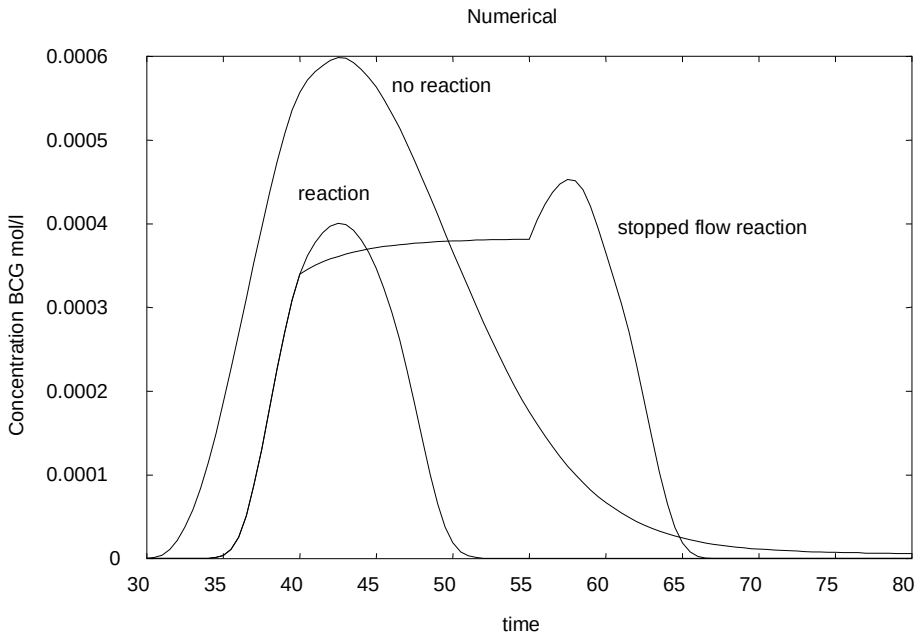

Figure (6.9) Numerical results 3 μl/min.

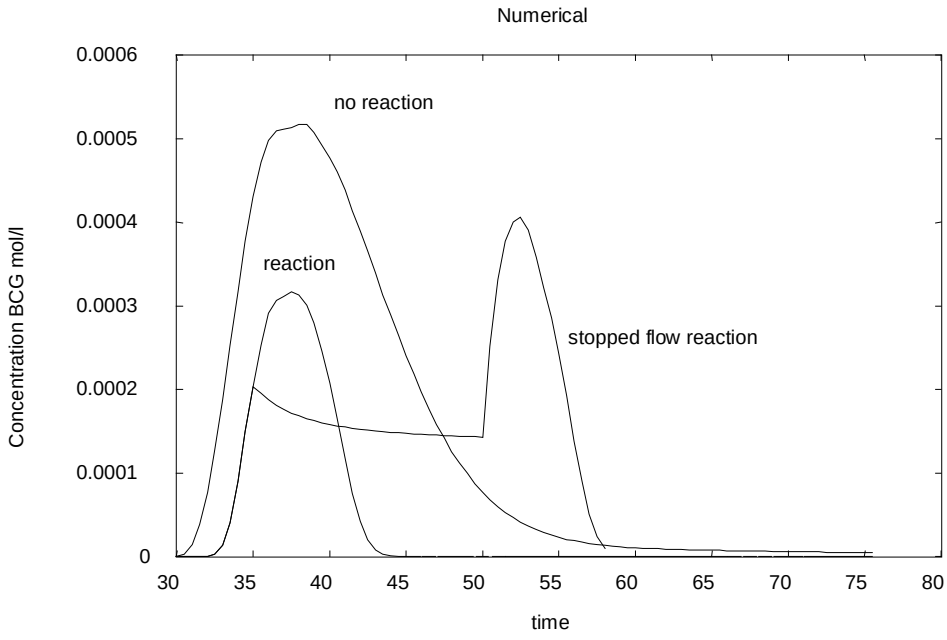

Figure (6.10) Numerical results 5 μl/min.

The total hypochlorite concentration versus time can be seen in Figure (6.11) in case of stopped flow. From this figure it can be seen that total hypochlorite concentration is (almost) zero during the stop period (40 – 55 seconds).

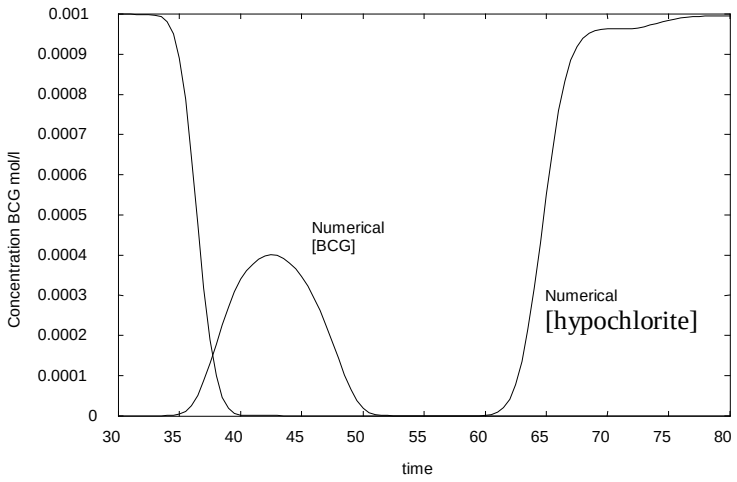

Figure (6.11) The total hypocholride concentration versus time for 3 µl/min.

6.4.2.1.1 The influence of the NaOCl concentration.

Figure (6.12) shows the effect of increasing the NaOCl concentration in the carrier in the numerical stopped flow experiments. The numerical calculations in Figure (6.12) were done with a time step of 1 second to speed up the calculations. Although not accurate the results should give an indication of what happens.

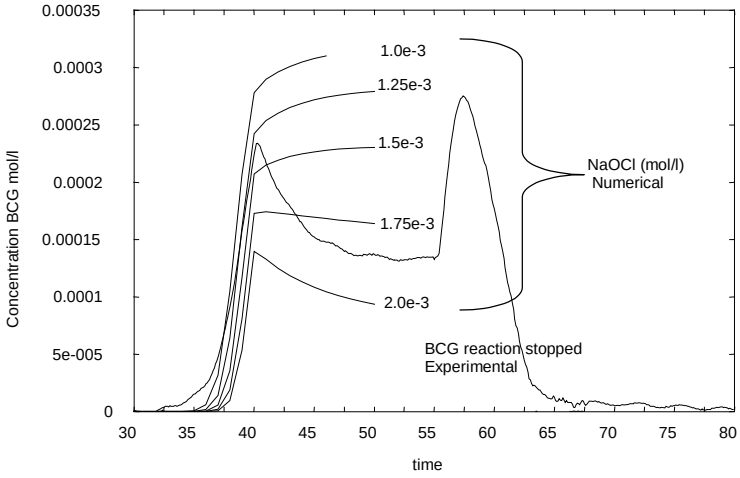

Figure (6.12) The effect of different NaOCl concentrations (k=1600).

6.4.2.1.2 The influence of the reaction constant.

Figure (6.13) shows that changing the reaction constant has very little effect on the response curve up to the stopping point (for 3 µl/min).

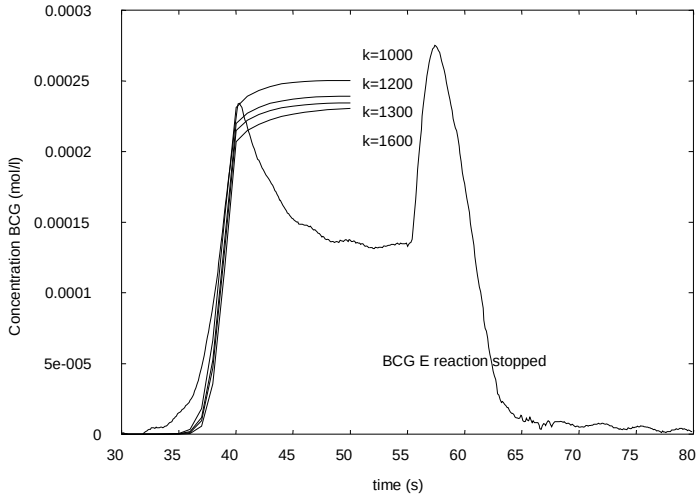

Figure (6.13) The effect of the reaction constant (NaOCl = 1.5e-3 mol/l).

6.4.2.1.3 The influence of the diffusion coefficient of the attacking species

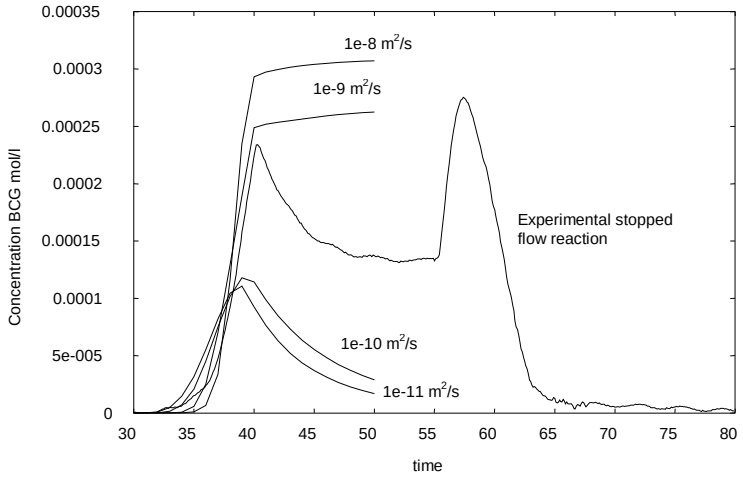

Figure (6.14) The effect of the diffusion coefficient of the hypochoride.

BCG reacts with the attacking species (see section 6.2). In Figure (2.8) we have seen the effect of different diffusion coefficients on the dispersion of

BCG in a flow system. Figure (6.14) shows the effect of the diffusion coefficient of attacking species (HOCl).

6.4.2.2 The complex reaction scheme

The complex reaction scheme is the reaction scheme with Cl_2 as the attacking species (see Equation (6.20) and Equation (6.21)).
Figure (6.15) shows the calculated results with this complex reaction scheme.

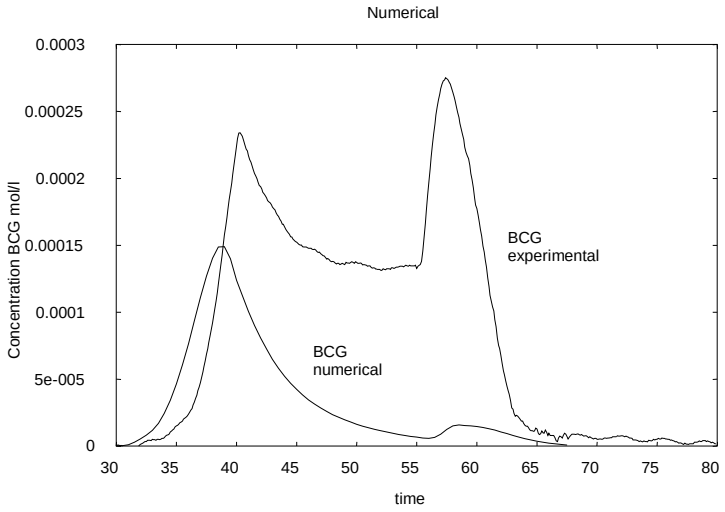

Figure (6.15) Stopped flow reaction with Cl_2 as the attacking species.

Only the stopped flow results for the flow rate of 3 µl/min are shown in Figure (6.15). The decrease of BCG during the stop time is clearly visible.

6.5 Discussion and conclusions

At all the chosen flow rates the numerical results show a good correspondence to the experimental results regarding the response curve without a reaction. The ability to calculate the dispersion of BCG in a flow system was also established in the previous chapters. The results also show that the numerical injection method is correct (switching between two flow profiles).

The numerical results for the simple reaction scheme and the experimental results are different. In the real experiments more BCG reacts and the reaction proceeds over a longer period, which is clearly visible during the stopped flow period.
In the numerical model with the simple reaction scheme the concentration of the oxidizing species in the detector has been exhausted at the start of

the stop period (see Figure (6.11)). In reality this is clearly not the case as can be seen from the decrease of the BCG concentration in the detector during the stopped flow period in Figure (6.4), Figure (6.5) and Figure (6.6). The calculation with the use of the complex reaction scheme (see Figure (6.15) does show this experimentally observed decrease of the BCG concentration during the stopped flow period. Quantitatively , however, the agreement between the calculations and measured signal is bad, presumably because of the errors in the assumptions on the data with regard to the formation of the Cl_2 species.
Nevertheless these results indicate that the complex reaction scheme is the more probable one and certainly show that the CFD-tools described in this thesis can be used to identify and quantify parameters that are important in the optimization of the reactor section of a micro flow injection analysis system.

6.6 References

[1] A. Greenberg, J. Connors, D Jenkins, “Standard methods; For the examination of water and wastewater, fifteenth ed., Washington, American Public Health Association, 1980

[2] B.C. Cox, “Modern Liquid Phase Kinetics”, Oxford University press, 1994

[3] M. Pickering, D. Heiler, “Kinetics of oxidation of bromcresol green.”, *J. Chem. Educ.* 1987 *64* 81.

[4] M.J. Pilling, P.W. Seakins, “Reaction kinetics”, Oxford University Press, 1995

[5] W.J. Moore, “Physical Chemistry”, Prentice-Hall, 1972

Chapter 7

Conclusions and suggestions for further research

7.1 Conclusions

The general conclusion is that it is possible to accurately predict the dispersion of a sample, with the use of the Navier-Stokes equations, in a micro flow system. A one to one translation can be made which means that only fundamental parameters are needed to successfully model a flow injection system. The fundamental parameters, in this thesis, are the concentrations, the diffusion coefficients, the geometry, the flow rates and in case of a reaction the reaction constant, equations and order. There is no need for a “match” or fitting factor.

Some conclusions that can be made from the numerical simulations in this thesis:

- The numerical problems with the convection term can best be solved by the use of the “quick” or “ccct” scheme.
- The element length of a control-volume, in the neighbourhood of a steep variation of the dependent variable with one of the space coordinates, should be smaller than 15 μm.
- The largest time step that produces realistic and accurate results is about 0.01 second. The best time stepping scheme was Crank-Nicolson.
- The application of a non-uniform grid is recommended to solve the a problem, because it saves considerable calculation time and does not result in an excessive amount of memory needed. A well constructed non-uniform grid can give the same accuracy as a uniform grid.
- To further save calculation time, it was shown that it is allowed to decouple the flow calculation from the convection-diffusion calculation. Further more it could be seen that the time based injection can be replaced with an injection block. This procedure allows elimination of the injection calculation, thereby reducing also the calculation time.

The appropriate time step and element length should be established separately for each different problem.

In chapter 4 the effect of sharp or smooth bends on the dispersion of a sample injected into a flow system was studied. The conclusions that can be made from this chapter are:

- The use of sharp bends to establish a flow system with a certain travelling distance within a small area has minimal effects on the dispersion of a sample (under the conditions described in chapter 4).
- The comparison, between numerical and experimental results (in chapter 4), shows that the numerical model used in this chapter could be used as a numerical pre-analysis tool. The general numerical model allows the calculation of the flow profile, pressure distribution and the concentration distribution of the sample, three dimensional, throughout an arbitrary channel.

In chapter 5 the effect of different flow conditions on the dispersion of a sample injected into a flow system was studied. The conclusions that can be made from this chapter are:

- The assumption that in a μ-system the diffusion is dominant shortly after the injection, as a result of the small dimensions, is invalid for the μ-system and sizes used in this chapter 5.
- The stopped flow period has little effect on the dispersion of the sample. (This is also the case in macro flow systems).
- From the experimental results, it can be concluded that in the flow system, used in chapter 5, the frequency of the pump (pulsed flow) has to be above 1 Hz and below 3 Hz to get (experimental) results that correspond with the continuous flow results.
- The numerical results support the previous statement for the lower frequency range.
- To establish a certain residence time in a μ-FIA system, with the sizes used in this thesis, the flow rate should be adapted. A decrease in flow rate shows a decrease in dispersion. If for some reason a decrease of the flow rate is not possible, stopped flow should be used with virtually no effect on the sample dispersion. This decrease in flow rate will effect the sample throughput.

In chapter 6 a reaction was studied. It was found that the situation gets a lot more complicated when a reaction is involved. The reaction that was taken for the comparison between experimental measurements and numerical calculations was perhaps not a very good choice. The numerical calculations suggest the same trend as the experimental measurements but there is a difference and this it likely to be caused by the reaction scheme used in the calculations.

It should be clear that the numerical model, used in this thesis, is able to accurately predict the dispersion of a sample in a flow injection system (with the restrictions mentioned in this thesis). The three-dimensional model used in this thesis allows the investigations of different geometries, flow rates, reaction (schemes) and different types of detectors. The applicability is only restricted by the imagination of the user. To illustrate the versatility of the numerical approach we refer back to the 4 modules, mentioned in chapter 1, that construct a flow injection system, and give some pointers on the use of numerical modeling with each module.

The pump module

Different flow rates and pulsed flows were investigated in this thesis. There are of course different mechanisms of propulsion that could be investigated.

The injection module

Different injection modules can be modeled. Normally an injection is done with a fixed sample loop. This method is more accurate than the time based injection. One major advantage of a numerical model is the ability to vary the injection volume quite easily. In macro FIA systems the injection model is usually build up with the use of a fixed sample loop. The sample loop usually is a piece of tubing that can be replaced but this takes some work. In micro systems, however, the sample loop is fixed. Changing the injection volume would mean the construction of a new device. The advantage is information about the effect of the injected volume and perhaps an accurate estimate of the optimal sample loop can be obtained.

The transport module

The transport module consists of tubing, connectors, reactors and mixing devices. This thesis investigated the effect of bends on the dispersion. Again a lot more is possible. The throughput of a device could be investigated in conjunction with different geometries and flow rates. Reactors and mixing devices depend on the ability of the device to bring (a) substance(s) in contact with (an)other substance(s). The effect of different geometries and flow rates on the mixing quality or the production of a reactor could be investigated numerically. Especially the effect of the geometry is experimentally difficult to investigate without making a lot of devices.

The detection module

The ability to investigate the effect of the geometry or placement of a detector on the response curve. This could be a three-dimensional detector (used in this thesis) or a two-dimensional detector. Again experimental investigation of the

different detectors is not possible without the (costly) construction of different detectors.

7.2 Suggestions for further research

7.2.1 Positioning of a two dimensional detector

An interesting topic for further research could be the optimization of the channel structure for the use of a two dimensional detector. In this thesis the detection principle was based on absorption of light that passed through the flow channel. A lot of detectors, such as electro-chemical sensors, have to be placed along the channel wall. Preliminary numerical studies show that with a small adaption of the channel structure the two-dimensional (wall) detector should give a better response.
Figure (7.1) shows for example the effect of a detector placed with an offset from the channel. The placement of an obstacle results in a better response of the detector.

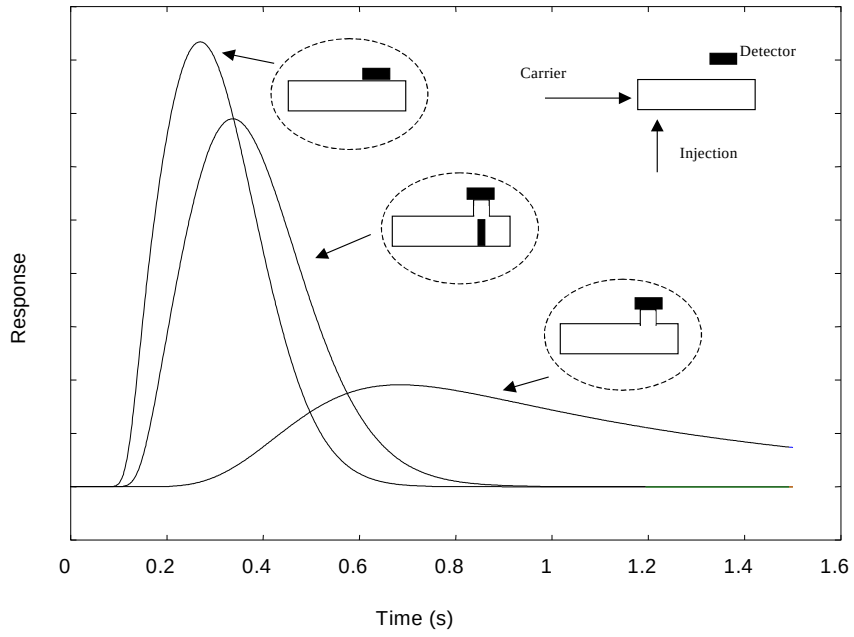

Figure (7.1) The different detector positions.

The previous example is a simple one, but shows that the effect can be large and deserves attention. A numerical tool allows the investigation off all sorts of different geometrical options.

7.2.2 The effect of downscaling on the dispersion

Another aspect that needs further attention is what happens to the dispersion when the size of the channel gets even smaller. The effects of miniaturization can best be explained with the use of Figure (7.2). This figure shows the different regions of validity for different solutions to the convection-diffusion equation. The (radial) Péclet number (P) is plotted against reduced time (τ) [1]. The Péclet number represents the ratio of mass transport by convection and by diffusion:

$$\mathrm{Pe_R} = \frac{2 < v > R}{D} \qquad \text{Equation (7.1)}$$

where R is a characteristic length equal to the tube diameter, D is the diffusion coefficient and <v> is the mean linear velocity.

τ represents the dimensionless number related to the residence time (t_v):

$$\tau = \frac{t_v D}{R^2} \qquad \text{Equation (7.2)}$$

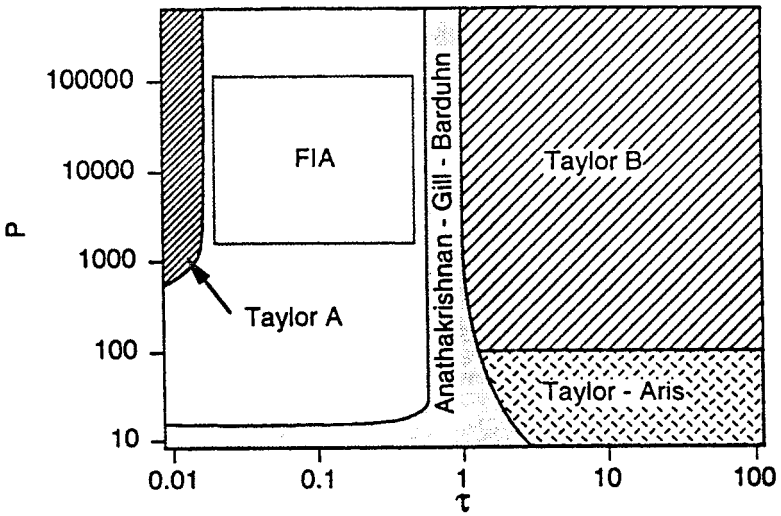

Figure (7.2) Regions of validity for various solutions of the convection diffusion equation.

In the Taylor and Taylor-Aris regions, the dispersion, can be descibed with relatively simple equations. The Taylor B regime assumes a predomination of molecular diffusion [2]. Aris provided an adaption to the Taylor approximation by allowing for a substantial increase in radial mixing by diffusion [3], the Taylor-Aris regime. In the Taylor A regime, convection predominates. The

macro FIA working area is placed outside any of these regimes. The numerical model used in this thesis describes the total area, but takes a lot of computer power and time. So it would be very useful if we could describe dispersion in a μFIA system with equations that are as simple as the Taylor equations.
Luckily with miniaturization the working area of FIA shifts to the Taylor B and Taylor-Aris regions. Figure (7.3) shows the position of a FIA system with a decrease in the diameter while keeping the flow rate, length and diffusion coefficient constant (for a straight round tube). This figure shows that downscaling to a diameter of 25 μm brings the system into the Taylor area. Further downscaling brings the system into the Taylor-Aris area.
The dimensions of the flow system are shown in Figure (7.3). The system goes through three regions. The expectation is that in the left part of Figure (7.3) (convection dominates) a sharp peak is followed by a long tailing section. In the Taylor region a perfect gaussian peak should be observed. In the Aris-Taylor regime the peak should still be gaussian, but less high and a bit broader than in the Taylor section.
The optimal dimensions, regarding dispersion should be between 50 μm and 20 μm.

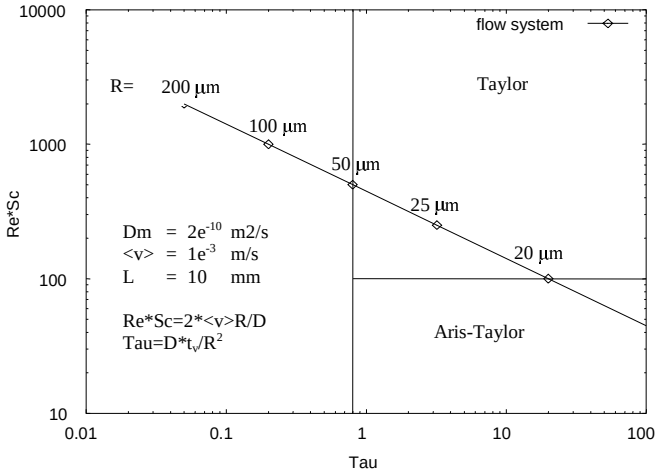

Figure (7.3) Regions of validity.

Figure (7.4) shows the response curve for different diameters. The response curve with a diameter of 200 μm is as expected. It seems however that the transition to the Aris-Taylor region is not between 25 μm and 10 μm.
Calculations of dimensions smaller than 10 μm were troublesome, or even impossible. The solver was unable to converge the solution. The reason for this is probably the high pressure drop over the channel.

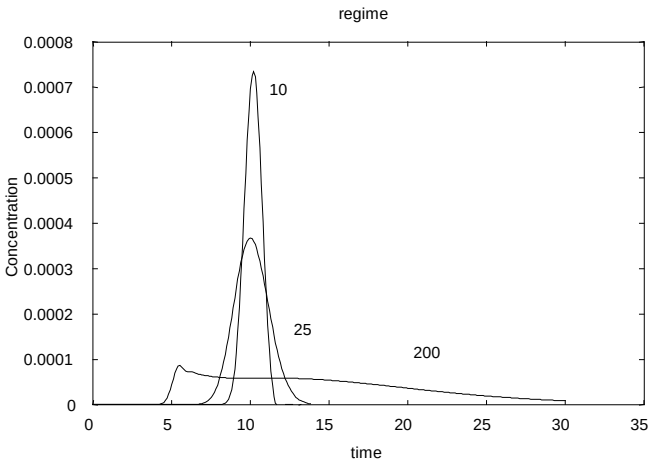

Figure (7.4) The response curve for different diameters.

According to Van der Linden [4] the pressure drop should be kept constant, this means that both <v> and L have to be decreased, otherwise problems with the pump and tightness of the connections can be expected. The numerical solver doesn't have these problems, but the increased pressure drop introduces numerical problems. Proper investigation should be conducted.

7.3 References

[1] R.D. Hull, Flow injection dispersion phenomena : simulation and evaluation of theoretical models, UMI Dissertation Services, 1993

[2] G.I. Taylor, ' Disperson of Soluble Matter in Solvent Flowing Slowly through a Tube' ,Proc. Roy. Soc., London, 219 A (1953) 186

[3] R. Aris, Proc. Roy. Soc., 'On the dispersion of Solute in a Fluid in laminar Flow Through a Tube', London, 235 A(1956)67

[4] W.E. van der Linden, "Miniaturisation in flow injection analysis", Trends in analytical chemistry, vol 6, no22, 1987

Curriculum Vitae

De schrijver van dit proefschrift werd geboren op 16 januari 1968 te Nijmegen. In 1985 behaalde hij aan het “BAC” te Schagen het HAVO diploma. Na twee jaar aan de “RSG”, te Schagen, volgde het VWO diploma. In hetzelfde jaar (1987) begon de schrijver zijn studie Chemische Technologie aan de Universiteit Twente. Binnen het vrij doctoraal programma koos hij voor de onderwijsstroom CT-Informatica. De stage werd verricht bij DOW Chemicals in Terneuzen. De afstudeeropdracht werd verricht bij de Vakgroep Chemische Analyse. Op 31 Augustus 1992 werd de inzet beloond met het doctoraal diploma.
Na het behalen van het doctoraal diploma werd de schrijver gedwongen tot een jaar dienstplicht. Tijdens de diensplicht was hij werkzaam als chauffeur bij de Infanterie Beveiligings Compagnie (IBC). Na de dienstplicht volgde een tweejarige (fulltime) baan bij het ingenieursbureau “BBV Software BV”. Dit ingenieursbureau houdt zich bezig met het ontwerpen en numeriek modelleren van geïntegreerde optische structuren. Van 1 september 1995 tot 1 september 1999 was hij werkzaam als Assistent in Opleiding (AIO) bij de vakgroep Chemische Analyse binnen de faculteit Chemische Technologie aan de Universiteit Twente. Tijdens de eerste drie jaar was hij ook nog werkzaam bij het ingenieursbureau op parttime basis. Het onderzoek werd uitgevoerd onder supervisie van prof. dr. W.E. van der Linden.

Dankwoord

Het is onmogelijk alle mensen te bedanken die de laatste vier jaar een bijdrage hebben geleverd aan dit proefschrift. Deze bijdrage kan natuurlijk inhoudelijk zijn maar ook de steun op niet inhoudelijke gebieden kan belangrijk zijn. Om te voorkomen dat het een te lange lijst van mensen wordt heb ik mij beperkt tot de belangrijkste. Dit betekent echter niet dat de bijdrage van mensen die niet met name genoemd worden niet gewaardeerd werd.

- Allereerst wil ik natuurlijk mijn hoogleraar Wim van der Linden bedanken voor de mogelijkheid om vier jaar lang aan een fascinerend onderwerp te kunnen werken en ondersteuning bij deze werkzaamheden.
- Als directe begeleider kan ik mij niemand beter voorstellen als Ties Bos. De vele aangename gesprekken, suggesties en kritische opmerkingen werden zeer op prijs gesteld.
- De vakgroep Chemische Analyse als geheel en in het bijzonder Bert Hoogendam en Ron Hulst voor de vele koffie en videoavond sessies. Ook de bijdrage van Bert op het gebied van experimentele opstellingen was essentieel.
- Mijn kamergenoten Marcel Hulsman en Jos Brunink voor de prettige gesprekken en plezierige werksfeer.
- De studenten Maarten Oosterkamp en Wim Hoeijenbos voor hun bijdrage en Tomás Marín Fernández voor zijn werk op het gebied van reactie kinetiek.
- Ik wil Albert van den Berg bedanken voor zijn rol als coördinator en de vele ideeën en oplossingen die hij naar voren bracht.
- Edwin Oosterbroek, Vincent Spierink, Johan Bomer, Olivier Parriaux, Anton Hollink, Paul Lambeck, Lucien Falco en vele anderen van de faculteit Electrotechniek.
- Mijn huisgenoten Herman Beunk en Jerre van Engen.
- En natuurlijk mijn ouders en broer.

Kortom bedankt !

Appendix

a.1 The command and Fortran files used in Chapter 4 .

a.1.1 The flow command file

```
/*********************************************************************/
/* command file for chapter 4 flow calculation structure 1       */
/*********************************************************************/
>>CFXF3D
   >>OPTIONS
      THREE DIMENSIONS
      BODY FITTED GRID
      CARTESIAN COORDINATES
      LAMINAR FLOW
      ISOTHERMAL FLOW
      INCOMPRESSIBLE FLOW
      USE DATABASE
      STEADY STATE
>>MODEL DATA
   >>TITLE
      PROBLEM TITLE 'STRAIGHT EELCO'
   >>PHYSICAL PROPERTIES
      >>STANDARD FLUID
         FLUID 'WATER'
         STANDARD FLUID REFERENCE TEMPERATURE 2.9315E+02
>>SOLVER DATA
   >>PROGRAM CONTROL
      MAXIMUM NUMBER OF ITERATIONS 300
      MASS SOURCE TOLERANCE 1.0000E-15
>>CREATE GRID
   >>INPUT GRID
      READ GRID FILE
>>MODEL BOUNDARY CONDITIONS
   >>MASS FLOW BOUNDARY CONDITIONS
      FLUXES 1* 1.000000E+00
      FRACTIONAL MASS FLOW SPECIFIED
   >>SET VARIABLES
      PATCH NAME 'INLET1'
      NORMAL VELOCITY 4.1666667e-4
>>OUTPUT OPTIONS
   >>LINE GRAPH DATA
      RESIDUAL
      FILE NAME 'output.dat'
      EACH ITERATION
      ALL VARIABLES
>>STOP
```

a.1.2 The convection-diffusion command file

```
/*********************************************************************/
/* command file for chapter 4 scalar calculation structure 1     */
/*********************************************************************/
>>CFXF3D
   >>OPTIONS
      THREE DIMENSIONS
      BODY FITTED GRID
      CARTESIAN COORDINATES
      LAMINAR FLOW
      ISOTHERMAL FLOW
      INCOMPRESSIBLE FLOW
      USE DATABASE
      USER SCALAR EQUATIONS 1
      TRANSIENT FLOW
   >>USER FORTRAN
      USRCVG
      USRINT
      USRTRN
   >>VARIABLE NAMES
      USER SCALAR1 'DYE001'
>>MODEL DATA
   >>TITLE
      PROBLEM TITLE 'STRAIGHT EELCO'
   >>PHYSICAL PROPERTIES
      >>STANDARD FLUID
         FLUID 'WATER'
         STANDARD FLUID REFERENCE TEMPERATURE 2.9315E+02
   >>SCALAR PARAMETERS
      >>DIFFUSIVITIES
         DYE001 2.03e-7
      >>TRANSIENT PARAMETERS
         >>FIXED TIME STEPPING
            TIME STEPS 2500*0.1
            INITIAL TIME 0.00
            BACKWARD DIFFERENCE
   >>DIFFERENCING SCHEME
      ALL EQUATIONS 'QUICK'
   >>SET INITIAL GUESS
      >>SET CONSTANT GUESS
         DYE001 0.00E+00
>>SOLVER DATA
   >>PROGRAM CONTROL
      MINIMUM NUMBER OF ITERATIONS 3
      MAXIMUM NUMBER OF ITERATIONS 12
      MASS SOURCE TOLERANCE 1.0000E-18
      ITERATIONS OF HYDRODYNAMIC EQUATIONS 0
>>CREATE GRID
   >>INPUT GRID
      READ GRID FILE
>>MODEL BOUNDARY CONDITIONS
   >>MASS FLOW BOUNDARY CONDITIONS
      FLUXES 1* 1.000000E+00
      FRACTIONAL MASS FLOW SPECIFIED
   >>SET VARIABLES
      PATCH NAME 'INLET1'
      NORMAL VELOCITY 4.1666667e-4
>>OUTPUT OPTIONS
   >>DUMP FILE OPTIONS
      INITIAL GUESS
      FINAL SOLUTION
>>STOP
```

a.1.3 The convection-diffusion Fortran file

This user file consists of three Fortran files. The files are very long so only the important items are given.

The first one is usrcvg.f

```
SUBROUTINE USRCVG(U,V,W,P,VFRAC,DEN,VIS,TE,ED,RS,T,H,RF,SCAL
     +                 ,XP,YP,ZP,VOL,AREA,VPOR,ARPOR,WFACT,CONV,IPT
     +                 ,IBLK,IPVERT,IPNODN,IPFACN,IPNODF,IPNODB,IPFACB
     +                 ,CMETH,MNSL,MXSL,RDFC,RESOR,URFVAR,LCONVG
     +                 ,WORK,IWORK,CWORK)
C
C**********************************************************************
C
C   THIS SUBROUTINE ALLOWS USERS TO MONITOR CONVERGENCE, ALTER
C   UNDER RELAXATION FACTORS, REDUCTION FACTORS ETC
C   AND WRITE SOLUTION DATA AS A FUNCTION OF ITERATION
```

<<SNIP>>

```
C+++++++++++++++++ USER AREA 4 ++++++++++++++++++++++++++++++++++++++++
C---- TO USE THIS USER ROUTINE FIRST SET IUSED=1
C
       IUSED=1
C
C+++++++++++++++++ END OF USER AREA 4 +++++++++++++++++++++++++++++++++
```

<<SNIP>>

```
C+++++++++++++++++ USER AREA 5 ++++++++++++++++++++++++++++++++++++++++
C
      CALL GETVAR('USRCVG','SCAL  ',ISCAL)
      CALL GETSCA('DYE001',IS1,CWORK)
      IVAR = ISCAL + IS1 - 1
C
      URESM=0.0
      DO 10 IPHASE=1,NPHASE
      URESM=MAX(URESM,RESOR(IVAR,IPHASE))
 10   CONTINUE
C
      LCONVG = URESM .LT. 1.0E-15
C
      OPEN(UNIT=4,NAME='../test.cvg',ACCESS='APPEND',
     +     STATUS='OLD')
      WRITE(4,3020)URESM,NITER,LCONVG
 3020 FORMAT(' Scalar : ',E12.5,
     +     ' Niter : ',I8,' LCONVG : ',I8)
      CLOSE(UNIT=4)
C
C+++++++++++++++++ END OF USER AREA 5 +++++++++++++++++++++++++++++++++
```

<<SNIP>>

```
RETURN
      END
```

The second one is usrint.f

```
      SUBROUTINE USRINT(U,V,W,P,VFRAC,DEN,VIS,TE,ED,RS,T,H,RF,SCAL
     +                 ,CONV,XC,YC,ZC,XP,YP,ZP
     +                 ,VOL,AREA,VPOR,ARPOR,WFACT,DISWAL,IPT
     +                 ,IBLK,IPVERT,IPNODN,IPFACN,IPNODF,IPNODB,IPFACB
     +                 ,WORK,IWORK,CWORK)
```

```
C
C*********************************************************************
C
C   UTILITY SUBROUTINE FOR USER-SUPPLIED INITIAL FIELD.
C
C*********************************************************************
```

<<SNIP>>

```
C+++++++++++++++++ USER AREA 4 +++++++++++++++++++++++++++++++++++++++
C---- TO USE THIS USER ROUTINE FIRST SET IUSED=1
C
       IUSED=1
C
C+++++++++++++++++ END OF USER AREA 4 +++++++++++++++++++++++++++++++++
```

<<SNIP>>

```
C+++++++++++++++++ USER AREA 5 +++++++++++++++++++++++++++++++++++++++
C
C---- AREA FOR INITIALISING VARIABLES U,V,W,P,VFRAC,TE,ED,RS,T,SCAL
C     ONLY.
C
      CALL IPALL('USER3D_INJECTION','USER3D','PATCH','CENTRES',IPT,NPT,
     +           CWORK,IWORK)
      CALL GETSCA('DYE001',IS1,CWORK)
      DO 200 I=1,NPT
       INODE=IPT(I)
       SCAL(INODE,1,IS1)=1e-3
 200   CONTINUE
C
C+++++++++++++++++ END OF USER AREA 5 +++++++++++++++++++++++++++++++++
C
      RETURN
      END
```

The third one is usrtn.f

```
      SUBROUTINE USRTRN(U,V,W,P,VFRAC,DEN,VIS,TE,ED,RS,T,H,RF,SCAL,
     +                  XP,YP,ZP,VOL,AREA,VPOR,ARPOR,WFACT,CONV,IPT,
     +                  IBLK,IPVERT,IPNODN,IPFACN,IPNODF,IPNODB,IPFACB,
     +                  WORK,IWORK,CWORK)
C
C*********************************************************************
C
C   USER SUBROUTINE TO ALLOW USERS TO MODIFY OR MONITOR THE SOLUTION AT
C   THE END OF EACH TIME STEP
C   THIS SUBROUTINE IS CALLED BEFORE THE START OF THE RUN AS WELL AS AT
C   THE END OF EACH TIME STEP
```

<<SNIP>>

```
C+++++++++++++++++ USER AREA 4 +++++++++++++++++++++++++++++++++++++++
C---- TO USE THIS USER ROUTINE FIRST SET IUSED=1
C
       IUSED=1
C
C+++++++++++++++++ END OF USER AREA 4 +++++++++++++++++++++++++++++++++
```

<<SNIP>>

```
C+++++++++++++++++ USER AREA 5 +++++++++++++++++++++++++++++++++++++++
C
      IF (KSTEP.EQ.0) THEN
      OPEN(UNIT=4,NAME='../detect1.dat',ACCESS='SEQUENTIAL',
```

```
     +     STATUS='UNKNOWN')
      WRITE(4,100)NSTEP
 100  FORMAT(I8)
      CLOSE(UNIT=4)
      OPEN(UNIT=4,NAME='../detect2.dat',ACCESS='SEQUENTIAL',
     +     STATUS='UNKNOWN')
      WRITE(4,100)NSTEP
 101  FORMAT(I8)
      CLOSE(UNIT=4)
      OPEN(UNIT=4,NAME='../detect3.dat',ACCESS='SEQUENTIAL',
     +     STATUS='UNKNOWN')
      WRITE(4,100)NSTEP
 102  FORMAT(I8)
      CLOSE(UNIT=4)
      ENDIF
C
      IF (KSTEP.NE.3) THEN
      TIMET=TIME+30.0
      RESULT1=0
      CALL IPALL('USER3D_DETECTION1','USER3D','PATCH','CENTRES',IPT,NPT,
     +           CWORK,IWORK)
      CALL GETSCA('DYE001',IS1,CWORK)
      DO 2001 I=1,NPT
       INODE=IPT(I)
       RESULT1=RESULT1+SCAL(INODE,1,IS1)
 2001 CONTINUE
      RESULT1=RESULT1/NPT
      OPEN(UNIT=4,NAME='../detect1.dat',ACCESS='APPEND',
     +     STATUS='OLD')
      WRITE(4,2020)TIMET,RESULT1
 2020 FORMAT(F20.15,' ',F20.15,' ')
      CLOSE(UNIT=4)
C
      RESULT2=0
      CALL IPALL('USER3D_DETECTION2','USER3D','PATCH','CENTRES',IPT,NPT,
     +           CWORK,IWORK)
      CALL GETSCA('DYE001',IS1,CWORK)
      DO 2002 I=1,NPT
       INODE=IPT(I)
       RESULT2=RESULT2+SCAL(INODE,1,IS1)
 2002 CONTINUE
      RESULT2=RESULT2/NPT
      OPEN(UNIT=4,NAME='../detect2.dat',ACCESS='APPEND',
     +     STATUS='OLD')
      WRITE(4,2030)TIMET,RESULT2
 2030 FORMAT(F20.15,' ',F20.15,' ')
      CLOSE(UNIT=4)
C
      RESULT3=0
      CALL IPALL('USER3D_DETECTION3','USER3D','PATCH','CENTRES',IPT,NPT,
     +           CWORK,IWORK)
      CALL GETSCA('DYE001',IS1,CWORK)
      DO 2003 I=1,NPT
       INODE=IPT(I)
       RESULT3=RESULT3+SCAL(INODE,1,IS1)
 2003 CONTINUE
      RESULT3=RESULT3/NPT
      OPEN(UNIT=4,NAME='../detect3.dat',ACCESS='APPEND',
     +     STATUS='OLD')
      WRITE(4,2040)TIMET,RESULT3
 2040 FORMAT(F20.15,' ',F20.15,' ')
      CLOSE(UNIT=4)
C
      OPEN(UNIT=10,NAME='SYS$OUTPUT')
      WRITE(10,300)TIMET,RESULT1,RESULT2,RESULT3
 300  FORMAT(F20.15,' ',F20.15,' ',F20.15,' ',F20.15)
      CLOSE(UNIT=10)
C
      ENDIF
C+++++++++++++++++ END OF USER AREA 5 +++++++++++++++++++++++++++++++++
C
      RETURN
      END
```

a.2 The command and Fortran files used in Chapter 6 .

a.2.1 The flow command file

```
/*********************************************************************/
/* flow command file for inlet carrier                               */
/*********************************************************************/
>>CFXF3D
  >>OPTIONS
    THREE DIMENSIONS
    BODY FITTED GRID
    CARTESIAN COORDINATES
    LAMINAR FLOW
    ISOTHERMAL FLOW
    INCOMPRESSIBLE FLOW
    USE DATABASE
    STEADY STATE
  >>USER FORTRAN
    USRCVG
>>MODEL DATA
  >>TITLE
    PROBLEM TITLE 'STRAIGHT EELCO'
  >>PHYSICAL PROPERTIES
    >>STANDARD FLUID
      FLUID 'WATER'
      STANDARD FLUID REFERENCE TEMPERATURE 2.9315E+02
    >>FLUID PARAMETERS
     VISCOSITY 1.0e-3
     DENSITY   998.0
>>SOLVER DATA
  >>PROGRAM CONTROL
    MAXIMUM NUMBER OF ITERATIONS 300
    MASS SOURCE TOLERANCE 1e-18
>>CREATE GRID
  >>INPUT GRID
    READ GRID FILE
>>MODEL BOUNDARY CONDITIONS
  >>MASS FLOW BOUNDARY CONDITIONS
    FLUXES 1* 1.000000E+00
    FRACTIONAL MASS FLOW SPECIFIED

 >>SET VARIABLES
    PATCH NAME 'INLET1'
    NORMAL VELOCITY 1.15207e-3

 >>SET VARIABLES
    PATCH NAME 'INLET2'
    NORMAL VELOCITY 1.041666e-3

>>OUTPUT OPTIONS
  >>LINE GRAPH DATA
    RESIDUAL
    FILE NAME 'output.dat'
    EACH ITERATION
    ALL VARIABLES
>>STOP
```

The italics part is used for the calculation of the flow profile during the sample injection.

a.2.2 The flow Fortran file

Both the flow profile have to be written to file to be able to read them during the convection-diffusion calculation.

```
      SUBROUTINE USRCVG(U,V,W,P,VFRAC,DEN,VIS,TE,ED,RS,T,H,RF,SCAL
     +                 ,XP,YP,ZP,VOL,AREA,VPOR,ARPOR,WFACT,CONV,IPT
     +                 ,IBLK,IPVERT,IPNODN,IPFACN,IPNODF,IPNODB,IPFACB
     +                 ,CMETH,MNSL,MXSL,RDFC,RESOR,URFVAR,LCONVG
     +                 ,WORK,IWORK,CWORK)
C
C*****************************************************************
C
C   THIS SUBROUTINE ALLOWS USERS TO MONITOR CONVERGENCE, ALTER
C   UNDER RELAXATION FACTORS, REDUCTION FACTORS ETC
C   AND WRITE SOLUTION DATA AS A FUNCTION OF ITERATION
C
```

<<SNIP>>

```
C+++++++++++++++++ USER AREA 5 ++++++++++++++++++++++++++++++++++++++++
C
      RESULTA=0
      RESULTB=0
      CALL GETVAR('USRCVG','P      ',IPRESS)
      URESM=RESOR(IPRESS,1)
      CALL IPALL('USER3D_DETECTION1','USER3D','PATCH','CENTRES',IPT,
     +           NPT,CWORK,IWORK)
C
      DO 2011 I=1,NPT
       INODE=IPT(I)
       RESULTA=MAX(W(INODE,1),RESULTA)
       RESULTB=RESULTB+ W(INODE,1)
 2011 CONTINUE
      RESULTB=RESULTB/NPT
C
      OPEN(UNIT=10,NAME='SYS$OUTPUT')
      WRITE(10,3030)NITER,RESULTB,RESULTA,URESM
 3030 FORMAT(' I: ',I3,' AVGW : ',E24.8,' WM : ',E24.8,' R : ',E12.5)
      CLOSE(UNIT=10)
C
      DUM=0.0
      IF (URESM.LT.0.5e-9.OR.NITER.EQ.299) THEN
      LCONVG=1
      OPEN(UNIT=4,NAME='../../inlet1.dat',ACCESS='APPEND',STATUS='OLD')
       DO 30 I=1,NFACE
        DUM=CONV(I  ,1)
        WRITE(4,3021)DUM
 3021 FORMAT(E12.5)
 30    CONTINUE
      CLOSE(UNIT=4)
      ENDIF
C
C+++++++++++++++++ END OF USER AREA 5 +++++++++++++++++++++++++++++++++
```

The flow profile is written to file. After the flow profile calculation for inlet2 the output file inlet2.dat is used.

a.2.3 The convection-diffusion (and reaction) command file

```
/*******************************************************/
/* SIMPLE CHEMICAL REACTION                            */
/*******************************************************/
>>CFX4
  >>OPTIONS
    THREE DIMENSIONS
    BODY FITTED GRID
    LAMINAR FLOW
    INCOMPRESSIBLE FLOW
    CHEMICAL SPECIES EQUATIONS 6
    USE DATABASE
    ISOTHERMAL FLOW
    TRANSIENT FLOW
    END
  >>USER FORTRAN
    USRCVG
    USRINT
    USRTRN
    USRSRC
  >>VARIABLE NAMES
    SPECIES1 'A'
    SPECIES2 'B'
    SPECIES3 'C'
    SPECIES4 'D'
    SPECIES5 'E'
    SPECIES6 'BF'
  >>UNITS
    >>CHEMICAL SPECIES
      MASS FRACTIONS
      END
>>MODEL DATA
  >>TITLE
    PROBLEM TITLE 'REFERENCE EXAMPLE 33'
    END
    >>MATERIALS DATABASE
    >>SOURCE OF DATA
      PCP
    >>FLUID DATA
      FLUID 'WATER'
      MATERIAL PHASE 'LIQUID'
      MATERIAL TEMPERATURE 293.15
  >>PHYSICAL PROPERTIES
    >> FLUID PARAMETERS
       DENSITY   998
       VISCOSITY 1.0e-3
    >>TRANSIENT PARAMETERS
      >>FIXED TIME STEPPING
        TIME STEPS 200*0.5
        INITIAL TIME 0.00
        CRANK NICOLSON
  >>DIFFERENCING SCHEME
    ALL EQUATIONS 'QUICK'
  >>SET INITIAL GUESS
    >>SET CONSTANT GUESS
      BF 1.0e-2
  >>CHEMISTRY
    >>CHEMICAL SPECIES PROPERTIES
      >>DIFFUSIVITIES
        SPECIES 3.0E-7 30.0E-7 3.0E-7 3.0E-7 30.0E-7
        END
      >>MOLECULAR WEIGHTS
        SPECIES 698.05 51.45  749.5 698.05 51.45 18.02
        END
    >>CHEMICAL REACTION SCHEME
      >>REACTION
        >>REACTION NAME
          NAME 'SIMPLE REACTION'
          END
        >>REACTANTS
          A 1.0
          B 1.0
          END
        >>PRODUCTS
```

```
          C 1.0
          END
        >>FORWARD RATE
          PREEXPONENTIAL FACTOR 1000.0
          ACTIVATION ENERGY 0.0
          END
        >>HEAT RELEASE
          MOLAR ENTHALPY OF REACTION 0.0
          ENTHALPY REFERENCE TEMPERATURE 293.15
     >>CHEMISTRY SOLVER OPTIONS
       BACKGROUND FLUID 'BF'
>>SOLVER DATA
  >>PROGRAM CONTROL
    MINIMUM NUMBER OF ITERATIONS 3
    MAXIMUM NUMBER OF ITERATIONS 10
    MASS SOURCE TOLERANCE 1.0000E-18
    ITERATIONS OF HYDRODYNAMIC EQUATIONS 0
    END
>>CREATE GRID
  >>INPUT GRID
    READ GRID FILE
>>MODEL BOUNDARY CONDITIONS
  >>INLET BOUNDARIES
    #CALC
     CONB = (51.45 *1.5e-3)/998.0;
     CONE = (51.45 *1.5e-3)/998.0;
    #ENDCALC
    PATCH NAME 'INLET1'
    A 0.0
    B #CONB
    E #CONE
    END
  >>INLET BOUNDARIES
    #CALC
     CONA = (698.05 *1.0e-3)/998.0;
     COND = (749.5*1.0e-3) /998.0;
    #ENDCALC
    PATCH NAME 'INLET2'
    B 0.0
    A #CONA
    D #COND
    E 0.0
    END
>>STOP
```

a.2.4 The convection-diffusion (and reaction) Fortran file

```
      SUBROUTINE USRCVG(U,V,W,P,VFRAC,DEN,VIS,TE,ED,RS,T,H,RF,SCAL
     +                 ,XP,YP,ZP,VOL,AREA,VPOR,ARPOR,WFACT,CONV,IPT
     +                 ,IBLK,IPVERT,IPNODN,IPFACN,IPNODF,IPNODB,IPFACB
     +                 ,CMETH,MNSL,MXSL,RDFC,RESOR,URFVAR,LCONVG
     +                 ,WORK,IWORK,CWORK)
C
<<SNIP>>

C+++++++++++++++++ USER AREA 5 ++++++++++++++++++++++++++++++++++++++++
C
C---- EXAMPLE: (TEST ON MAX OF MASS RESIDUAL AND ENTHALPY RESIDUAL)
C
      RESULTC=0
      RESULTA=0
      RESULTB=0
      RESULTD=0
      RESULTE=0
      VOLUME=0
      CALL IPALL('USER3D_DETECTION1','USER3D','PATCH','CENTRES',IPT,
     +           NPT,CWORK,IWORK)
      CALL GETSCA('A     ',IS1,CWORK)
      CALL GETSCA('B     ',IS2,CWORK)
      CALL GETSCA('C     ',IS3,CWORK)
      CALL GETSCA('D     ',IS4,CWORK)
      CALL GETSCA('E     ',IS5,CWORK)
      DO 2001 I=1,NPT
       INODE=IPT(I)
       RESULTA=RESULTA+SCAL(INODE,1,IS1)*998.0/698.05
       RESULTB=RESULTB+SCAL(INODE,1,IS2)*998.0/51.45
       RESULTC=RESULTC+SCAL(INODE,1,IS3)*998.0/749.5
       RESULTD=RESULTD+SCAL(INODE,1,IS4)*998.0/698.05
       RESULTE=RESULTE+SCAL(INODE,1,IS5)*998.0/51.45
       VOLUME=VOLUME+VOL(INODE)
 2001 CONTINUE
      RESULTA=RESULTA/NPT
      RESULTB=RESULTB/NPT
      RESULTC=RESULTC/NPT
      RESULTD=RESULTD/NPT
      RESULTE=RESULTD/NPT
C
      ARESM=0.0
      BRESM=0.0
      CRESM=0.0
C

      CALL GETVAR('USRCVG','SCAL  ',ISCAL)
      CALL GETSCA('A     ',IS1,CWORK)
      CALL GETSCA('B     ',IS2,CWORK)
      CALL GETSCA('C     ',IS3,CWORK)
      IVARA = ISCAL + IS1 - 1
      IVARB = ISCAL + IS2 - 1
      IVARC = ISCAL + IS3 - 1
C
      DO 10 IPHASE=1,NPHASE
      ARESM=MAX(ARESM,RESOR(IVARA,IPHASE))
      BRESM=MAX(BRESM,RESOR(IVARB,IPHASE))
      CRESM=MAX(CRESM,RESOR(IVARC,IPHASE))
 10   CONTINUE
C
      CHECKA=ARESM .LT. 0.5E-11
      CHECKB=BRESM .LT. 1.0E-12
C
      LCONVG = 0
      IF (NITER.GT.100) THEN
       LCONVG = 1
      ENDIF
      IF (CHECKA.EQ.1.AND.CHECKB.EQ.1)  THEN
       LCONVG = 1
      ENDIF

      OPEN(UNIT=4,NAME='../test.cvg',ACCESS='APPEND',
     +     STATUS='OLD')
```

```
      WRITE(4,3020)TIME,NITER,LCONVG,RESULTA,ARESM,RESULTB,BRESM,
     +             RESULTC,CRESM
 3020 FORMAT('TIME : ',F12.5,' I: ',I4,' CVG ',I4,
     +       '  A: ',E12.5,' +/-  ',E12.5,
     +       '  B: ',E12.5,' +/-  ',E12.5,
     +       '  C: ',E12.5,' +/-  ',E12.5)
      CLOSE(UNIT=4)
C
      OPEN(UNIT=10,NAME='SYS$OUTPUT')
      WRITE(10,3120)TIME,NITER,LCONVG,RESULTA,ARESM,RESULTB,BRESM,
     +             RESULTC,CRESM
 3120 FORMAT('TIME : ',F12.5,' I: ',I8,' CVG ',I8,
     +       '  A: ',E12.5,' +/-  ',E12.5,
     +       '  B: ',E12.5,' +/-  ',E12.5,
     +       '  C: ',E12.5,' +/-  ',E12.5)
      CLOSE(UNIT=10)
C
C----END OF EXAMPLE
C
C+++++++++++++++++ END OF USER AREA 5 +++++++++++++++++++++++++++++++++
C
```

<<SNIP>>

```
C
SUBROUTINE USRINT(U,V,W,P,VFRAC,DEN,VIS,TE,ED,RS,T,H,RF,SCAL
     +                ,CONV,XC,YC,ZC,XP,YP,ZP
     +                ,VOL,AREA,VPOR,ARPOR,WFACT,DISWAL,IPT
     +                ,IBLK,IPVERT,IPNODN,IPFACN,IPNODF,IPNODB,IPFACB
     +                ,WORK,IWORK,CWORK)
C
```

<<SNIP>>

```
C+++++++++++++++++ USER AREA 5 +++++++++++++++++++++++++++++++++++++++++
C
C---- AREA FOR INITIALISING VARIABLES U,V,W,P,VFRAC,TE,ED,RS,T,SCAL
C     ONLY.
C
      CALL GETSCA('A     ',IS1,CWORK)
      CALL GETSCA('B     ',IS2,CWORK)
      CALL GETSCA('C     ',IS3,CWORK)
      CALL GETSCA('D     ',IS4,CWORK)
      CALL GETSCA('E     ',IS5,CWORK)
C
      CALL IPALL('*','*','BLOCK','CENTRES',IPT,
     +           NPT,CWORK,IWORK)
      DO 200 I=1,NPT
       INODE=IPT(I)
       SCAL(INODE,1,IS1)= 0.0
       SCAL(INODE,1,IS2)= (51.45 *1.5e-3)/998.0
       SCAL(INODE,1,IS3)= 0.0
       SCAL(INODE,1,IS4)= 0.0
       SCAL(INODE,1,IS5)= (51.45 *1.5e-3)/998.0
 200   CONTINUE
C
C  mass fraction y= MW * []/ density
C
      CALL IPALL('USER3D_INJECTION','USER3D','PATCH','CENTRES',IPT,
     +           NPT,CWORK,IWORK)
      DO 201 I=1,NPT
       INODE=IPT(I)
       SCAL(INODE,1,IS1)=(698.05 *1.0e-3)/998.0
       SCAL(INODE,1,IS2)=0.0
       SCAL(INODE,1,IS4)=(749.5 *1.0e-3)/998.0
       SCAL(INODE,1,IS5)=0.0
 201   CONTINUE
C
      DO 33 I=1,NFACE
        CONV(I  ,1)= 0.0
 33    CONTINUE

C
      CALL SETPER('USRINT','WORK  ','ILE1  ',NFACE,I1VEL)
      CALL SETPER('USRINT','WORK  ','ILE2  ',NFACE,I2VEL)
C
      OPEN(UNIT=4,NAME='../../../inlet2.dat',READONLY,
     +     STATUS='OLD')
```

```
      REWIND 4
      DO 31 I=1,NFACE
        READ(4,3022)DUM
 3022   FORMAT(E12.5)
        CONV(I  ,1)    =DUM
        WORK(I2VEL+I-1)=DUM
 31    CONTINUE
C
      CLOSE(UNIT=4)
C
      OPEN(UNIT=4,NAME='../../../inlet1.dat',READONLY,
     +     STATUS='OLD')
      REWIND 4
      DO 39 I=1,NFACE
        READ(4,3023)DUM
 3023   FORMAT(E12.5)
        CONV(I  ,1)    =DUM
        WORK(I1VEL+I-1)=DUM
 39    CONTINUE
C
      CLOSE(UNIT=4)
C
C+++++++++++++++++ END OF USER AREA 5 +++++++++++++++++++++++++++++++++
```

<<SNIP>>

```
      SUBROUTINE USRTRN(U,V,W,P,VFRAC,DEN,VIS,TE,ED,RS,T,H,RF,SCAL,
     +                  XP,YP,ZP,VOL,AREA,VPOR,ARPOR,WFACT,CONV,IPT,
     +                  IBLK,IPVERT,IPNODN,IPFACN,IPNODF,IPNODB,IPFACB,
     +                  WORK,IWORK,CWORK)
C
```

<<SNIP>>

```
C+++++++++++++++++ USER AREA 5 +++++++++++++++++++++++++++++++++++++++++
C
      IF (KSTEP.EQ.0) THEN
      OPEN(UNIT=4,NAME='../detect.dat',ACCESS='SEQUENTIAL',
     +     STATUS='UNKNOWN')
      WRITE(4,100)NSTEP
 100  FORMAT(' ')
      CLOSE(UNIT=4)
      ENDIF
C
      IF (1) THEN
      TIMET=TIME+10
      RESULTC=0
      RESULTA=0
      RESULTB=0
      RESULTD=0
      RESULTE=0
      VOLUME=0
      CALL IPALL('USER3D_DETECTION1','USER3D','PATCH','CENTRES',IPT,
     +           NPT,CWORK,IWORK)

      CALL GETSCA('A     ',IS1,CWORK)
      CALL GETSCA('B     ',IS2,CWORK)
      CALL GETSCA('C     ',IS3,CWORK)
      CALL GETSCA('D     ',IS4,CWORK)
      CALL GETSCA('E     ',IS5,CWORK)
      DO 2001 I=1,NPT
       INODE=IPT(I)
       RESULTA=RESULTA+SCAL(INODE,1,IS1)*998.0/698.05
       RESULTB=RESULTB+SCAL(INODE,1,IS2)*998.0/51.45
       RESULTC=RESULTC+SCAL(INODE,1,IS3)*998.0/749.5
       RESULTD=RESULTD+SCAL(INODE,1,IS4)*998.0/698.05
       RESULTE=RESULTE+SCAL(INODE,1,IS5)*998.0/51.45
C
       VOLUME=VOLUME+VOL(INODE)
 2001 CONTINUE
      RESULTA=RESULTA/NPT
      RESULTB=RESULTB/NPT
      RESULTC=RESULTC/NPT
      RESULTD=RESULTD/NPT
      RESULTE=RESULTE/NPT
```

```
      OPEN(UNIT=4,NAME='../detect.dat',ACCESS='APPEND',
     +     STATUS='OLD')
      WRITE(4,2020)TIMET,RESULTA,RESULTB,RESULTC,RESULTD,RESULTE
 2020 FORMAT(F20.15,' ',F20.15,' ',F20.15,' ',F20.15,' ',F20.15,
     +      ' ',F20.15)
      CLOSE(UNIT=4)
C
      ENDIF
C+++++++++++++++++ END OF USER AREA 5 +++++++++++++++++++++++++++++++++++
```

<<SNIP>>

```
      SUBROUTINE USRSRC(IEQN,ICALL,CNAME,CALIAS,AM,SP,SU,CONV
     +                 ,U,V,W,P,VFRAC,DEN,VIS,TE,ED,RS,T,H,RF,SCAL
     +                 ,XP,YP,ZP,VOL,AREA,VPOR,ARPOR,WFACT,IPT
     +                 ,IBLK,IPVERT,IPNODN,IPFACN,IPNODF,IPNODB,IPFACB
     +                 ,WORK,IWORK,CWORK)
C
```

<<SNIP>>

```
C+++++++++++++++++ USER AREA 6 +++++++++++++++++++++++++++++++++++++++++
C
C SECTION WHERE THE DIFFERENT FLOW VALUES ARE SET
C
      CALL GETVAR('USRSRC','SCAL  ',ISCAL)
      CALL GETADD('USRSRC','PERMR ','ILE1  ',ILEVEL,I1VEL)
      CALL GETADD('USRSRC','PERMR ','ILE2  ',ILEVEL,I2VEL)

C
      IF (ISCAL.EQ.IEQN) THEN
C
      IF (TIME.GT.20.0) THEN
       DO 30 I=1,NFACE
        CONV(I  ,1)= WORK(I1VEL+I-1)
 30    CONTINUE
      ELSE
       DO 31 I=1,NFACE
        CONV(I  ,1)= WORK(I2VEL+I-1)
 31    CONTINUE
      ENDIF
C
C IF FLAGSIGN IS ZERO THE COPY IS SET BACK (SEE USERINT)
C STANDARD ALL IS SET TO ZERO
C
C      FLAGSIGN=(TIME .GT. 30.0 .AND. TIME .LE. 45.0)
C
C       IF (FLAGSIGN.EQ.0) THEN
C
C       ELSE
C       DO 33 I=1,NFACE
C         CONV(I  ,1)=0
C 33    CONTINUE
C       ENDIF
C
      ENDIF
C
C
C+++++++++++++++++ END OF USER AREA 6 +++++++++++++++++++++++++++++++++++
C
```

<<SNIP>>